UNIVERSITÀ DEGLI STUDI DI PARMA

Dottorato di Ricerca in Fisiopatologia Sistemica

Ciclo XXVIII

Microenvironment and microvascular wall modulate cancer cell progression

Coordinatore:
Chiar.mo Prof. Enrico Maria Silini

Tutor:
Chiar.mo Prof. Roberto Perris
Dott.ssa Domenica Mangieri

Dottoranda: Carlotta Alias

“Above all, don't fear difficult moments. The best comes from them”

Rita Levi-Montalcini

“On the other side of clouds, the sky is blue”

E.M.

Summary

Abstract

Tumour progression is a complex process that frequently brings to cancer metastasis, the first cause of poor prognosis of cancer affected patients. Metastasis are generated by cells escaped from a primary mass and able to enter in the circulation, survive and proliferate in a new, distant site of the organism. To reach all these goal, many different phenomena had occur within both the cancer cells and the surrounding microenvironment.

In the first part of this thesis, the focus was pointed on the metastatic potential of a leiomyosarcoma cell model. The studied cancer cells demonstrated a strong invasive capacity of the ECM *in vitro*, principally by production of matrix metalloproteinases 2 and 9, and robust pro-angiogenic activity in the chick CAM model, that facilitate its dissemination through same chick embryo internal organs. This study, with the title "MMPs and angiogenesis affect the metastatic potential of a human vulvar leiomyosarcoma cell line", is presented in the published form.

In the second part of this work, the emphasis was given to the microvascular element of the tumour microenvironment and specifically to the perivascular pericytes. These are intriguing cells due to their uncertain involvement in the biology of cancer. It is not clear how pericytes change within the tumour microenvironment and which is their contribute during the tumour dissemination. After the characterization of the chosen pericytic cell model, an *in vitro* study of the interaction between pericytes and different cancer cell lines where performed. Indirect and direct cell-cell interaction as well as movement of cancer cells in presence of pericytes conditioned media was analysed, in order to investigate the reciprocal influence of pericytes and tumour cells in the context of cancer progression.

Abbreviations

α-SMA	Alpha smooth muscle actin
BBB	Blood brain barrier
BDNF	Brain-derived neurotrophic factor
BM	Basement Membrane
CAFs	Cancer-associated fibroblasts
CAM	Chorio-allantoic membrane
cc-CM	Co-culture conditioned medium
CCD	Charge-coupled device
CI	Cell index
CM	Conditioned medium
CNS	Central nervous system
CXCL-5	Chemokine (C-X-C motif) ligand 5
DAB	Diaminobenzidine
DAPI	4',6-diamidino-2-phenylindole
Dkk-1	Dickkopf-1
DMEM	Dulbecco's modified Eagle's medium
DT	Doubling time
ECs	Endothelial cells
EDTA	Ethylenediaminetetraacetic acid
EGF	Epidermal Growth Factor
EMMPRIN	Extracellular matrix metalloproteinase inducer
FBS	Foetal bovine serum
FGF basic	Fibroblast growth factor basic
FGF-19	Fibroblast growth factor 19
FITC	Fluorescein isothiocyanate
FU	Units of fluorescence
GalNAz	N-azidoacetyl-galactosamine
GDF-15	Growth differentiation factor 15
GFR	Growth factor reduced
GlcNAz	N-azidoacetyl-glucosamine
gLMS	Gynaecological leiomyosarcoma
GM-CSF	Granulocyte macrophage colony stimulating factor

HBVP	Human brain vascular pericytes
HB-EGF	Heparin-binding EGF-like growth factor
IGFBP-2	Insulin-like growth factor-binding protein-1
IL-8	Interleukin 8
IL-11	Interleukin 11
IL-17A	Interleukin 17A
INF-γ	Interferon gamma
LIF	Leukemia inhibitory factor
LMS	Leiomyosarcoma
ManNAz	N-azidoacetyl-mannoosamine
MIF	Macrophage migration inhibitory factor
MMPs	Matrix metalloproteases
NGS	Normal goat serum
NPD	Normalized pixel density
NuMA	Nuclear mitotic apparatus protein
PCR	Polymerase chain reaction
PDGF-AA	Platelet-derived growth factor A
PDGF-B	Platelet-derived growth factor B
PDGFR-β	Platelet-derived growth factor receptor beta
PFA	Paraformaldehyde
PGS	Pericyte growth supplements
PM	Pericyte medium
PTX3	Pentraxin 3
RIPA buffer	Radioimmunoprecipitation assay buffer
RT	Room temperature
RTCA	Real-Time cell analysis
S1P	Sphingosine-1-phosphate
STS	Soft-tissue sarcoma
TAE buffer	Tris-acetate-EDTA buffer
TBS buffer	Tris-buffered saline buffer
TBST buffer	TBS containing 0,1% Tween-20 buffer
TGFβ1	Transforming growth factor beta 1

TGFβR-II	Transforming growth factor beta receptors II
TLDA	TaqMan low density array
TME	Tumour microenvironment
uPAR	Urokinase plasminogen activator receptor
VEGF	Vascular endothelial growth factor
vLMS	Vulvar leiomyosarcoma

Background

Tumour progression and dissemination

Tumorigenesis is a multistep process: every step reflect genetic alterations that drive the progressive transformation of normal cells into highly malignant derivatives[1]. Genetic transformations give to cancer cells many abnormal capabilities well described by D. Hanahan and R. Weinberg (Figure 1).

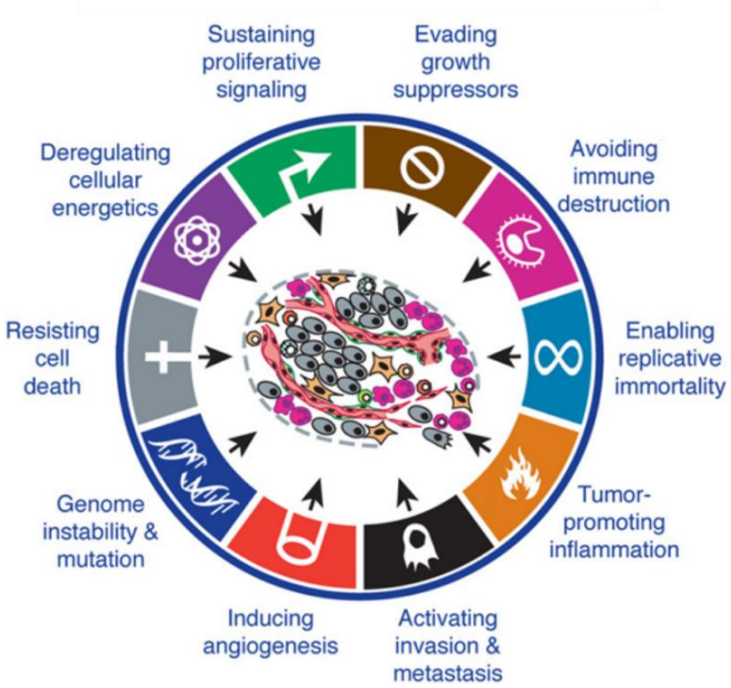

Figure 1. Cancer hallmark capabilities necessary for tumour growth and progression. Modified from Hanahan & Weinberg (1).

Metastasis is the phenomenon through which cells of a primary tumour mass spread to distant sites and grow as secondary tumours (Figure 2). This ability to invade the body is one of the recognized hallmarks of cancer[1] and occurs in a series of progressive steps called "metastatic cascade"[2]:

- tumour cells dissociation from the primary mass;
- local invasion through the surrounding BM and stromal cell layers such as ECs and pericytes;
- intravasation into the lumen of the blood vessel;
- survival to the hard microenvironment in the blood flow;
- arrest at a distant organ site;
- extravasation into the parenchyma of a tissue;

- survival in this new microenvironment;
- formation of micro metastases.

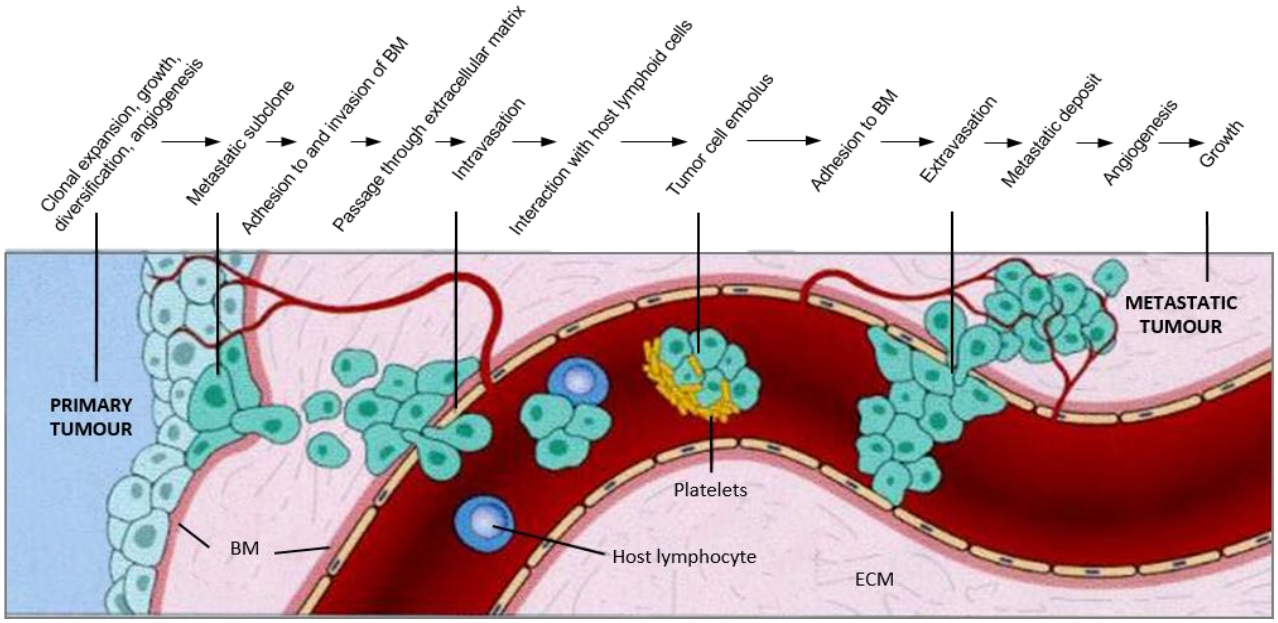

Figure 2. Schematic representation of the metastatic cascade, from the primary mass to metastasis. Modified from Kumar et al. (3).

Despite this accurate description, the phenomenon it is still one of the lesser understood events in cancer biology[4,5]. What is known is that the metastatic cascade is a highly inefficient process[5–7], because blood and lymph, the major route of transport of cancer cells, represent hostile environments for these cells[8]. The majority of cancer cells enter the bloodstream, but most of these die for loss of survival signal[9] or are eliminated by the immune system[10]. In fact, it has been demonstrated that lesser than 0,01% of the cancer cells that undertake the metastatic cascade develop into metastases[11,12]. However, metastasis are the primary cause of tumour morbidity and mortality[13]: in fact, primary tumours are responsible only for 10% of the cancer-related deaths while the remaining 90% are caused by metastasis[14]. That attests the difficulties in blocking the tumour once it disseminates through the body[13].

For this purpose, a larger interest is currently given to the tumour microenvironment[15]: fibroblasts, myofibroblasts, leukocytes, endothelial cells, pericytes and ECM[16]. Indeed, the various steps that leads to metastasis involve not only the malignant cells of the tumour, but also non-malignant cells and ECM composing the tumour microenvironment, which influence and sometimes regulate various points of the metastatic cascade[17,18].

An effective treatment of the cancer phenomenon is largely based on the capacity to block the process of metastasis[2], both blocking the malignant cells before dissemination and controlling the tumour microenvironment .

These dual aspects of tumorigenesis will be discuss in Part I and II.

Part I

Introduction

Soft tissue sarcoma consists of a rare (1% of malignant tumour19) and heterogeneous group (including 70 different histotype20) of solid tumours of mesenchymal origin. Leiomyosarcoma is the most frequent with an incidence of 20% of all STS dianosticated in Europe21. LMS could be classified according to the anatomic distribution into gynaecologic type (particularly uterus or vulvar leiomyosarcoma) and non-gynaecologic type22. The subtype of gynaecological LMS account for 13% of STS diagnoses23. Gynaecological LMS represent a risk for the women after the age of 40 years23 due to high aggressiveness and propensity to infiltrate secondary organs24–30, which leads to poor prognosis. Despite decades of clinical approaches, gLMS represent nowadays one of the most resistant sarcomas31 without available effective treatments23,32,33.

Tumorigenesis and angiogenesis are events reciprocally stimulating[1,34,35]. The formation of new blood vessels permits expansion of tumour mass, which may enhance its metastatic potential. Thus, tumour dissemination and invasion are closely related to tumour-induced neoangiogenesis[36]. Furthermore, the cleavage of ECM due to the MMPs activity is a phenomenon linked to the promotion of angiogenesis and tumour spreading[37]. Both because of the release of angiogenic factors stored in the ECM (particularly VEGF and bFGF), growth factors, cytokines[38] and of the degradation of the matrix scaffold.

While a lot of experimental and clinical studies documented many of the mechanisms involved in the development of several types of carcinomas[1,39], by contrast, the molecular and cellular mediators involved in dissemination of STSs and, more in detail in gLMS, remain mostly unknown.

For these reasons, a focus on some aspects of progression and dissemination of a subtype of gLMS, vulvar LMS, was taken into account. Using a vulvar LMS-derived cell line namely SK-LMS-1, an *in vitro* (invasion of ECM, evasion from ECM) and *in vivo* (CAM assay) investigation of tumoral cells behaviour was carried on. The invasive capacity observed in all the *in vitro* assays was attributed at the activity of MMPs 2 and 9, while in the *in vivo* evaluations SK-LMS-1 demonstrated a strong angiogenic response and dissemination capacity to the chick embryo liver. Together, these results indicated that MMP-2 and MMP-9 are crucial elements involved in the spreading and invasion of the studied vLMS derived cell line. However, further studies are require to clarify the molecular and cellular machinery involved in the progression of this malignancy.

The published paper is presented below.

J. Cell. Mol. Med. Vol 19, No 9, 2015 pp. 2098-2107

MMPs and angiogenesis affect the metastatic potential of a human vulvar leiomyosarcoma cell line

Carlotta Alias [a, #], Laura Rocchi [b, #], Domenico Ribatti [c], Stefano Caraffi [b], Alessandra D'Angelo [a], Roberto Perris [a, d], Domenica Mangieri [b, d, *]

[a] *Department of Life Sciences, University of Parma, Parma, Italy*
[b] *Surgical Pathology Unit, University Hospital of Parma, Parma, Italy*
[c] *Department of Basic Medical Sciences, Neurosciences and Sensory Organs, Section of Human Anatomy and Histology, University of Bari Medical School, National Cancer Institute "Giovanni Paolo II", Bari, Italy*
[d] *Centre for Molecular and Translational Oncology (COMT), University of Parma, Parma, Italy*

Received: June 16, 2014; Accepted: January 20, 2015

Abstract

Gynaecological leiomyosarcoma (gLMS) represent a heterogeneous group of soft tissue sarcoma, characterized by rare incidence, high aggressiveness and propensity to infiltrate secondary organs, poor prognosis and lethality, because of the lack of biological mechanisms that underlying their progression and effective pharmaceutical treatments. This study was focused on some of the aspects of progression and dissemination of a subtype of gLMS namely vulvar LMS (vLMS). We therefore used a vulvar LMS-derived cell line namely SK-LMS-1, coupled with *in vitro* and *in vivo* assays. We observed that SK-LMS-1 cells have a strong invasive capacity *in vitro*, through the activity of matrix metalloproteinases 2 and 9, while *in vivo* these cells induce a strong angiogenic response and disseminate to the chick embryo liver. Therefore, we postulate that metalloproteinases are involved in the spreading behaviour of SK-LMS-1. Further investigations are necessary to better understand the molecular and cellular machinery involved in the progression of this malignancy.

Keywords: tumour progression • human vulvar leiomyosarcoma • matrix metalloproteinases • angiogenesis • chicken CAM

Introduction

Gynaecological leiomyosarcomas (gLMS) represent a heterogeneous group of soft tissue sarcoma [1–3] of mesenchymal origin [1], that although have a rare incidence, present high aggressiveness, and propensity to infiltrate secondary organs [4–10], poor prognosis and lethality because of the lack of effective treatments [11, 12].

While a lot of experimental and clinical studies documented many of the mechanisms involved in the progression of several types of carcinomas [13, 14], by contrast, the molecular and cellular mediators involved in progression and dissemination of STSs, and more in detail, in gLMS, remain mostly unknown.

The cleavage of extracellular matrix (ECM) proteins is a pivotal phenomenon in tumour spreading and during metastatic cascade [15, 16], facilitating movement of malignant cells and angiogenesis.

In this context, matrix metalloproteinases (MMPs), a group of Zn-dependent enzymes comprising more than 20 members, seem to play a major role [16, 17].

In this study, we performed combined *in vitro* and *in vivo* assays on a vulvar LMS cell line, namely SK-LMS-1, to clarify some aspects of progression and dissemination of this lethal disease.

Materials and methods

Cell line and conditioned medium

Human vulvar SK-LMS-1 cells were purchased from ATCC (Manassas, VA, USA) and cultured in DMEM (Lonza, Cologne GmbH, Germany) supplemented with 10% foetal bovine serum (FBS; Sigma-Aldrich,

[#]These authors equally contributed to this work.
*Correspondence to: Domenica MANGIERI
E-mail: domenica.mangieri@unipr.it

doi: 10.1111/jcmm.12565

Milan, Italy), 2 mM L-Glutamine (Lonza) and antibiotics (100 U of penicillin G and 100 μg/ml of streptomycin sulfate, Lonza). Cell cultures were maintained at 37°C under a humidified 5% CO_2 atmosphere. Conditioned medium (CM) was prepared from confluent SK-LMS-1 cells culture maintained in DMEM without serum. After 72 hrs the CM was collected, centrifuged at 500 × g for 5 min. at 4°C and filtered through a 0.22 μm pore size membrane.

Invasion assay

The invasion potential of SK-LMS-1 cells was assessed by using the EnzChek Gelatinase Kit (Life Technologies, Milan, Italy), based on a DQ™ Gelatin fluorescein isothiocyanate. Under the proteolytic action of MMPs, fluorescent peptides were released. The assay was employed as follows: a mixture containing 50 μl of growth factor reduced (GFR) Matrigel (BD Biosciences, Milan, Italy) and 100 μg/ml of DQ™ Gelatin was added to each well of a 96-well plates and allowed to solidify at 37°C for 1 hr. Each well was filled with 1.5×10^4 SK-LMS-1 cells suspended in 100 μl DMEM supplemented with 10% FBS, in presence or absence of metalloproteases (MMPs) inhibitor 1,10-Phenanthroline (1 mM final concentration; Life Technologies). Cultures were monitored at 3 and 72 hrs under an inverted microscope equipped with a CCD camera (DS-Fi2; Nikon Instruments, Florence, Italy) at 100× magnification, and the fluorescence emitted by proteolysis of the FITC-conjugated gelatin was measured using a microplate fluorescence reader (SPECTRAFluor; Tecan Group, Männedorf, Switzerland) at a wavelength range of 485/535 nm. Results were plotted and expressed as arbitrary units of fluorescence (FU).

Matrigel evasion assay

2×10^4 SK-LMS-1 resuspended in 2 μl of serum-free DMEM were included in a 2 μl mixture of GFR-Matrigel (BD Biosciences) and the above described DQ™ Gelatin (100 μg/ml; Life Technologies). Each drop was seeded at the centre of each well of a 24-well plate and allowed to solidify al 37°C for 30 min. Wells were then filled with DMEM containing 10% FBS in presence or absence of metalloproteases (MMPs) inhibitor 1,10-Phenanthroline (1 mM final concentration; Life Technologies). Cells were monitored daily and images were captured with an inverted fluorescence microscope equipped with a CCD camera (DS-Qi1Mc; Nikon Instruments) at 40× and 200× magnification. Fluorescence emitted by peptides after proteolysis of gelatin was measured using a microplate fluorescence reader (SPECTRAFluor; Tecan Group) at 485/535 nm. Results were plotted and expressed as arbitrary units of fluorescence (FU). Supernatant from each well was collected to prepare CM, as described previously.

MMPs western blotting analysis

SK-LMS-1 cells inside the Matrigel drops from the evasion assay were collected for Western blot analysis. After 3 and 72 hrs, cells from eight drops were recovered from Matrigel using Recovery Solution (BD Biosciences) according to manufacturer's instruction and lysed with radioimmunoprecipitation buffer containing a cocktail of protease inhibitors (Roche, Milan, Italy). The protein content was quantified using Bradford reagent (Sigma-Aldrich), and 40 μg aliquots were mixed in Laemmli buffer, boiled at 90°C for 5 min. and loaded on each lane of a precast 4–15% gradient SDS-polyacrylamide gel (Bio-Rad, Segrate (Mi), Italy). After electroforetic resolution, proteins were transferred to a nitrocellulose membrane by a Trans-Blot Turbo Blotting System (BioRad). Blots were then blocked for 1 hr with TBS containing 0.1% Tween-20 (TBST) and 5% skim milk and incubated for 2 hrs with the following primary antibodies, diluted in TBST: 4 μg/ml rabbit polyclonal anti-MMP-2 (ab37150; Abcam, Cambridge, UK); 1:250 mouse monoclonal anti-MMP-9 (ab119906, clone 5G3; Abcam); 1:400 rabbit polyclonal anti-β-actin (A2066; Sigma-Aldrich). Membranes were incubated with specific horseradish peroxidase-conjugated secondary antibodies (1:400; Sigma-Aldrich) at room temperature for 1 hr. Immunocomplexes were visualized using WestarECL system (Cyanagen, Bologna, Italy) and exposure to radiograph film (Kodak, Rochester, NY, USA).

Angiogenic factors array

Expression of angiogenesis-related proteins contained in the CM derived from the drops was determined with the Human Angiogenesis Array Kit (R&D Systems Ltd., Abingdon, UK), consisting of 55 antibodies against angiogenesis-related proteins spotted on a nitrocellulose membrane. The array was performed following the manufacturer's instructions using 1 ml of CM or cell supernatant from SK-LMS-1 drops. The data from developed X-ray film were digitalized with a transmission-mode scanner and quantified using ImageJ analysis software (http://rsb-web.nih.gov/ij/). The positive controls were spot couples distributed in the upper left, upper right, and lower left corners of each array kit, whereas the negative controls spot couples were located in the lower right corner of each membrane. The averaged background signal was subtracted and the arrays were calibrated based on the signal strength of the positive controls. The average signal (pixel density) of the pair of duplicated spots representing each angiogenesis protein was determined as above and the corresponding signals on different arrays were compared.

CAM assay

Fertilized chicken eggs were incubated at 37°C and constant humidity. On day 3 of incubation, a window was opened in the eggs shell after removal of 2–3 ml of albumen so as to detach the developing CAM from the shell, then eggs were sealed with tape and returned to the incubator. On day 8, 5×10^5 cancer cells were labelled with lipophilic dye FastDiO (Life Technologies) and resuspended in 10 μl of GFR-Matrigel (BD Biosciences); 20 μl of total suspension were carefully placed on top of each CAM and eggs were returned to the incubator. Vascular structures were visualized using a stereomicroscope equipped with a CCD camera (DS-Fi2; Nikon Instruments) and pictures were taken daily for 7 days, both in bright field and fluorescence, until embryos were sacrificed on day 15. Blood vessels entering the implant on the focal plane of the CAM were counted at a magnification of 50× using Nikon NIS software. After sacrifice, using a stereomicroscope, samples of CAM (in correspondence of tumour cell graft and as far as possible from the tumour implant) and embryo organs were dissected. Samples were processed for molecular analysis and immunohistochemistry as described below.

Journal of Cellular and Molecular Medicine published by John Wiley & Sons Ltd and Foundation for Cellular and Molecular Medicine.

Table 1 Primers for human angiogenic factors analysis

Factor	Forward primer (5′–3′)	Reverse primer (5′–3′)	Ta (°C)
FGF-2	CCGTTACCTGGCTATGAAG	ACTGCCCAGTTCGTTTCAG	65
MMP-2	AATACCATCGAGACCATGC	GTCCAGATCAGGTGTGTAGC	65
MMP-9	CCTTTGGACACGCACG	CCTAGTCCTCAGGGCACT	61
VEGFA	AGAGCAAGACAAGAAAATCCCT	ATCTGGTTCCCGAAACCCT	61
RPL-27	TGGGAAGGTGGTGCTTGT	GGGGTAGCGGTGAATTCC	54

Table 2 Primers for chicken angiogenic factors analysis

Factor	Forward primer (5′–3′)	Reverse primer (5′–3′)	Ta (°C)
VEGFA	GAAAGGCCGGTACAAACCA	TTAACTCAAGCTGCCTCGAC	56
β-Actin	CCGCAAATGCTTCTAAACCG	AAAGCCATGCCAATCTCGTC	56

Immunohistochemistry

Samples from CAM and embryo organs were fixed in 4% paraformaldehyde, dehydrated in a graded ethanol series, cleared in xylene and embedded in paraffin. CAM blocks were cut into 8 μm thick sections, whereas embryo internal organs were cut into 6 μm thick sections; all were subjected to immunohistochemical analysis. To discover human cancer cell infiltrates, we used 1 mg/ml rabbit polyclonal anti-human NuMA (Nuclear mitotic apparatus protein; ab97585; Abcam) and 1:50 rabbit monoclonal anti-human mitochondria (MA5-12017, clone MTC02; Thermo Scientific, Waltham, MA, USA) antibodies, diluted in PBS. After 12 hrs of incubation at 4°C, immunodetection was performed by using diaminobenzidine DAKO kit (DAKO, Cernusco sul Naviglio, Milan, Italy) according to the manufacturer's protocol. Sections were then washed in distilled water, counterstained with haematoxylin (Polysciences, Warrington, PA, USA) and mounted using buffered glycerine. Specific pre-immune serum replacing the primary antibodies served as a negative control. Sections were examined with a Nikon light microscope as described above.

Alu sequences detection assay

Frozen chick embryo tissues were subjected to DNA extraction using DNeasy Blood and Tissue kit (Qiagen, Milan, Italy) according to the manufacturer's protocol. PCR was performed on 100 ng of purified DNA using GoTaq® Flexi DNA Polymerase (Promega, Milan, Italy) and human *Alu* specific primers (forward: 5′-ACGCCTGTAATCCCAGCACTT-3′; reverse: 5′-TCGCCCAGGCTGGAGTGCA-3′) [18] at an annealing temperature (Ta) of 60°C. After 20 cycles, the amplification product (244 bp) was electrophoresed on 1.8% agarose gel in Tris-Acetate-EDTA buffer. Images of gels were collected with a gel documentation system (AlphaImager, Alpha Innotech, San Jose, CA, USA).

Real-time PCR for angiogenic factors

Angiogenic factor transcripts from human tumour cells were detected *via* RT-PCR. Total RNA was extracted from tumour-treated CAM/chick embryo tissues at 4 and 7 days after SK-LMS-1 inoculum using Trizol Reagent (Life Technologies) following the manufacturer's instructions. For chicken targets, RNA was reverse-transcribed using the QuantiTect Reverse Transcription Kit (Qiagen) and then amplified using the *Power* SYBR® Green PCR Master Mix (Life Technologies). For better sensitivity, human targets were retrotranscribed and amplified in a single step using *Power* SYBR® Green RNA-to-CT™ 1-Step Kit (Life Technologies), according to the manufacturer's protocol. Both reactions were carried out in a DNA Engine Opticon System (MJ Research Incorporeted, St. Bruno, QC, Canada) with the primer pairs (IDT DNA, Leuven, Belgium) described in Tables 1 and 2, using human RPL27 and chicken β-actin as endogenous controls. Each sample was run in triplicate and analysed with the $2^{-\Delta\Delta Ct}$ method.

Statistical analysis

All experiments were performed in triplicate, and data were expressed as mean ± S.D. The statistical correlation between groups was analysed by Student's *t*-test, where $P < 0.05$ was considered significant.

Results

Invasive propensity of SK-LMS-1 requires the production and activation of MMPs

To assess the invasive ability of SK-LMS-1 and to verify if MMPs are implicated in this phenomenon we performed a series of complementary invasion/evasion experiments. During invasion assay (Fig. 1), in standard culture conditions, we observed that 3 hrs after seeding in absence of MMPs inhibitor, SK-LMS-1 cells were able to invade the surrounding scaffold, forming well organized tubular-like structures (Fig. 1A), by contrast, in presence of MMPs inhibitor, cells were incapable to form a network (Fig. 1B). After 72 hrs of culture, the tumour cells arranged in discrete aggregates with many branches, invadopo-

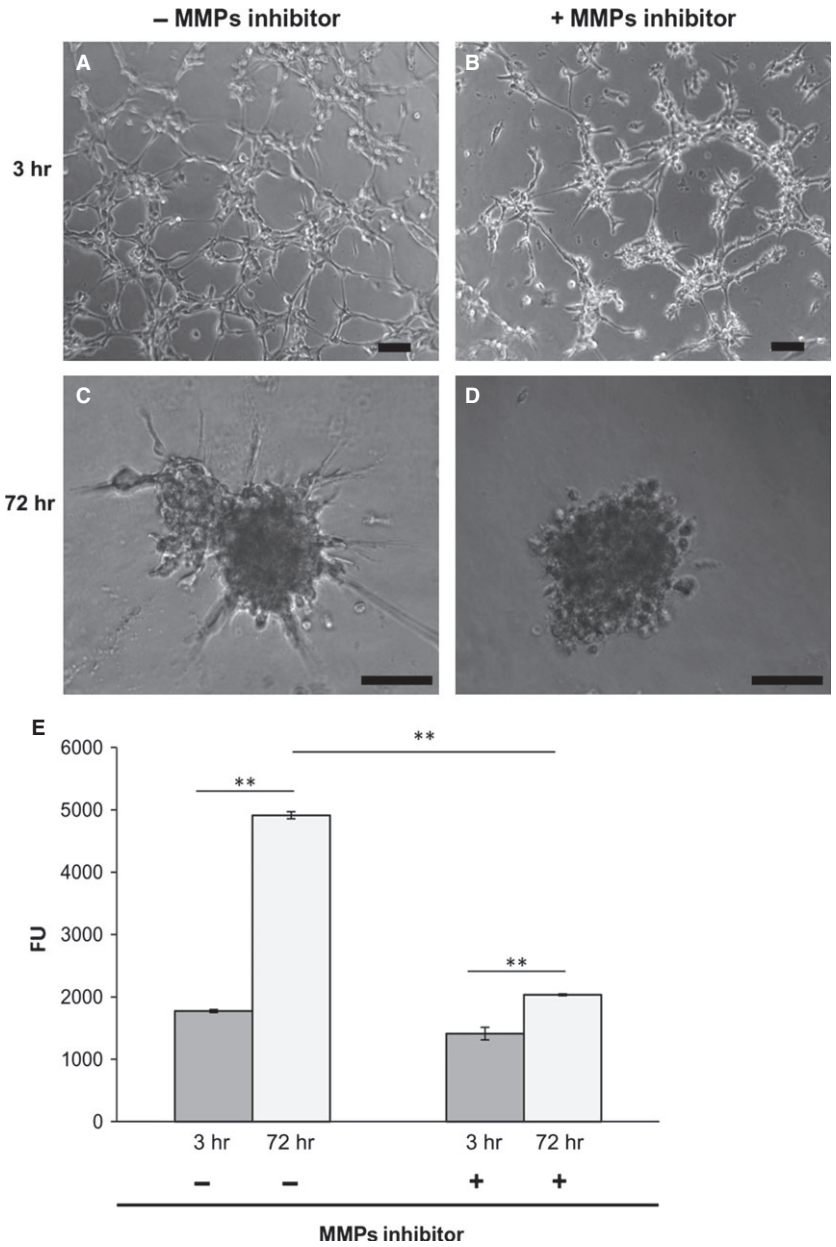

Fig. 1 Matrigel invasion assay. (**A**–**D**) Phase contrast images of cells on Matrigel layer at indicated time-points; scale bar: 100 μm. (**E**) Endogenous collagenases activity indirectly measured by fluorescence emitted by DQ™ Gelatin degradation at indicated time-points. Data represent mean of three independent experiments ± S.D. $^{**}P < 0.01$.

dia-like protrusions penetrating the matrix (Fig. 1C) suggesting a clear invasive propensity of the SK-LMS-1. By contrast, adding 1,10-Phenantroline, cells aggregated in rounded, non-invading clusters (Fig. 1D). Quantitatively, as shown in Figure 1E, after 72 hrs of culture, the MMPs activity of SK-LMS-1 was significantly higher in culture without MMPs inhibitor compared to the control (FU = 4093 ± 56 *versus* FU = 1774 ± 25; $P < 0.001$). In the evasion assay (Fig. 2), we found that the cancer cells after 3 and 72 hrs of culture with medium alone already arranged in well organized invadopodia-like structures (Fig. 2A and C) when compared with SK-LMS-1 embedded in presence of MMPs inhibitor (Fig. 2B and D). Proteolytic activity of MMPs was documented by fluorescence emission in absence (Fig. 2E, upper panel) or presence (Fig. 2E, lower panel) of MMPs inhibitor. The activity in terms of Fluorescence Units was plotted in Figure 2F (FU = 177.5 ± 21 *versus* FU = 86 ± 6; $P < 0.05$). To asses which MMPs were involved, we performed a Western blot analysis on cell lysates derived from drops, and results indicated that MMP-2 and MMP-9 were expressed. In particular, MMP-9 was expressed early, while the expression of MMP-2 arose 72 hrs after seeding (Fig. 2G). When the samples were treated with the MMPs inhibitor a reduction in MMPs levels was detectable (Fig. 2G).

Journal of Cellular and Molecular Medicine published by John Wiley & Sons Ltd and Foundation for Cellular and Molecular Medicine.

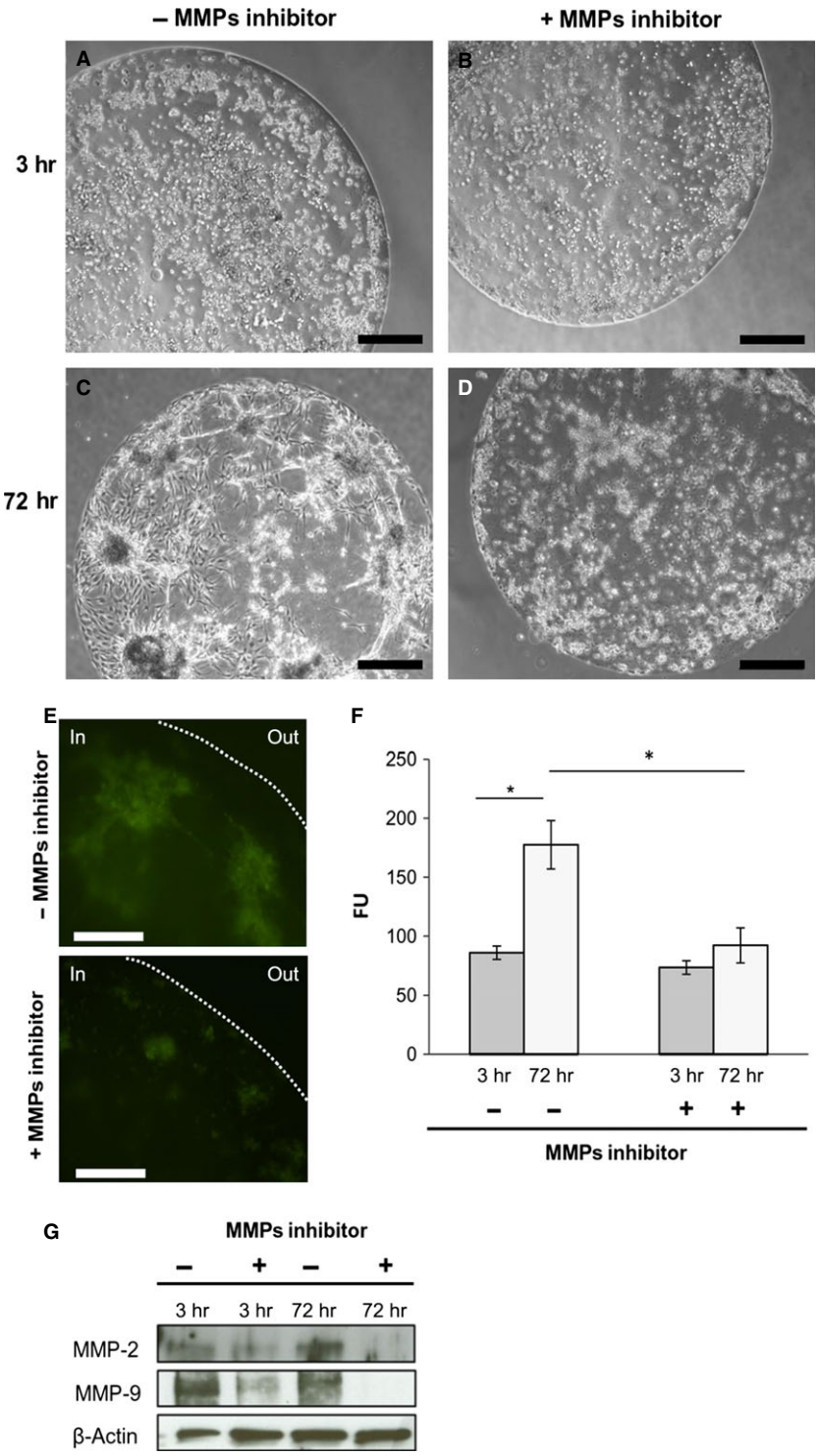

Fig. 2 Matrigel drops evasion assay. (**A**–**D**) Phase contrast images of drops at indicated time-points; scale bar: 500 μm. (**E**) Fluorescent images of cells in Matrigel drops 72 hrs after seeding in absence or presence of MMPs inhibitor 1,10-Phenantroline. The dotted line indicates the border of drop; scale bar: 100 μm. (**F**) Measure of endogenous collagenases activity. Fluorescence was emitted by DQ™ Gelatin degradation at indicated time-points. Data represent mean of three independent experiments ± S.D. (**G**) Western blot analysis of protein extracted from drops 3 and 72 hrs after seeding. $^{**}P < 0.01$.

To ascertain whether the evasion capacity of SK-LMS-1 was because of the release of pro-invasive/angiogenic molecules, we performed antibody based protein array analysis (Fig. 3A). The analysis was performed on CM obtained both from cancer cells seeded in monolayer (CM) and embedded in drops (drops CM). A significant up-regulation of two pro-invasive factors, endothelin-1 and pentraxin

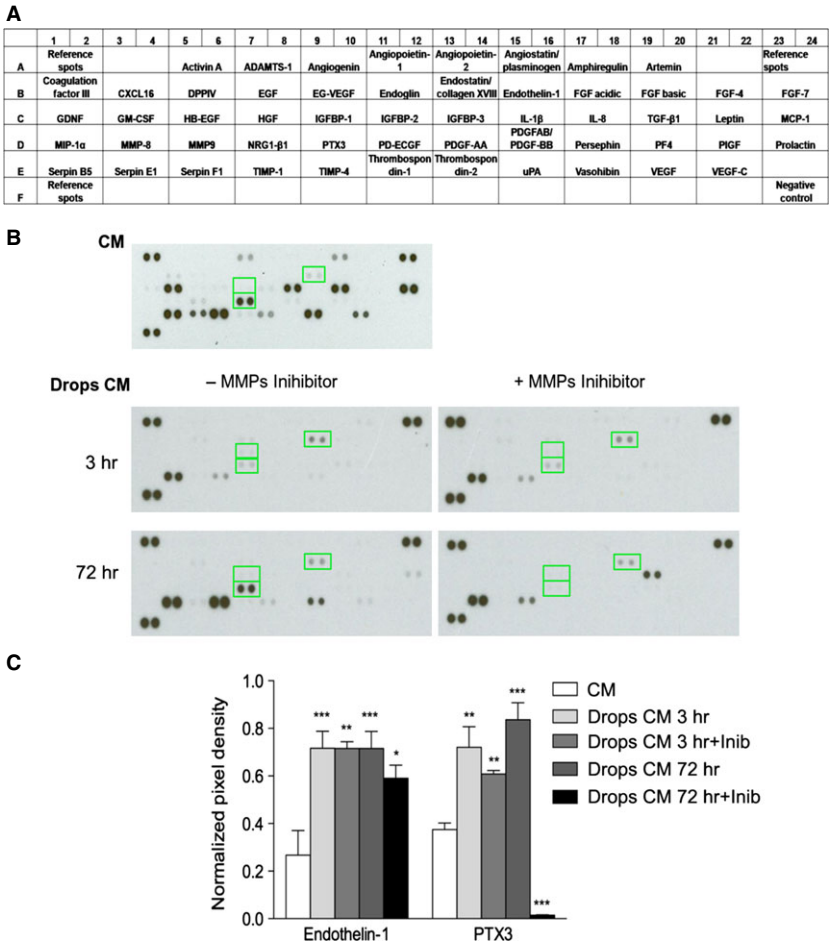

Fig. 3 Assessment of angiogenesis-related proteins. (**A**) Schematic representation of the angiogenic array. (**B**) Relative expression of 55 different angiogenesis-related proteins are determined from CM or Drops CM at 3 and 72 hrs in absence or presence of MMPs inhibitor 1,10-Phenantroline. All proteins are determined in duplicate and based on optical densitometry of the corresponding spots. The up-regulated expression of proteins in CM and in Drops CM are indicated with green squares. (**C**) The expression of proteins was quantified and plotted in the reported histogram. IGFBP1 is expressed only in the Drops CM while Endothelin-1 and PTX3 expression is increased in Drops CM in respect to CM. $^{*}P < 0.05$; $^{**}P < 0.01$; $^{***}P < 0.001$.

3 (PTX3) was observed in drops CM both after 3 and 72 hrs (Fig. 3B, left). Indeed, in drops CM we observed the presence of another pro-invasive protein, insulin-like growth factor binding protein-1 (IGFBP-1; Fig. 3B, left). MMPs inhibitor reduced the expression of these proteins (Fig. 3B, right). The data were quantified and the normalized pixel density was reported in Figure 3C. No expression of MMP-9 was detected in drops CM. This was probably due by the local *in situ* retirement of the gelatinase, degradating the Matrigel embed structure.

In vivo angiogenic and invasive potential

To study SK-LMS-1 behaviour in term of angiogenic potential, spreading aptitude and metastasis formation *in vivo,* we employed a chicken CAM assay. A schematic representation of the model used is reported in Figure 4A. Four days after SK-LMS-1 cells implant, stereoscopic observation documented many neovessels that developed radially towards the tumour implant arranged in a classical 'spoked-wheel' pattern (mean number of blood vessels = 35 ± 4; Fig. 4B). Angiogenic effect was comparable to that induced by FGF-2, a widely recognized angiogenic factor (mean number of blood vessels = 28 ± 5; Fig. 4C). By contrast, only few blood vessels directed towards the implant composed of GFR-Matrigel alone (mean number of blood vessels = 5 ± 1.5; Fig. 4D) were identifiable. The angiogenic response was indeed demonstrated by real time PCR showing an up-regulation of the chicken VEGF expression (Fig. 4E). To further investigate if the angiogenic response might be related to the secretion of pro-angiogenic factors produced by SK-LMS-1 cells implants, we used a one step real time PCR system to detect human VEGF and FGF-2 in the SK-LMS-1 CAM seeding site and distal area (Fig. 5A). We observed that human VEGF is not significantly increased in the seeding site while it is strongly up-regulated after 7 days in the distal area (Fig. 5A, left). Expression of human FGF-2 is increased in the site of SK-LMS-1 cells implant 4 and 7 days after engraftment as compared with control (Fig. 5A, right). Instead, in the distal areas of the implant a weak increase in FGF-2 expression can be observed only after 4 days (Fig. 5A, right). Moreover, we demonstrated that MMP-2 was strongly expressed in the seeding site at 4 and 7 days after implant. Indeed, in the distal area both MMP-2 and MMP-9 were up-regulated 7 days after engraft (Fig. 5B). To explore if SK-

Journal of Cellular and Molecular Medicine published by John Wiley & Sons Ltd and Foundation for Cellular and Molecular Medicine.

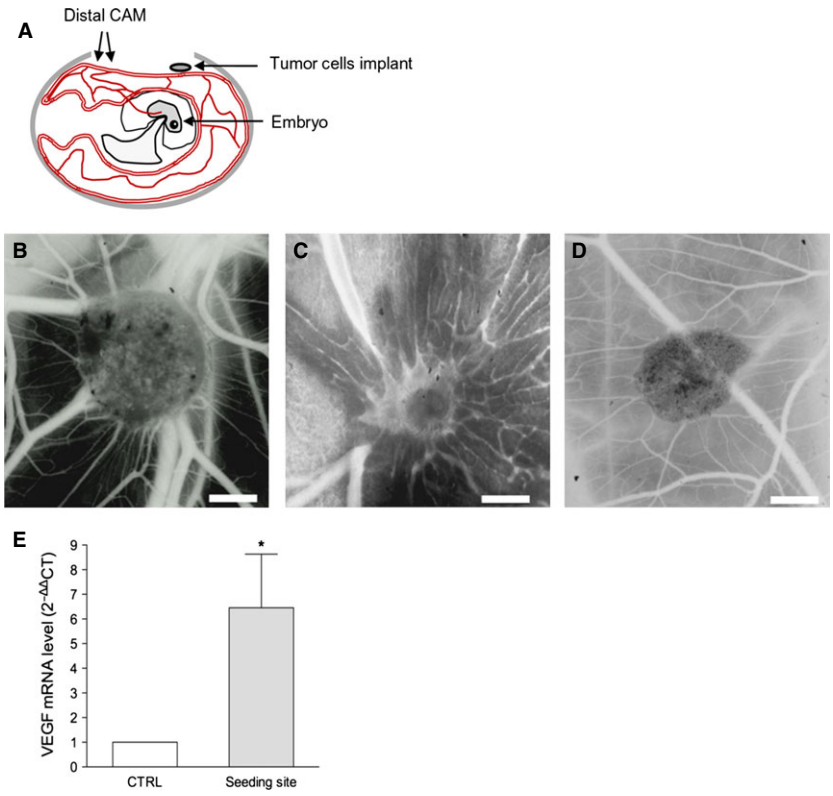

Fig. 4 CAM assay. (**A**) Schematic representation of CAM assay. (**B**) Stereomicroscopic images of SK-LMS-1 embedded in Matrigel implanted on the CAM. After 4 days numerous allantoic vessels formed radially towards the implant. (**C**) 200 ng of human FGF-2 resospended in Matrigel was used as positive control. (**D**) Matrigel alone was used as negative control; scale bar: 1000 μm. (**E**) Quantification of avian VEGF in tumour-treated CAM samples by RT-PCR. $*P < 0.05$.

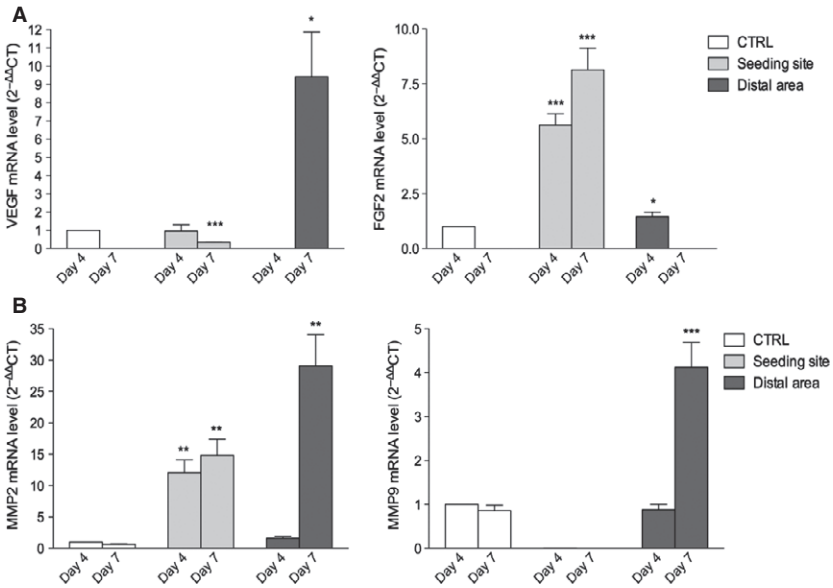

Fig. 5 Molecular analysis of human angiogenic factors in SK-LMS-1 treated CAM by RT-PCR. (**A**) A one step real time PCR system was used to detect the expression of human VEGF (left) and FGF-2 (right) in the SK-LMS-1 CAM seeding site and distal area. (**B**) The same system was used to asset the expression of both human MMP-9 (left) and MMP-2 (right). Histograms represent means and S.D.s from three independent experiments. $*P < 0.05$; $**P < 0.01$; $***P < 0.001$.

LMS-1 cells were able to migrate from the site of implant, we performed human Alu sequences analysis by PCR followed by immunohistochemistry (Fig. 6). Results obtained by amplification of Alu sequences (Fig. 6A) revealed the presence of human genome in CAM in the site of implant, as expected, and in some embryo organs, such as the liver. Microscopic results confirmed infiltrates of human cells detectable not only in the site of implant (Fig. 6B and C) but also in the chicken liver (Fig. 6E and F).

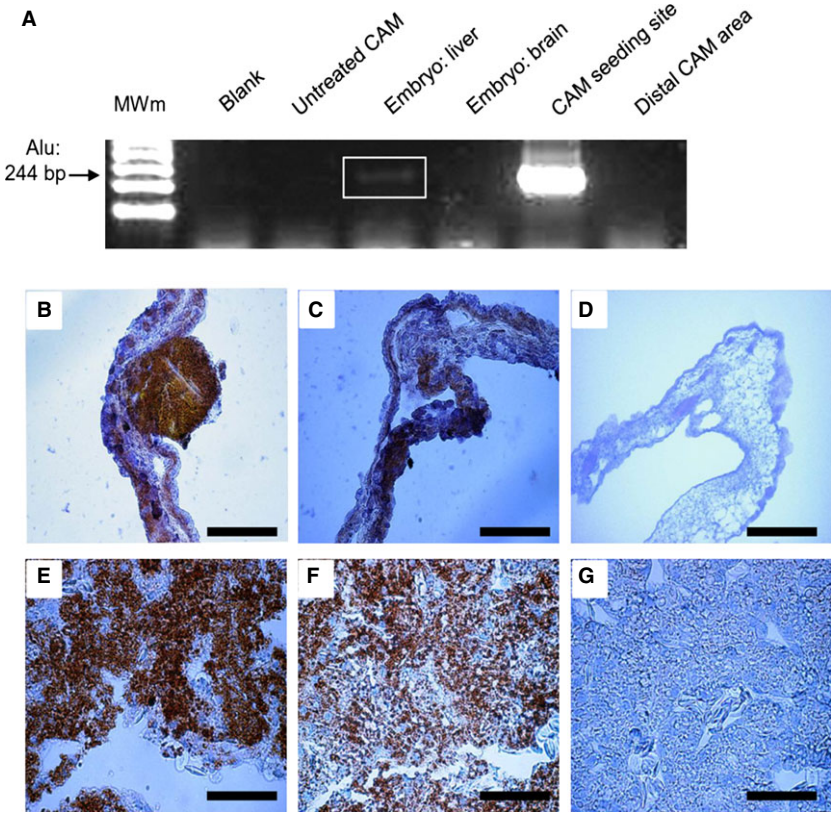

Fig. 6 SK-LMS-1 infiltration on CAM and in chick embryo organs. (**A**) RT-PCR detection of human Alu sequences in different samples of the SK-LMS-1 treated CAM and embryo organs. (**B**–**G**) Immunohistochemical analysis of CAM and embryo liver: slides were stained with anti-human mitochondria (**B** and **E**) and with anti-human NuMA antibodies (**C** and **F**). Negative controls was performed by replacing primary antibodies with specific pre-immune serum (**D** and **G**); scale bar: 50 μm.

Discussion

The molecular mechanisms underlying the progression and metastasis of vLMS are still unknown.

Here, we have identified MMP-2 and MMP-9 as crucial enzymes in modulating the invasive activity of vLMS SK-LMS-1 cell line; we have shown that vLMS progression and angiogenesis are correlated. In addition we observed a propensity of the SK-LMS-1 tumour cells to colonize internal organs, such as liver, when the cells were implanted on the CAM surface.

In this study, we found that in invasion/migration assays, in standard culture conditions, SK-LMS-1 cells were able to penetrate the gelatinous scaffold in which they were seeded; by contrast, in the presence of MMPs inhibitor 1,10-Phenanthroline, this capacity is significantly reduced. 1,10-Phenatroline is a MMPs inhibitor because of its ability to chelate metals (Zn^{2+}, Ca^{2+}, Cu^{2+}) [19, 20]. MMPs are frequently implicated in ECM degradation during tumour progression, promoting angiogenesis [15–17], spreading and metastasis [15–17, 21, 22]. Since their activity contributes to the evolution of many tumours [22–26], MMPs have been considered as potential therapeutic targets in cancer treatment [27], and some specific inhibitors have been tested in clinical trials [27, 28].

By analysing the molecular composition of CM derived from SK-LMS-1 drops after the evasion assay, we have identified different factors related to the expression and activation of MMPs. At least three molecules were up-regulated: Endothelin-1, PTX3 and IGFBP-1. Endothelin-1 is over-expressed in a number of cancers, influencing different aspects of tumour progression [29], and it induces expression of several MMPs [30]. PTX3 has recently been found to affect cell spreading and metastasis formation in breast cancer [31] and other tumours [32]. We hypothesize that both Endothelin-1 and PTX3 could influence the expression of MMPs in SK-LMS-1 cells *in vitro*. IGFBP-1 plays a role in promoting the survival and growth of some tumour types [33, 34]; however, the underlying mechanisms have not been established yet. It is unclear whether the presence of IGFBP-1 in the SK-LMS-1 CM is directly related to MMPs activity.

The use of CAM as a host for SK-LMS-1 cells allowed us to observe two concomitant events: the angiogenic response and the metastatic diffusion of cancer cells, a phenomenon already documented for other tumour types [35–38]. Regarding the angiogenic response, we hypothesize that it is mainly under the control of both human and chick VEGF. VEGF is one of the most potent angiogenic factors [39]. Since the CAM is a vascularized extraembryonal annex, continuously undergoing blood vessel formation and remodelling is under the control of endogenous angiogenic factors, including VEGF and FGF-2 [39, 40]. In our experimental condition, SK-LMS-1 cells might enable their own growth and spreading by both expressing pro-angiogenic factors and modulating the expression of chick angiogenic factors.

Journal of Cellular and Molecular Medicine published by John Wiley & Sons Ltd and Foundation for Cellular and Molecular Medicine.

The propensity of SK-LMS-1 cells to spread to distal portions of the CAM mesenchyme as well as to the embryo liver is consistent with the high propensity of vLMS to infiltrate secondary organs [4–10].

Taken together, our results suggest that MMP-2 and MMP-9 are pivotal elements in modulating the invasive activity of vulvar LMS-derived cells both *in vitro* and *in vivo*, and that the chick CAM provides an appropriate microenvironment for the study of human vLMS progression. Further studies are required to elucidate the involvement of the MMPs/angiogenesis axis in the spreading of vLMS and improve our knowledge of potential molecular targets for cancer treatment.

Acknowledgements

This study was supported by a grant from Italian Ministry of Health (project no. GR-2009-1574637 to DM). We are grateful to Prof. Enrico Maria Silini, who thoroughly endorsed our project. We also wish to thank Dr. Nicoletta Campanini and Prof. Paolo Govoni for their valuable technical assistance.

Conflicts of interest

The authors confirm that there are no conflicts of interest.

Author contribution

CA and LR designed and performed experiments, analysed data and wrote the paper; DR analysed data and supervised the manuscript; SC assisted manuscript preparation; AD'A performed immunohistochemistry assays; RP supervised the manuscript; DM wrote the manuscript and directed the project.

References

1. **Amankwah EK, Conley AP, Reed DR.** Epidemiology and therapies for metastatic sarcoma. *Clin Epidemiol*. 2013; 5: 147–62.
2. **D'Angelo E, Prat J.** Uterine sarcomas: a review. *Gynecol Oncol*. 2010; 116: 131–9.
3. **Novetsky AK, Powell MA.** Management of sarcomas of the uterus. *Curr Opin Oncol*. 2013; 25: 546–52.
4. **Yamada S, Yamada SM, Nakaguchi H, *et al.*** A case of multiple brain metastases of uterine leiomyosarcoma with a literature review. *Surg Oncol*. 2011; 20: e127–31.
5. **Gurram MK, Pulivarthi S, McGary CT, *et al.*** Brain and multiorgan metastases from uterine leiomyosarcoma. *Tumori*. 2014; 100: e8–13.
6. **Tan LA, Kasliwal MK, Nag S, *et al.*** A rare intramedullary spinal cord metastasis from uterine leiomyosarcoma. *J Clin Neurosci*. 2013; 20: 1309–12.
7. **Nguyen SKA, Wong F.** Right atrial metastasis of uterine leiomyosarcoma causing obstructive shock. *Curr Oncol*. 2012; 19: e292–4.
8. **Corcoran S, Hogan AM, Nemeth T, *et al.*** Isolated cutaneous metastasis of uterine leiomyosarcoma: case report and review of Literature. *Diagn Pathol*. 2012; 7: 85.
9. **Tunio MA, AlAsiri M, Saleh RM, *et al.*** Obstructive small bowel metastasis from uterine leiomyosarcoma: a case report. *Case Rep Obstet Gynecol*. 2014; 2014: 1–5.
10. **Alonso Gómez J, Arjona Sánchez Á, Martínez Cecilia D, *et al.*** Uterine leiomyosarcoma metastasis to the pancreas: report of a case and review of the literature. *J Gastrointest Cancer*. 2012; 43: 361–3.
11. **Sutton G.** Uterine sarcomas 2013 - State of the Science. *Gynecol Oncol*. 2013; 130: 3–5.
12. **Hensley ML, Wathen JK, Maki RG, *et al.*** Adjuvant therapy for high-grade, uterus-limited leiomyosarcoma - results of a phase 2 trial (SARC 005). *Cancer*. 2013; 19: 1555–61.
13. **Hanahan D, Weinberg RA.** Hallmarks of cancer: the next generation. *Cell*. 2011; 144: 646–74.
14. **Dvorak HF, Weaver VM, Tlsty TD, *et al.*** Tumor microenvironment and progression. *J Surg Oncol*. 2011; 103: 468–74.
15. **Deryugina EI, Quigley JP.** Matrix metalloproteinases and tumor metastasis. *Cancer Metastasis Rev*. 2006; 25: 9–34.
16. **Sato T, Sakai T, Noguchi Y, *et al.*** Tumor-stromal cell contact promotes invasion of human uterine cervical carcinoma cells by augmenting the expression and activation of stromal matrix metalloproteinases. *Gynecol Oncol*. 2004; 92: 47–6.
17. **Kessenbrock K, Plaks V, Werb Z.** Matrix metalloproteinases: regulators of the tumor microenvironment. *Cell*. 2010; 141: 52–7.
18. **Mira E, Lacalle RA, Gómez-Moutón C, *et al.*** Quantitative determination of tumor cell intravasation in a real-time polymerase chain reaction-based assay. *Clin Exp Metastasis*. 2002; 19: 313–8.
19. **Almendro V, Ametller E, Garcìa-Recio S, *et al.*** The role of MMP7 and its cross-talk with the FAS/FASL system during the acquisition of chemoresistance to oxaliplatin. *PLoS ONE*. 2009; 4: e4728.
20. **Mezyk-Kope R, Bzowska M, Stalinska K, *et al.*** Identification of ADAM10 as a major TNF sheddase in ADAM17-deficient fibroblasts. *Cytokine*. 2009; 46: 309–15.
21. **Bergers G, Brekken R, McMahon G, *et al.*** Matrix metalloproteinase-9 triggers the angiogenic switch during carcinogenesis. *Nat Cell Biol*. 2000; 2: 737–44.
22. **Giannelli G, Falk-Marzillier J, Schiraldi O, *et al.*** Induction of cell migration by matrix metalloprotease-2 cleavage of laminin-5. *Science*. 1997; 277: 225–8.
23. **Fernandes T, De Angelo-Andrade LA, Morais SS, *et al.*** Stromal cells play a role in cervical cancer progression mediated by MMP-2 protein. *Eur J Gynaecol Oncol*. 2008; 29: 341–4.
24. **Daniele A, Zito AF, Giannelli G, *et al.*** Expression of metalloproteinases MMP-2 and MMP-9 in sentinel lymph node and serum of patients with metastatic and non-metastatic breast cancer. *Anticancer Res*. 2010; 30: 3521–7.
25. **Libra M, Scalisi A, Vella N, *et al.*** Uterine cervical carcinoma: role of matrix metalloproteinases. *Int J Oncol*. 2009; 34: 897–903.
26. **Wang W, Shao R, Wu Q, *et al.*** Targeting gelatinases with a near-infrared fluorescent cyclic His-Try-Gly-Phe peptide. *Mol Imaging Biol*. 2009; 11: 424–33.
27. **Brown PD.** *Ongoing trials with matrix metalloproteinase inhibitors Expert Opin Investig Drugs*. 2000; 9: 2167–77.
28. **Hidalgo M, Eckhardt SG.** Development of matrix metalloproteinase inhibitors in cancer therapy. *J Natl Cancer Inst*. 2001; 93: 178–93.
29. **Rosanò L, Spinella F, Bagnato A.** Endothelin 1 in cancer: biological implications

and therapeutic opportunities. *Nat Rev Cancer*. 2013; 13: 637–51.

30. **Felx M, Guyot MC, Isler M, *et al.*** Endothelin-1 (ET-1) promotes MMP-2 and MMP-9 induction involving the transcription factor NF-kappaB in human osteosarcoma. *Clin Sci*. 2006; 110: 645–54.
31. **Choi B, Lee EJ, Song DH, *et al.*** Elevated Pentraxin 3 in bone metastatic breast cancer is correlated with osteolytic function. *Oncotarget*. 2014; 5: 481–92.
32. **Kondo S, Ueno H, Hosoi H, *et al.*** Clinical impact of pentraxin family expression on prognosis of pancreatic carcinoma. *Br J Cancer*. 2013; 109: 739–46.
33. **Fürstenberger G, Senn HJ.** Insulin-like growth factors and cancer. *Lancet Oncol*. 2002; 3: 298–302.
34. **Zhang P, Suidasari S, Hasegawa T, *et al.*** High concentrations of pyridoxal stimulate the expression of IGFBP1 in HepG2 cells through upregulation of the ERK/c-Jun pathway. *Mol Med Rep*. 2013; 8: 973–8.
35. **Ribatti D, Nico B, Vacca A, *et al.*** Chorioallantoic membrane capillary bed: a useful target for studying angiogenesis and anti-angiogenesis *in vivo*. *Anat Rec*. 2001; 264: 317–24.
36. **Ribatti D.** Chicken chorioallantoic membrane angiogenesis model. *Methods Mol Biol*. 2012; 843: 47–57.
37. **Mangieri D, Nico B, Coluccia AML, *et al.*** An alternative *in vivo* system for testing angiogenic potential of human neuroblastoma cells. *Cancer Lett*. 2009; 277: 199–204.
38. **Folkman J.** Role of angiogenesis in tumor growth and metastasis. *Semin Oncol*. 2002; 29: 15–8.
39. **Ferrara N.** Role of vascular endothelial growth factor in regulation of physiological angiogenesis. *Am J Physiol Cell Physiol*. 2001; 280: C1358–66.
40. **Ribatti D, Presta M.** The role of fibroblast growth factor-2 in the vascularization of the chick embryo chorioallantoic membrane. *J Cell Mol Med*. 2002; 6: 439–46.

Part II

Introduction

The pericyte

In vertebrates, vessels are composed of two major cell types, endothelial cells and mural cells. Mural cells associated to capillaries and venules are identified as specific cells first described in the second half of 19th century by Rouget as "adventitial cells"[40] and named in 1923 "pericytes" by Zimmermann[41] (Figure 3). Pericytes are scattered along the endothelial lining of microvessels, partially enveloping ECs and co-producing and sharing with them a basement membrane[18].

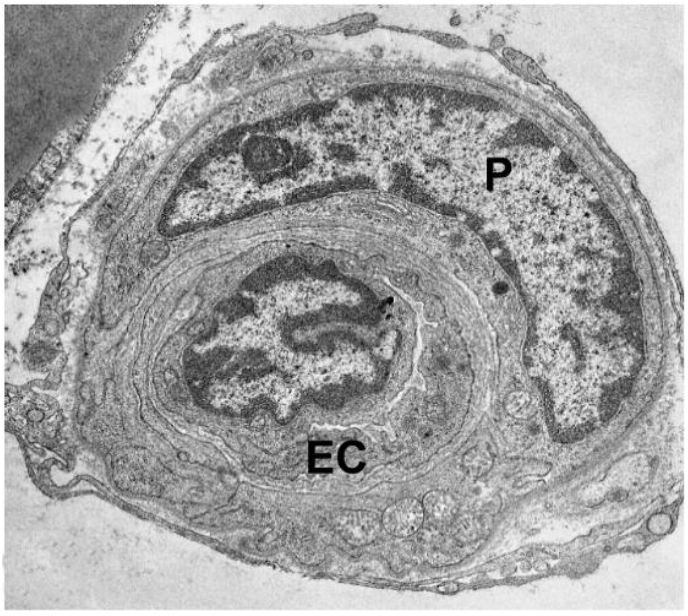

Figure 3. A pericyte (P) embracing an endothelial cell (EC) of a microvessel. Electron microscopy of an ultrathin section. Modified from Diaz-Flores et al. (42).

Notwithstanding the existence of these cells is well established, less is still known about pericytes. Currently, a mature pericyte is defined as a highly branched cell, embedded within the vascular basement membrane and incompletely enveloping the endothelial cells of the microvessels[42]. This definition may lead to think to pericyte as a static cell, which only task is to structurally support the vascular wall. However, it is even more evident that pericytes are dynamic cells, involved in various processes, both physiological and pathological[18,42].

Pericytes markers

Despite the progresses in visualizing techniques, morphology alone it is not sufficient for distinguishing pericytes from the heterogeneous cellular population that presents perivascular location. Widely accepted pericytes markers are α-SMA, NG2 and PDGFR-β[43–47]. Other markers, in support of the more known listed before, are also: CD10, CD44, CD73, CD90, CD94, CD105, CD106, CD146, CD184, , CD147, BP-1, Desmin[43–46]. However, these markers are not expressed merely by pericytes. The perivascular niche includes other cells, which express some of the same markers as pericytes do[18,48]. Moreover, as Dìaz-Flores and co-workers highlighted, these commonly used markers show a dynamic expression, resulting from different in vivo conditions (species of origin, localization, stages of vessels) and also in in vitro culturing. Until now, the lacking of a pan-pericyte marker has leave an open question about how unequivocally identify a pericyte[18].

Pericytes in health and disease

Since their discovery, pericytes were addressed as key regulators of blood pressure, due to the presence of contractile actin filaments in their cytoplasm[49]. These cells are also involved in important physiological phenomena, such as the formation of basement membrane[50], the maintenance of blood brain barrier[51], the control of microvessels stability and permeability[52], the formation of new microvessels from pre-existing ones and vascular stabilization[18,42,53,54].

Pericytes in tumour progression and metastasis

Apart from their physiological activities, pericytes are known to be involved in various diseases[55,56], including cancer progression and metastasis[43,46,57–59]. Pericytes of the tumour vasculature differ from their physiological counterpart for many features, including decrease amount of capillaries coverage, abnormal ECM contact and loose association with endothelial cells[46,60] (Figure 4).

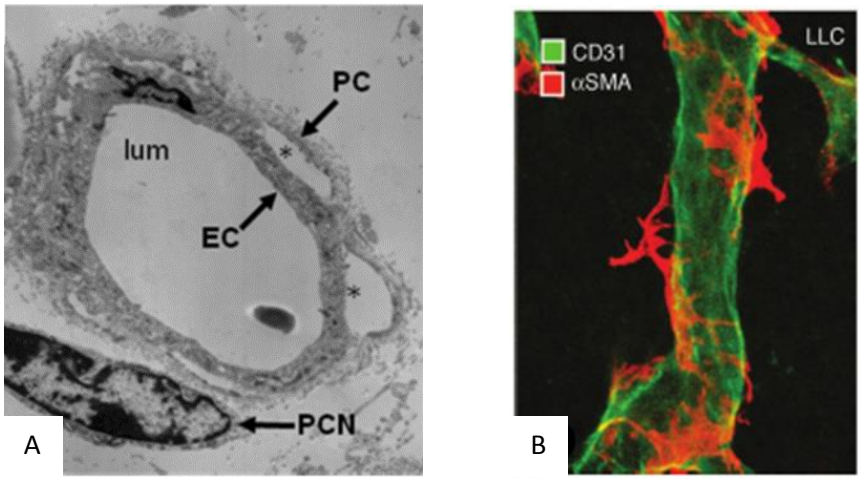

Figure 4. Abnormal endothelial-pericyte associations in tumours. A) Electron micrograph of a pericyte dissociated from endothelium in a M1 chloroma tumour. Modified from Barlow et al. (60); B) Confocal image of pericytes around a vessel of a Lewis lung carcinoma. Modified from Morikawa et al. (46).

All these characteristics observed in many tumour vessels may be seen as a co-factor in vessel abnormalities, enhancing their fragility and haemorrhagic propensity[16]. In several experimental models, defects in pericyte coverage result in leaky vessels and correlate with increased haematogenous dissemination of tumour cells to distant organs, independently of the invasive properties of the tumour cells[58,59,61,62]. Consistently, in a case study of colorectal carcinoma patients, reduced pericyte investiture of tumour microvessels has been correlated with a higher frequency of distant metastasis[63]. Morikawa and colleagues, using an insulinoma RIP-Tag2 transgenic mice, were the first to describe a peculiar phenomenon: pericytes partially dissociated from the endothelium extended their processes into the tumour parenchyma[46]. Other researcher have claimed similar observations in various models[64,65]. These observations raise several open questions, even hinting at the possibility that this peculiar interaction may be responsible for an enhanced metastatic capability of tumour cells. It is known that tumours show a propensity to metastasize to specific tissues and several theories have been proposed to explain this tendency, most of them centring on the relation between the origin of the disseminating cancer cells and the nature of the host tissue[66]. Few of these, however, take into account the contribution of the vascular wall and the complex interactions occurring between the surface receptors and adhesion molecules of circulating cancer cells and the microvascular layers[6,67]. Pericytes have been implicated in leukocyte adhesion and infiltration, helping to form a pro-inflammatory environment favourable to angiogenesis and tumour progression[68]. By the same token, tumour-activated mural cells may aid cancer cell extravasation and colonization at the metastatic site by contributing to create a permissive, pro-metastatic environment[62]. Most notably, liver stellate cells, a specialized form of pericytes, seemingly cooperate with tumour cells in the release of growth factors (VEGF, PDGF, HGF, TGFβ) that may

facilitate the establishment of melanoma metastases[69]. Furthermore, melanoma and a few other types of cancer, including breast and lung carcinoma, show a propensity to colonize the brain, forming metastases in close contact with the layer of pre-existing brain microvasculature[70–72]. Invasion and colonization of the target tissue are orchestrated by a series of complex interactions between cancer cells and microvasculature, many of which are still unknown. The fact that some tissues contains a rich and elaborate vascular network, with a high density of pericytes as compared to other tissues, raises challenging questions: may this "vascular niche" facilitate cancer cell extravasation, survival and colonization? May the contact with the pericytes promote metastatic foci formation? In addition, for the cancer cell homing it is possible that pericytes, together with other stromal cells can exert a pro-neoplastic effects on tissue-invading tumour cells. Accordingly, Bababeygy and co-workers using tumour mice experiments, has proposed that a pattern of hematopoietic stem cells may represent a population of committed pericytes within the neovascular tree and may play a role in shaping the angio-architecture in the vascular niche of target tumours[73]. Because of their involvement in all these aspects of tumour progression and dissemination, pericytes are consider new important targets of the anticancer therapy[74,75].

Material and Methods

Cell lines and conditioned medium

Tumour cell lines (A375 melanoma cells; MDA-MB-231 breast cancer cells; HT1080 fibrosarcoma cells) were maintained in DMEM with 1 g/L glucose (Life Technologies), supplemented with 10% FBS (Life Technologies), 2 mM L-glutamine (Lonza) and antibiotics (100U of penicillin G and 100 μg/mL of streptomycin sulfate, Lonza). HBVP (CellScience) were grown in PM (CellScience) supplemented with 2% FBS (CellScience), 1% PGS (CellScience) and 1% antibiotic solution (CellScience). Dishes and flasks were always previously coated with 1% porcine gelatin (Sigma-Aldrich) for at least 15 minutes at 37°C in a cell incubator. Pericytes were cultured until they reached the wanted passage. Pericytes passaged in culture 3-4-5 times are herein referred as "early", while pericytes passaged 8-9-10 time are herein referred as "late" pericytes. Cell cultures were maintained at 37°C under a humidified 5% CO_2 atmosphere.
CM was prepared from confluent cells culture maintained in DMEM without serum. After 72 hours the CM was collected, centrifuged at 500 g for 5 minutes at 4°C and filtered through a 0,22 μm pore size membrane.

Cytofluorimetric analysis

To perform cytofluorimetric analysis, HBVP were washed with PBS, detached with Accutase (GE Healthcare Life Sciences) and resuspended in complete PM. Three hundred thousand cells for each sample were centrifuged 5 minutes at 500 g, then washed with cold wash buffer (PBS containing 1% FBS and 0,1% sodium azide, Sigma-Aldrich) and incubated at 4°C in the dark for 30 minutes with fluorophore-conjugated primary antibodies (Appendix-Table 1, Becton Dickinson). In all the experiments, the corresponding isotype-matched antibodies were used as negative controls (Appendix-Table 2, Exalpha Biologicals). After two washes, cells were acquired on a BD FACSCalibur and analysed with Cell Quest Pro software (Becton Dickinson).

Immunocytochemistry

HBVP at different passages were detached and $2x10^4$ cells were seeded in complete PM on gelatin-coated glass coverslips. After 24 hours, cells were washed two times with PBS, fixed for 20 minutes with 4% PFA, washed three times with PBS (10 minutes each). To identify surface markers, cells were treated with a blocking solution (PBS containing 5% NGS, Life Technologies) for 20 minutes at RT. Cell were incubated with primary antibodies diluted in PBS containing 2% NGS (listed in Appendix-Table 3, all purchased from Abcam) overnight at 4°C in a humidified container. The next day, cells were washed three times with PBS (10 minutes each) and incubated

with the appropriate secondary antibody (listed in Appendix-Table 4, all purchased from Life Technologies) for 1 hour at RT. HBVP were washed three times with PBS (10 minutes each) and one time with distilled water, then coverslips were mounted with Vectashield Mounting Medium with DAPI (Vector Laboratoires). To assess intracellular protein expression, cell membranes were permeabilized with PBS containing 0,1% Triton X100 (Sigma-Aldrich) in for 15 minutes at RT and then processed as above described. Specific preimmune serum replacing the primary antibody was employed as a negative control. Cells were examined under a fluorescence microscope (Axio Observer, Zeiss) equipped with a CCD camera (LSM710, Zeiss) at 600X magnification.

Metabolic labelling of ECM

The extracellular matrix produced by HBVP was visualized through a Staudinger reaction between three azido sugars (GlcNAz, ManNAz and GalNAz, Thermo scientific), added to the cell medium, and a fluorescence-labelled Phosphine (DyLight 550-Phospine, Thermo Scientific). HBVP were detached and $3x10^5$ cells in complete PM were plated in each well of an 8-Well Falcon Culture Slide (BD) plate. Azido sugars were added to the medium of culture at a final concentration of 40 μM each and HBVP were incubated for five days. To visualize the ECM, fluorescence-labelled Phosphine was added at a final concentration of 50 μM, following manufacturer's protocol. HBVP enveloped into the matrix were revealed staining their nuclei. Cells were washed twice with PBS, fixed with 4% PFA (20 minutes, RT) and washed two times with PBS (5 minutes each). Nuclei were stained with 1 μg/ml Hoechst 33258 for 10 minutes at RT. After three washes with PBS (10 minutes each) and one with distilled water, coverslips were mounted using Aqua-Poly/Mount (BioSciences). Slides were visualized with a fluorescence microscope (Axio Observer; Zeiss) at 600X magnification.

RNA extraction and retrotranscription

Total RNA was extracted from $5x10^5$ HBVP at different passages using RNeasy Plus Mini Kit (Qiagen), following manufacturer's instructions. The RNA quantification was performed using NanoDrop 2000 (Thermo Scientific), while purity and integrity of RNA were evaluated with 2200 TapeStation instrument (Agilent Technologies). One μg of RNA was reverse-transcribed using the QuantiTect Reverse Transcription Kit (Qiagen) following manufacturer's protocol.

Pericytes gene expression analysis

To analyse the gene expression of pericytes, a Real-Time PCR was performed using a custom-designed TLDA Microfluidic Card (Life Technologies). This card consists of 192 TaqMan Gene Expression Assays preconfigured in a 384-well format (genes are listed in Appendix-Table 5). After the card reached RT, each of its 8 ports was filled according to manufacturer's protocol with 100 µl of mix made with Master Mix and one µl of cDNA. Upon loading, the card was briefly centrifuged, sealed and loaded into the thermal cycler. Real-Time PCR was performed in a 7900HT Real-Time PCR System (SDS 2.4, Life Technologies). The following cycling conditions were used: 50°C for 2 min, 94,5°C for 10 min, and 40 cycles of 97°C for 30 s followed by 59,7°C for 1 min. Data were analysed through RQ Manager 1.2.1 Software (Life Technologies). Gene expression values were normalized to the median expression of ACTB housekeeping gene and analysed with the $2^{-\Delta\Delta Ct}$ method.

Proliferation assay

Proliferation of pericytes at different passages was assessed using an xCELLigence RTCA DP instrument (Software Package 2.0, ACEA Biosciences) which was placed in a cell incubator 24 hours before the experiment. Each well of an E-plate 16 (ACEA BioSciences) was coated with 1% gelatin solution. A blank reading on the xCELLigence system was performed with 100µl of PM or sfPM in each well to measure background impedance. HBVP were detached and resuspended both in PM and in sfPM. A thousand cells were seeded in each well, four replicates for each condition. Impedance readings, expressed as a CI, were started and recorded at 15 minutes intervals for 96 hours.

Tubulogenesis assay

Tubulogenesis assay was performed using µ-Slide Angiogenesis plates (Ibidi) coated with GFR-Matrigel, following manufacturer's instructions. HBVP were detached, resuspended in PM $1{,}5x10^4$ cell were seeded on GFR-Matrigel layer. The formation of the tubes was documented with an inverted microscope (Eclipse TS100, Nikon) equipped with a CCD camera (DS-Qi1Mc, Nikon).

Pericytes-tumoral cells non-contact co-culture assay

Non-contact co-culture test was performed using 3 µm pore size transwell inserts (Corning) between HBVP at different passages and A375, MDA-MB-231 or HT1080 cell lines. HBVP at different passages were detached and $1x10^4$ cells were seeded in complete PM on gelatin-coated

glass coverslips positioned on the bottom of a 6-well plate. The upper chamber of each transwell insert was filled with 1 ml of complete PM with or without $1x10^5$ cancer cells. After 72 hours, supernatant from each well was collected to prepare cc-CM (co-culture Conditioned Medium), while HBVP were fixed with 4% PFA for immunocytochemistry analysis.

Pericytes-tumour cells interaction assay

To monitor and quantify the invasion of a monolayer of pericytes by tumour cells, an impedance-based detection platform was used. Each well of an E-plate 16 (ACEA BioSciences) was coated with 1% gelatin solution. HBVP were detached, resuspended in PM and $5x10^3$ cells were seeded into each well. Impedance readings were started and repeated at 15 minutes intervals. When HBVP reached a stable monolayer, readings were paused and tumour cells were added. Tumour cells were detached using 0,5mM EDTA (Sigma-Aldrich) and resuspended in complete medium. Two thousand tumour cells were added in each well, to reach a pericytes-to-tumour cells ratio of 2,5:1. The impedance readings were then restarted and recorded for 72 hours.

Tumour cells migration assay

A migration assay was performed using the same impedence-based detection platform above described. In this kind of experiment were used CIM-plates (ACEA BioSciences), the xCELLigence modified Boyden chamber system. Tumour cells were starved for 24 hours before experiment, than were detached and counted. One hundred and eighty μl of cc-CM were added in the bottom part of each well. Ten thousand cells in serum-free medium were seeded in each insert. Impedance readings were started and recorded for 36 hours.

Cytokine array

Expression of cytokines was determined with the Human XL Cytokine Array Kit (R&D Systems), consisting of 102 antibodies against soluble cytokines that mediate cell-to-cell communication spotted on a nitrocellulose membrane. The array was performed following manufacturer's instructions using 1 ml of cc-CM from each condition. The data from developed X-ray film were digitalized with a transmission-mode scanner and quantified using ImageJ analysis software (http://rsbweb.nih.gov/ij/). The positive controls were spot couples distributed in the upper left, upper right, and lower left corners of each array kit, whereas the negative controls spot couples were located in the lower right corner of each membrane. The averaged background signal was subtracted and the arrays were calibrated based on the signal strength of the positive controls. The average signal (pixel density) of the pair of duplicated spots

representing each cytokine was determined as above and the corresponding signals on different arrays were compared.

Statistical analysis

Experiments were performed at least in triplicate and data were expressed as mean ± standard deviation (SD). The statistical correlation between groups was analysed by Student's t test, where $P < 0,05$ was considered significant.

Results

Characterization of pericytes at different maturation degree

Phenotypic analysis

The expression of recognized markers of pericytes was assessed through both cytofluorimetric and immunocytochemistry analysis.

In cytofluorimetric examination (Figure 5), HBVP early passages phenotype was characterized by strong expression of CD44 and CD73 (both at 100%), high expression of CD90, CD146 and NG2 (82%, 80% and 74% respectively), low expression of CD106 and CD10 (21% and 3%), none expression of CD94 and CD184.

HBVP late passages phenotype shown a different pattern of markers, with a high expression of CD73 and CD90 (88% and 83%), low expression of CD44 and CD146 (47% and 32%), very low expression of CD10, NG2, CD106 (5%, 2% and 1%), none expression of CD94 and CD184.

HBVP differ also in term of cellular dimension: early passages shown FSC/SSC values clearly smaller than HBVP late passages, that appeared bigger.

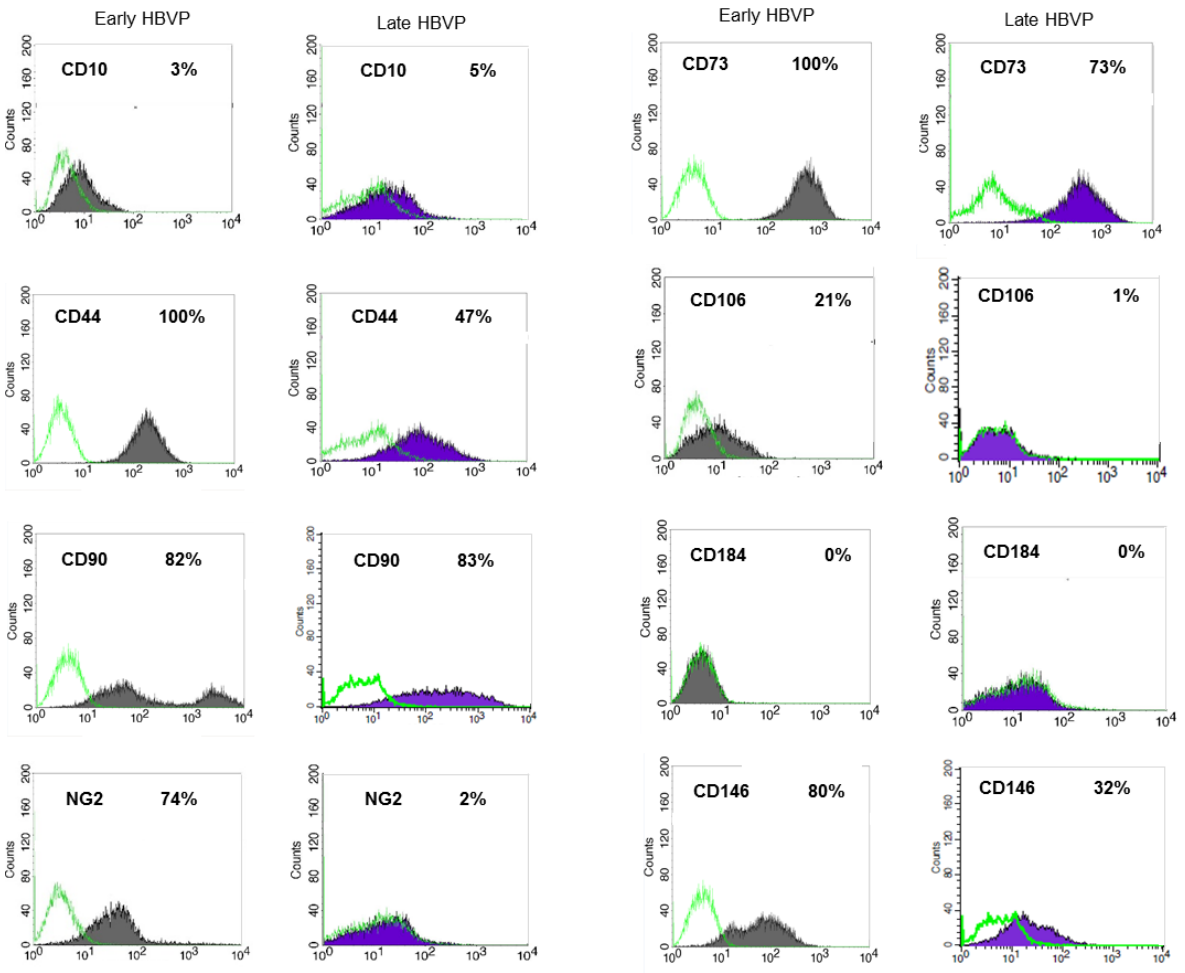

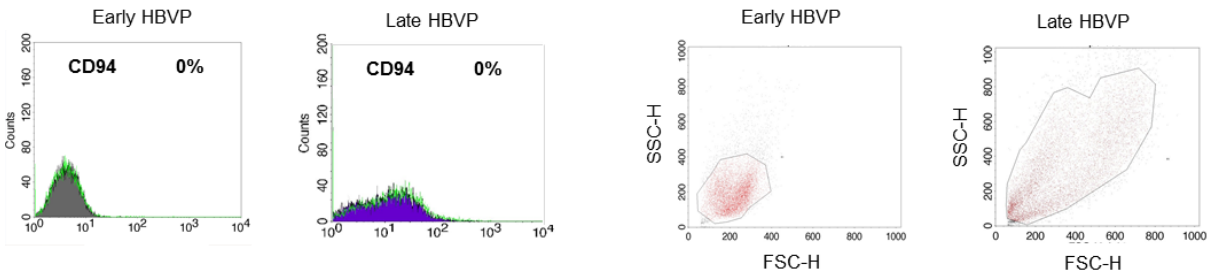

Figure 5. Expression of surface markers of pericytes at early and late passages of culture (grey and purple filled histogram represent indicated markers of early and late HBVP, green line histogram represent isotype controls).

In immunocytochemistry analysis (Figure 6), HBVP early passages showed high positivity for CD73 and CD147, NG2, positivity for BP-1 and PDGFR-β, poor expression of CD10, CD44 and CD90. Cytoplasmic marker α-SMA appeared clearly localized in the nucleus, while Desmin was not homogenously expressed through the cell population. HBVP late passages shown high positivity for CD73 and CD174, positivity for BP-1, PDGFR-β, CD44, CD90, and weak positivity for CD10 and NG2. Cytoplasmic markers α-SMA and Desmin were present as filaments along the whole cellular length. Differences in cellular dimension were also clearly confirmed.

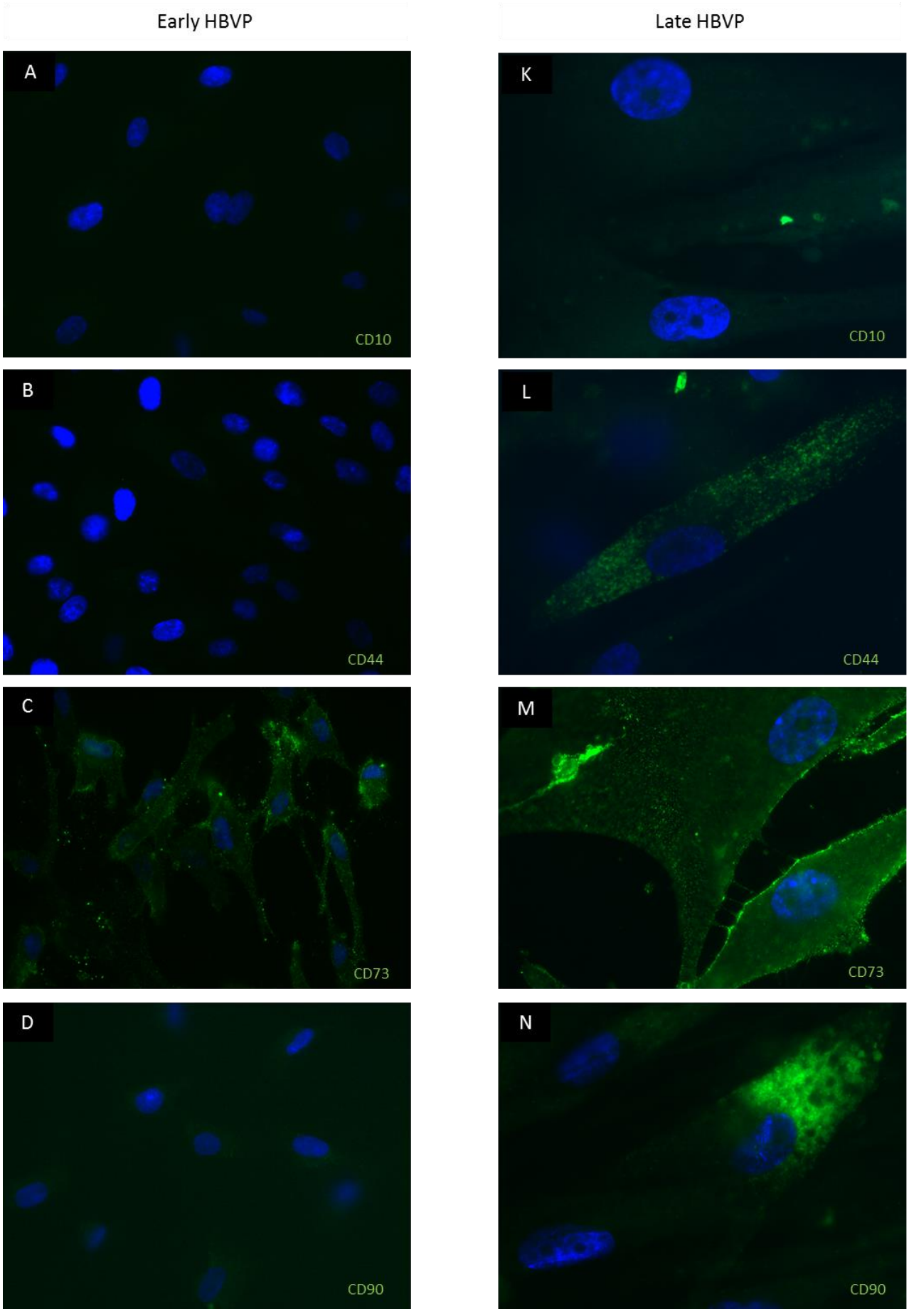
Early HBVP
Late HBVP
A
CD10
K
CD10
B
CD44
L
CD44
C
CD73
M
CD73
D
CD90
N
CD90

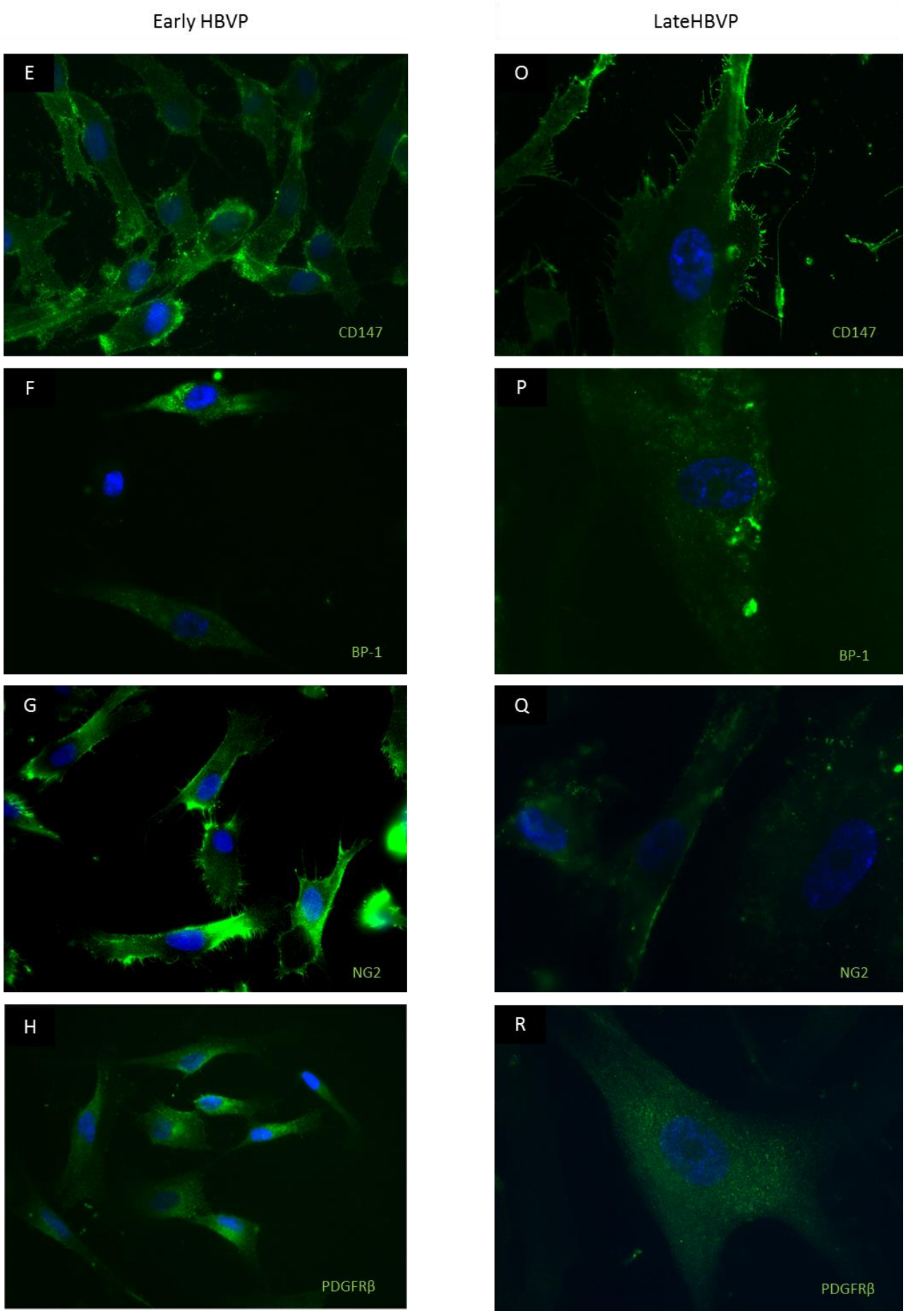
Early HBVP
LateHBVP
E
CD147
O
CD147
F
BP-1
P
BP-1
G
NG2
Q
NG2
H
PDGFRβ
R
PDGFRβ

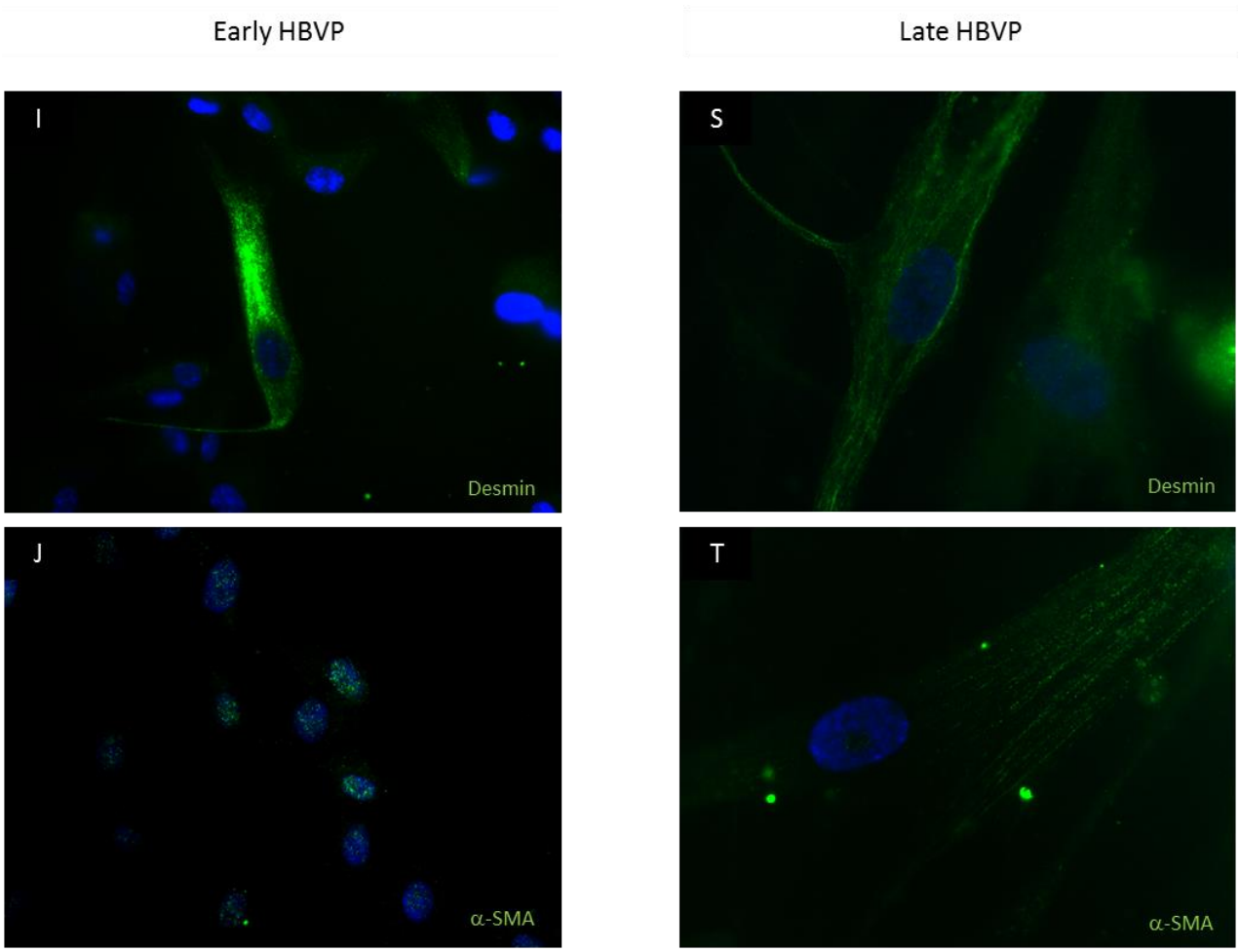

Figure 6. Expression of surface and cytoplasmic markers of early and late passage pericytes (green: CD10, CD44, CD73, CD90, CD147, BP-1, NG2, PDGFRβ, α-SMA and Desmin; blue: nuclei; magnification 600X).

Extracellular matrix production

The ECM produced by pericytes was visualized through a metabolic labelling with azido sugars incorporated into newly synthetized matrix. ECM of HBVP early appeared thin and loose (Figure 7 A), whereas ECM of HBVP late was more compact and firm (Figure 7 B).

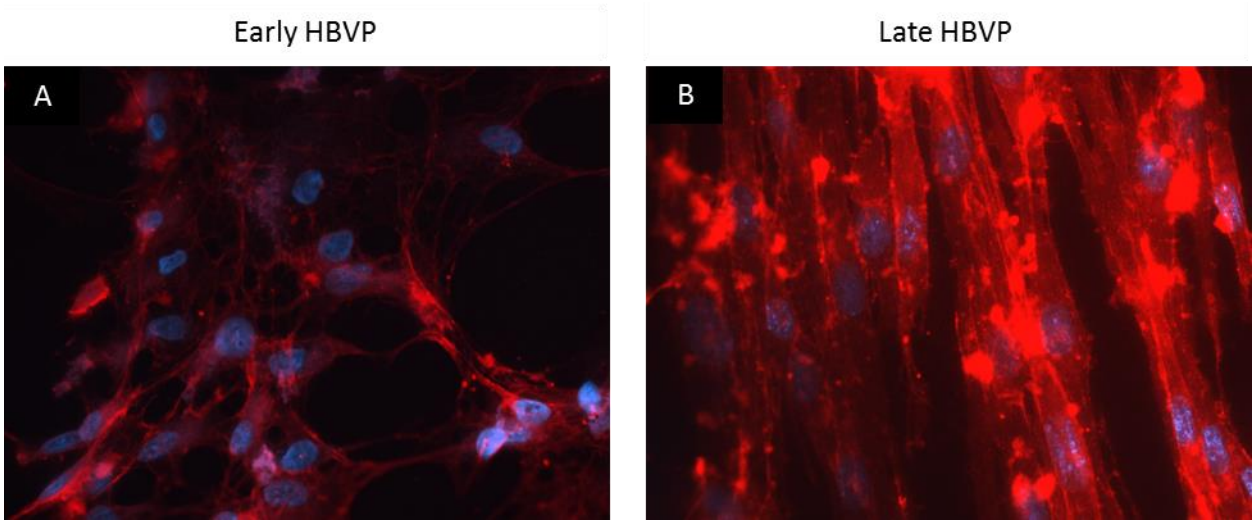

Figure 7. Metabolic labelling of the matrix produced by HBVP at early (A) and late (B) passages (red: ECM; blue: nuclei; magnification 600X).

ECM genes expression analysis

The expression of 192 selected genes was evaluated in early and late pericytes. Early HBVP expressed 131 genes of the totality of genes tested. In comparison to the basal expression of pericytes after one passage in culture, early pericytes overexpressed 69%, down regulated the expression of 27% and expressed *de novo* 4% of genes (Figure 8 A). Late HBVP expressed 136 of the 192 tested genes, overexpressing 54%, down regulating 39% and *de novo* expressing 7% of genes (Figure 8 B). Differences existed between early and late pericytes not only in the overall trend of the genes expression stated as number of genes up or down regulated, but also in the intensity of the expression regulated in the same way. In the "overexpressed genes" category, genes related with the production of basal lamina (as collagen type IV, laminins, thrombospondin,) are more expressed in early pericytes than in late (Figure 9), while genes implicated in the stabilization of the ECM (as collagen type I, fibulin, fubrillin, microfibrillar protein) are more represented in the late population than in the early one (Figure 10).

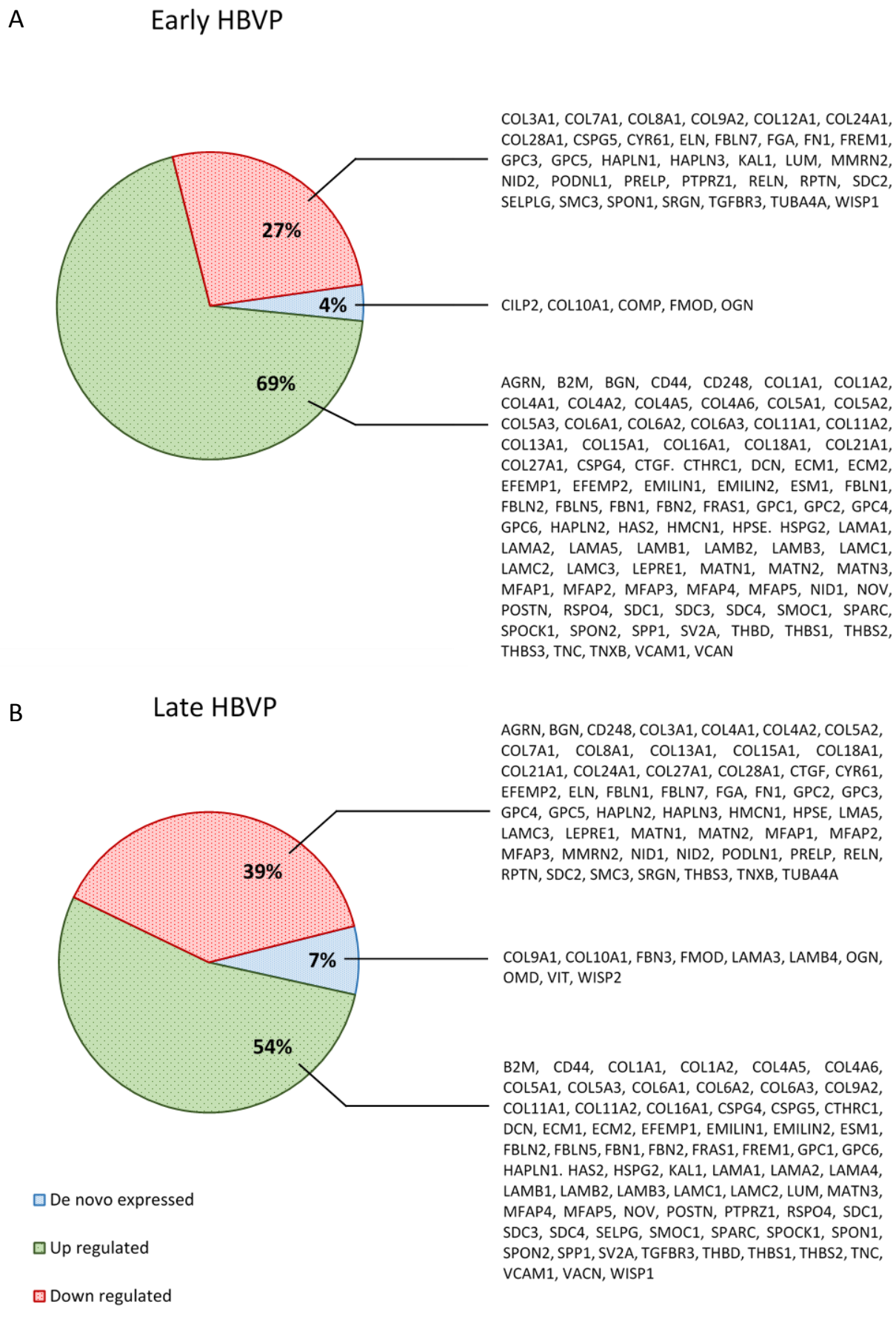

Figure 8. Gene expression of early (A) and late (B) HBVP.

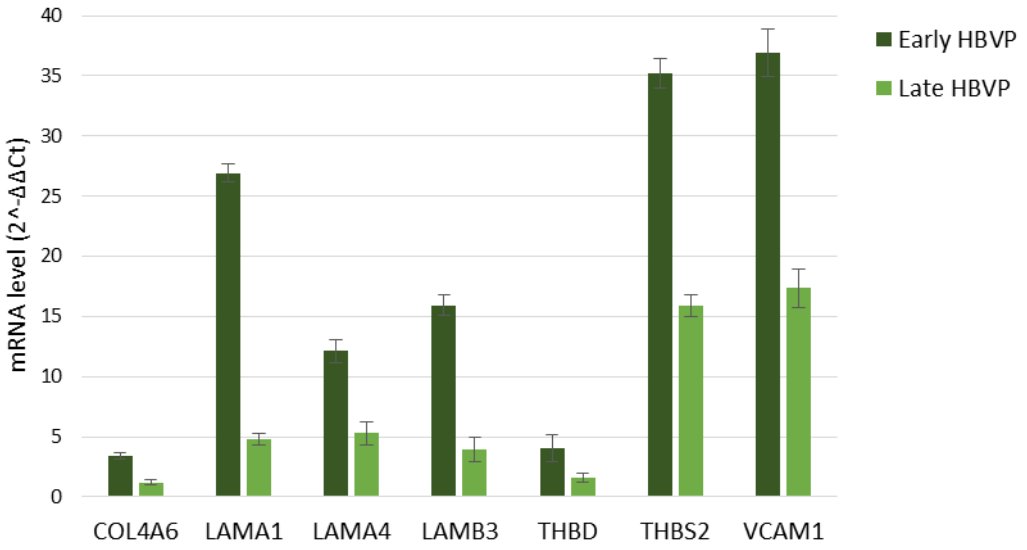

Figure 9. Genes up-regulated in both early and late pericytes but more expressed in early HBVP.

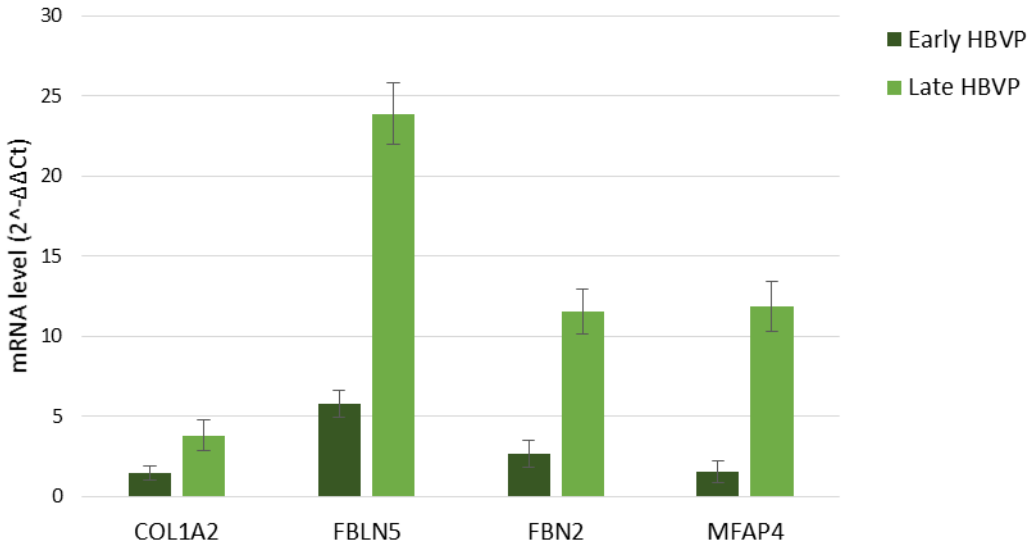

Figure 10. Genes up-regulated in both early and late pericytes but more expressed in late HBVP.

Proliferation assay

The proliferative capabilities of HBVP at early (Figure 11 A) and late (Figure 12 A) passages of culture was evaluated using an impedance-based assay. Seeded in complete PM, early pericytes duplicate every 16 hours (DT=16,25 ± 1,98, figure 11 B), whereas late pericytes show a twofold

proliferation rate (DT=31,12 ± 4,33, figure 12 B). In medium deprived of serum, both pericyte populations arrested their proliferation and, starting from 24-36 hours in culture, decreased their number.

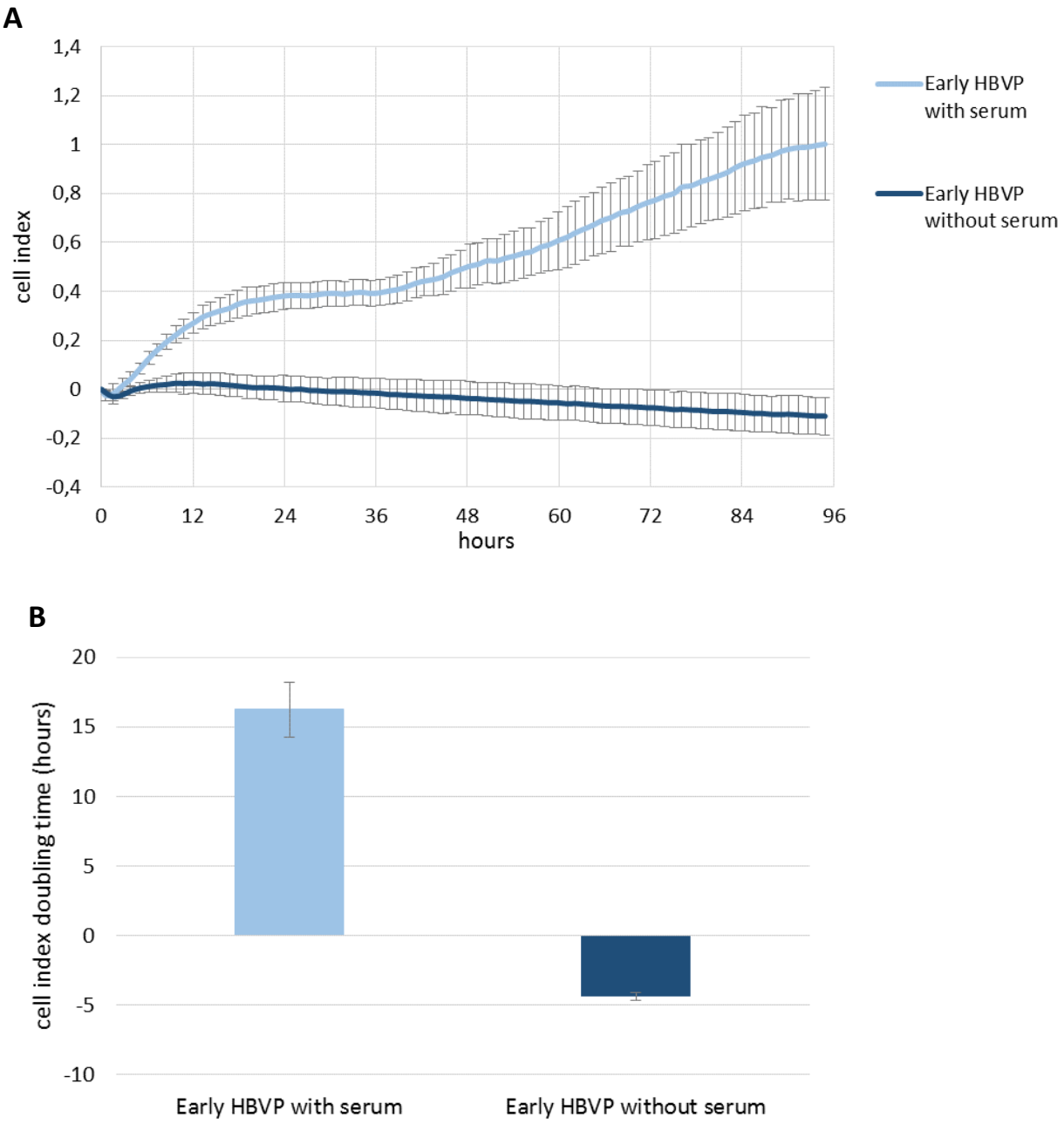

Figure 11. Proliferation capability of early HBVP in presence or absence of serum. Proliferation trend (A) and doubling time representation (B).

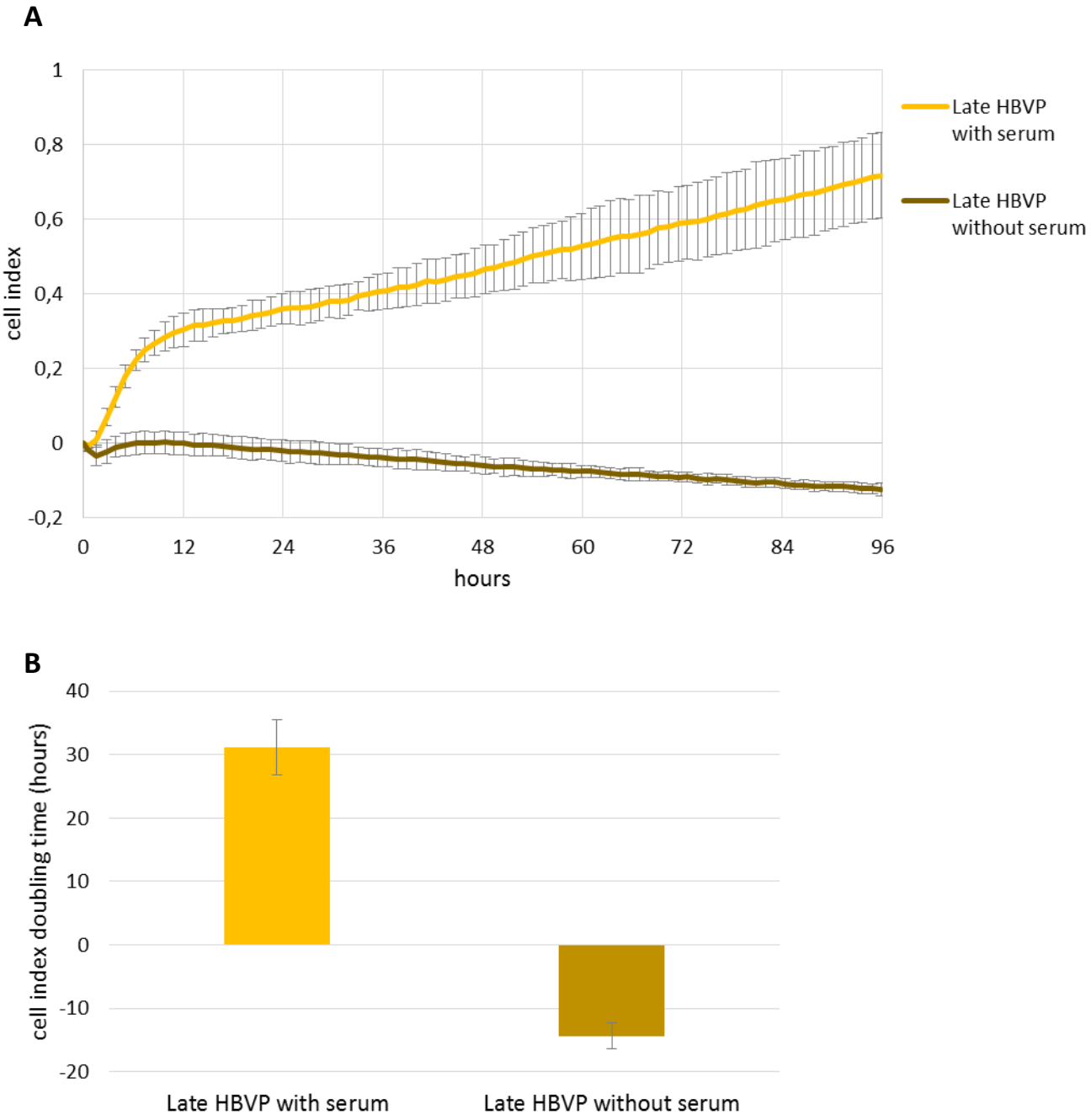

Figure 12. Proliferation capability of late HBVP in presence or absence of serum. Proliferation trend (A) and doubling time representation (B).

Tubulogenesis assay

Pericytes seeded on Matrigel aggregate and form tubule-like structures. Early HBVP formed tubular structures 4 hours after seeding (Figure 13 B) and maintained well-organised tubes until 24 hours (Figure 13 D). Instead, late HBVP made tubes only 1 hour after seeding (Figure 13 E), but after 6 hours the tubular structures started to disassemble (Figure 13 G) and 24 hours after seeding were completely disaggregated (Figure 13 H).

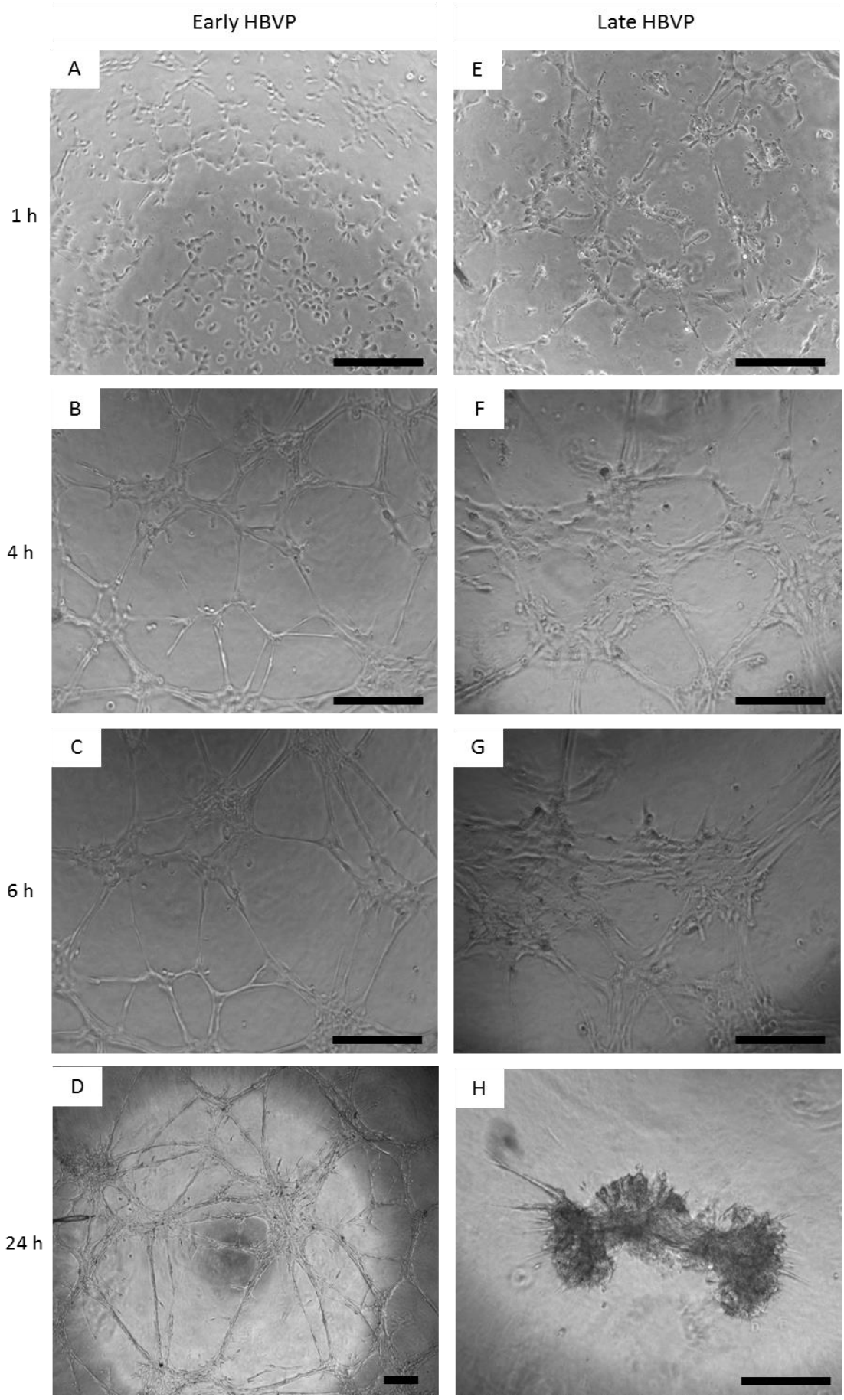

Figure 13. Tubulogenesis assay of early (A-D) and late (E-H) HBVP on Matrigel. Scale bar: 250 μm.

Pericytes-tumour cells interactions

Non-contact co-culture

In a non-contact co-culture system, pericytes at different passages were conditioned by three tumoral cell lines. After 72 hours, the analysis of the cellular markers CD44 (Figure 14), CD90 (Figure 15), NG2 (Figure 16) and PDGFR (Figure 17) demonstrated poor differences between pericytes co-cultured or not co-cultured with tumour cells. Only HBVP early passages shown a different expression of PDGFRβ after conditioning of HT1080 (Figure 17 B) and MDA-MB-231(Figure 17 D) cell lines.

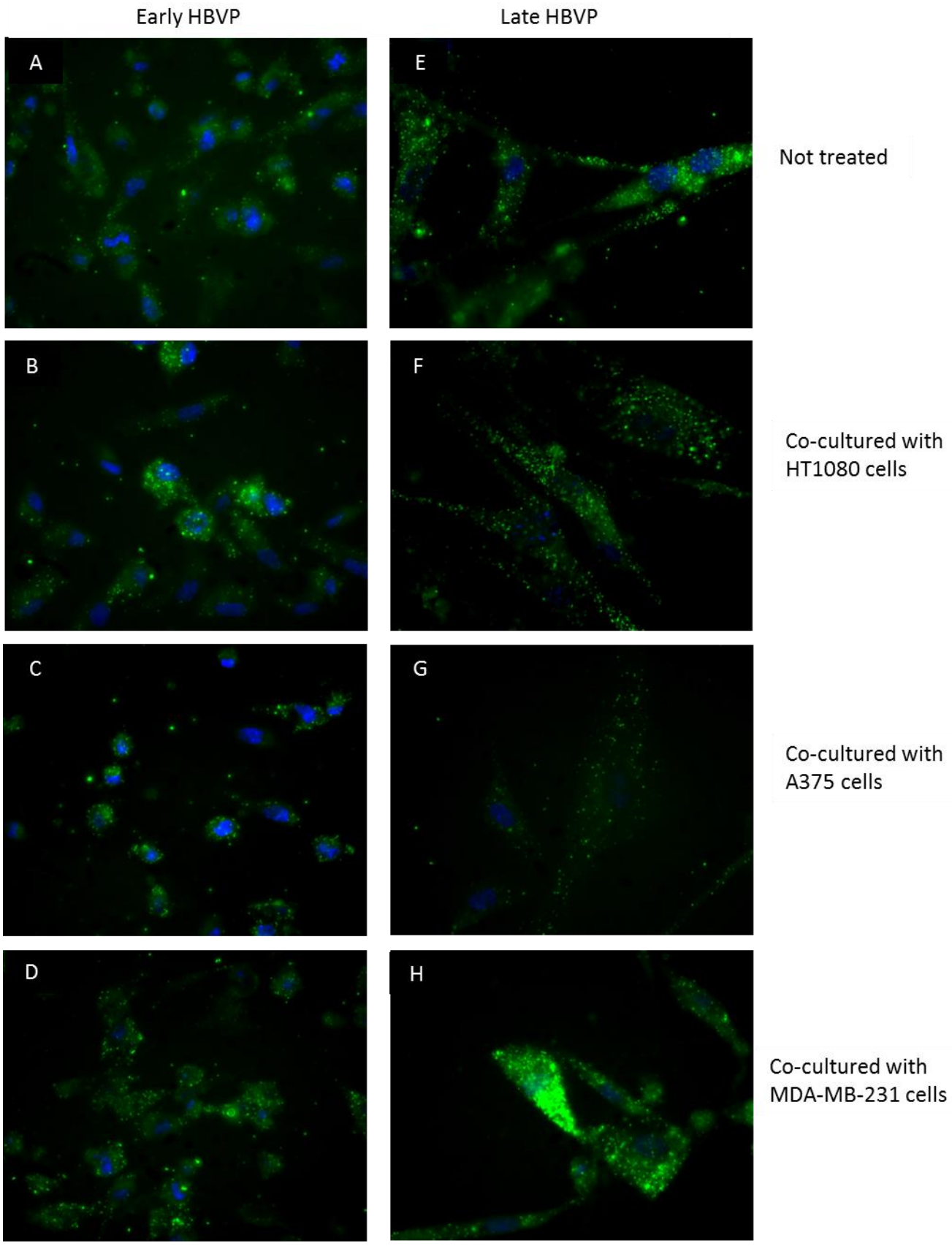

Figure 14. CD44 expression in pericytes at early and late passages alone or co-cultured with indicated tumoral cells (green: CD44; blue: nuclei; magnification 600X).

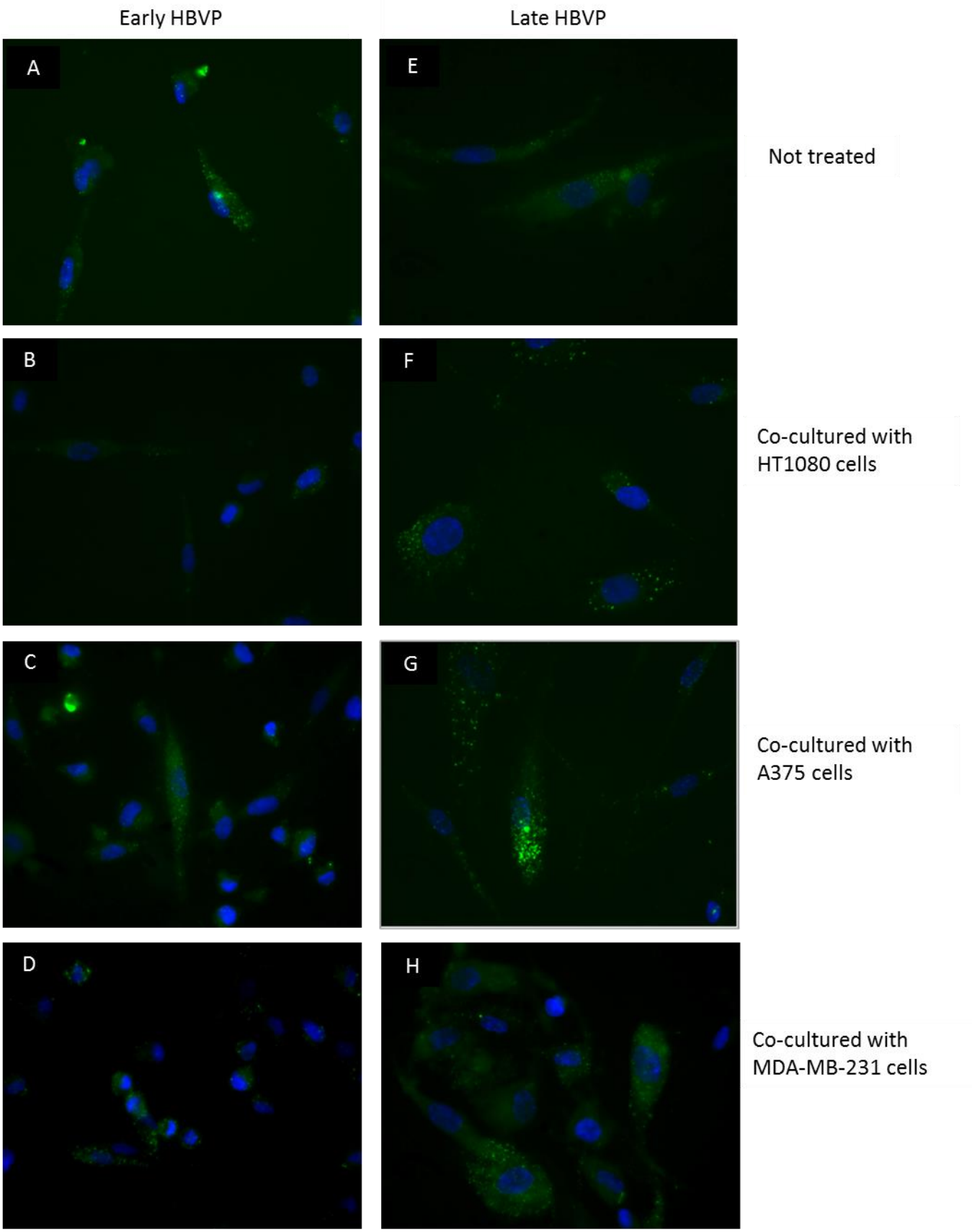

Figure 15. CD90 expression in pericytes at early and late passages alone or co-cultured with indicated tumoral cells (green: CD90; blue: nuclei; magnification 600X).

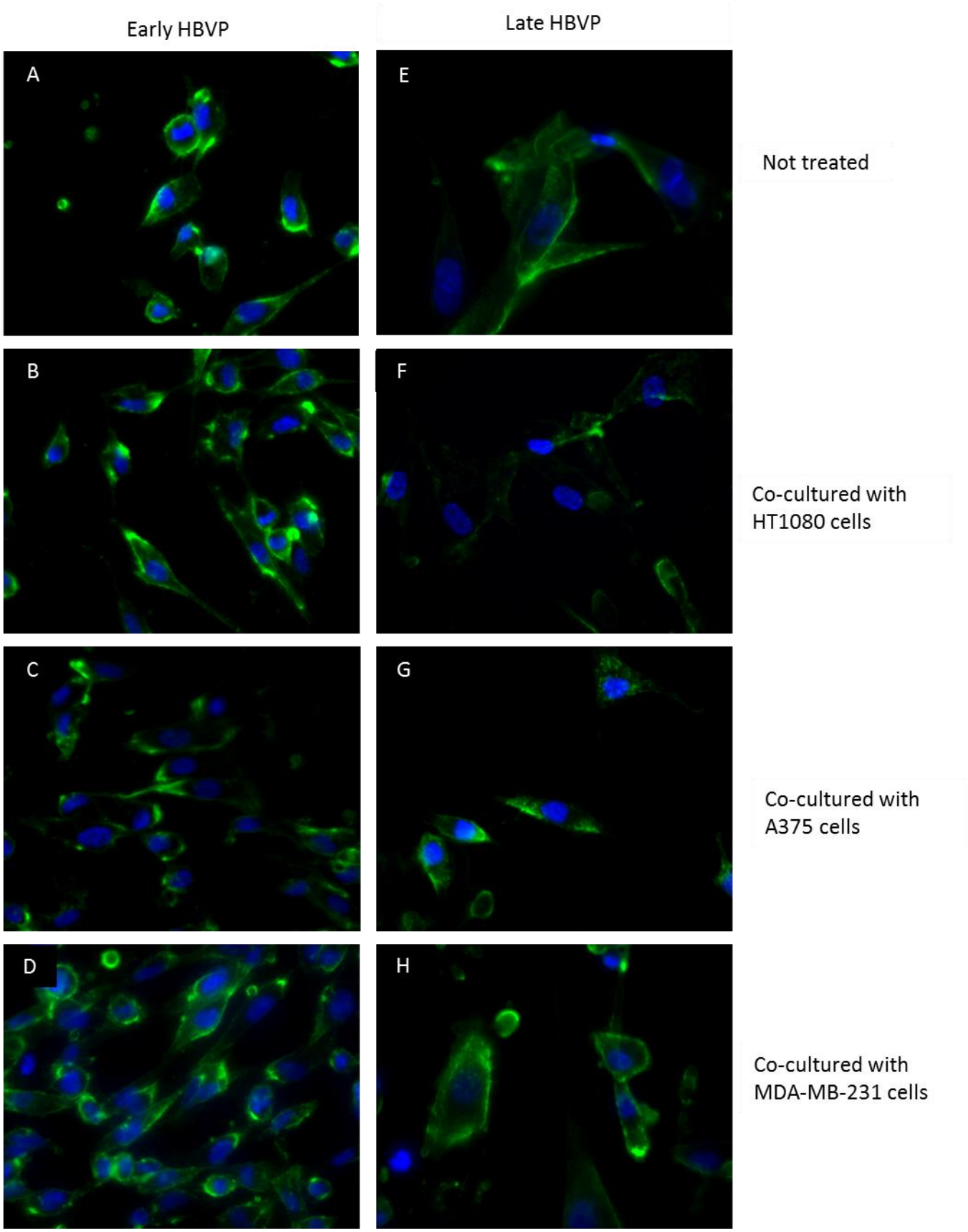

Figure 16. NG2 expression in pericytes at early and late passages alone or co-cultured with indicated tumoral cells (green: NG2; blue: nuclei; magnification 600X).

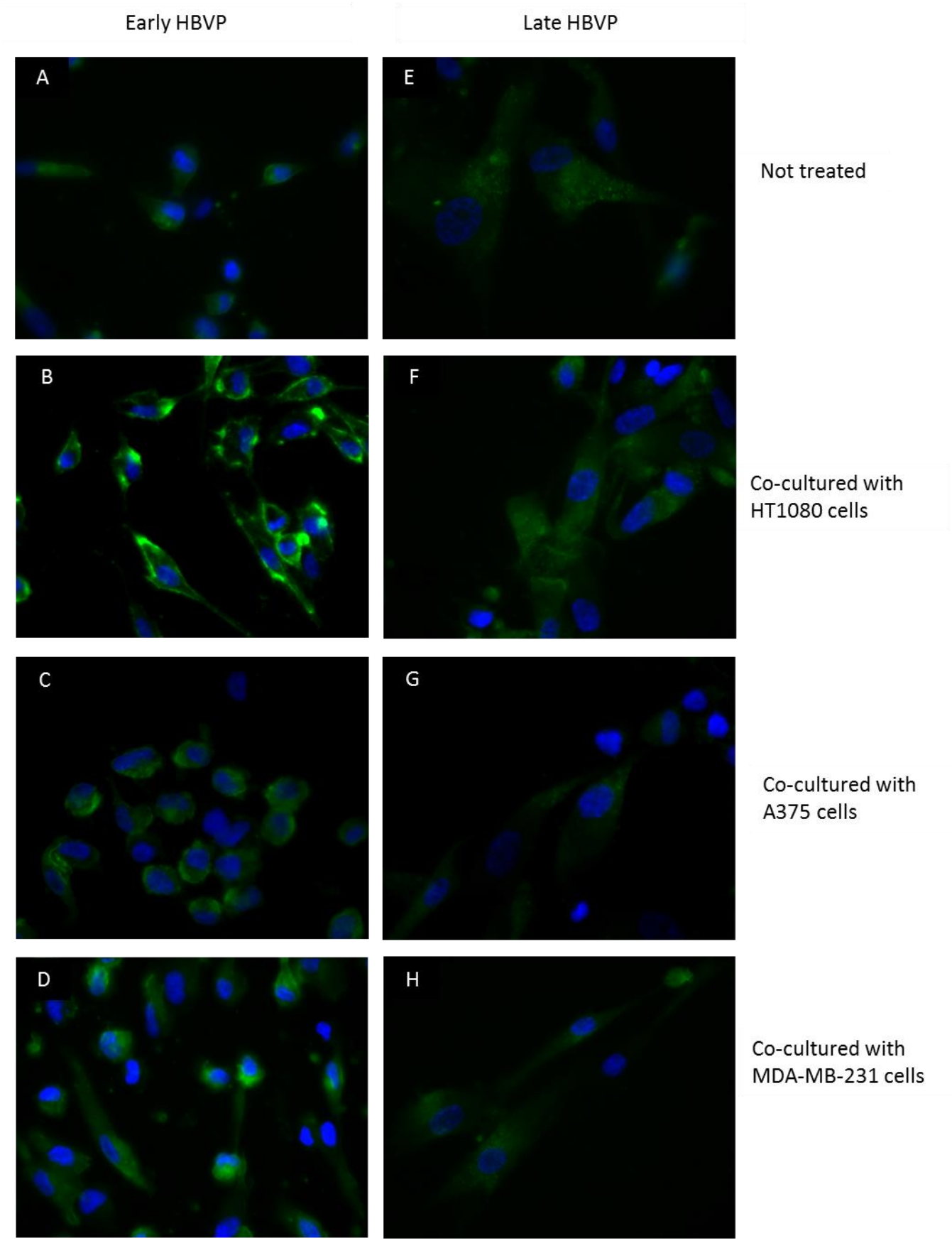

Figure 17. PDGFRβ expression in pericytes at early and late passages alone or co-cultured with indicated tumoral cells (green: PDGFRβ; blue: nuclei; magnification 600X).

Pericytes-cancer cell interaction assay

Then the direct interaction between pericytes and tumour cells was assayed. Early pericytes shown the strongest interaction with HT1080 cell line (Figure 18, orange line), as demonstrated by the constant growth of the CI values during 72 hours to the maximum value around 3,5 (3,49 ± 0,15). The interaction with MDA-MB-231 and HT1080 (Figure 18, blue and grey lines respectively) appeared different from the basal CI (Figure 18, yellow line), but lower, with maximum values of 1,62 ± 0,09 and 1,74 ± 0,07. On the other hand, late pericytes shown the same trend of interactions through cell lines but in a more homogeneous fashion (Figure 19), with CI values ranged between 2,31 ± 0,25 and 1,79 ± 0,10.

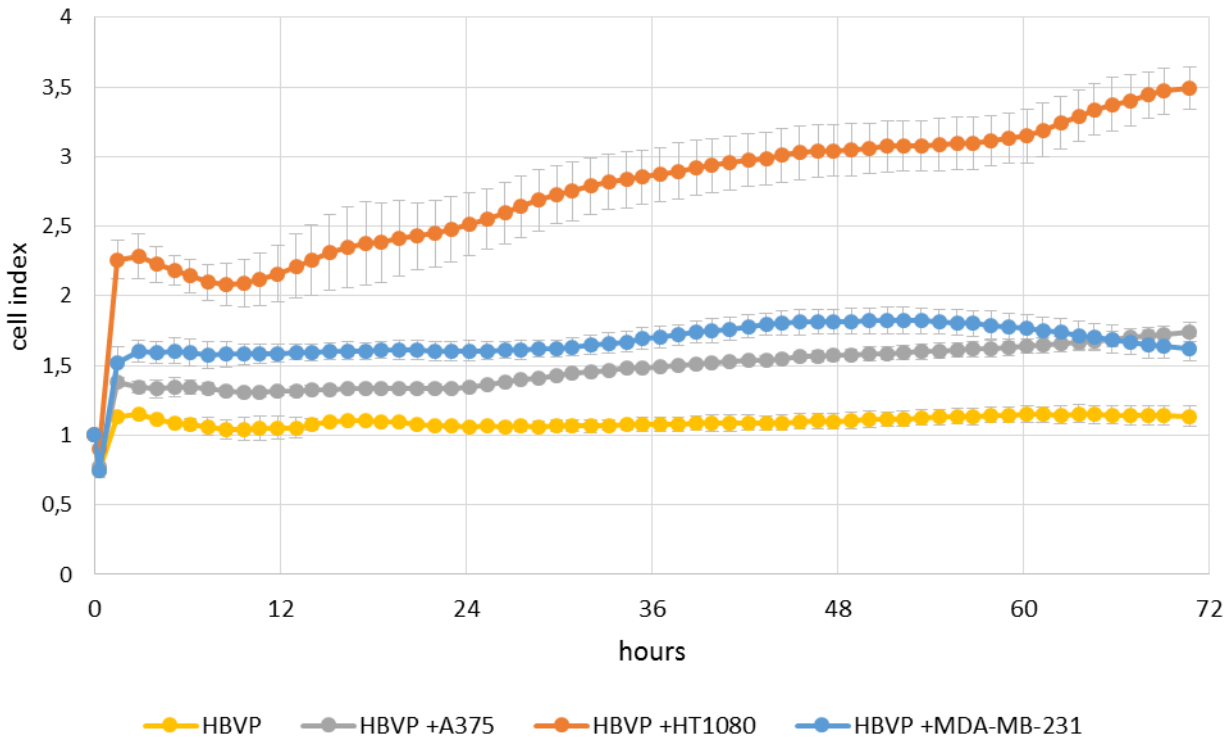

Figure 18. Direct interaction between early pericytes and tumour cell lines.

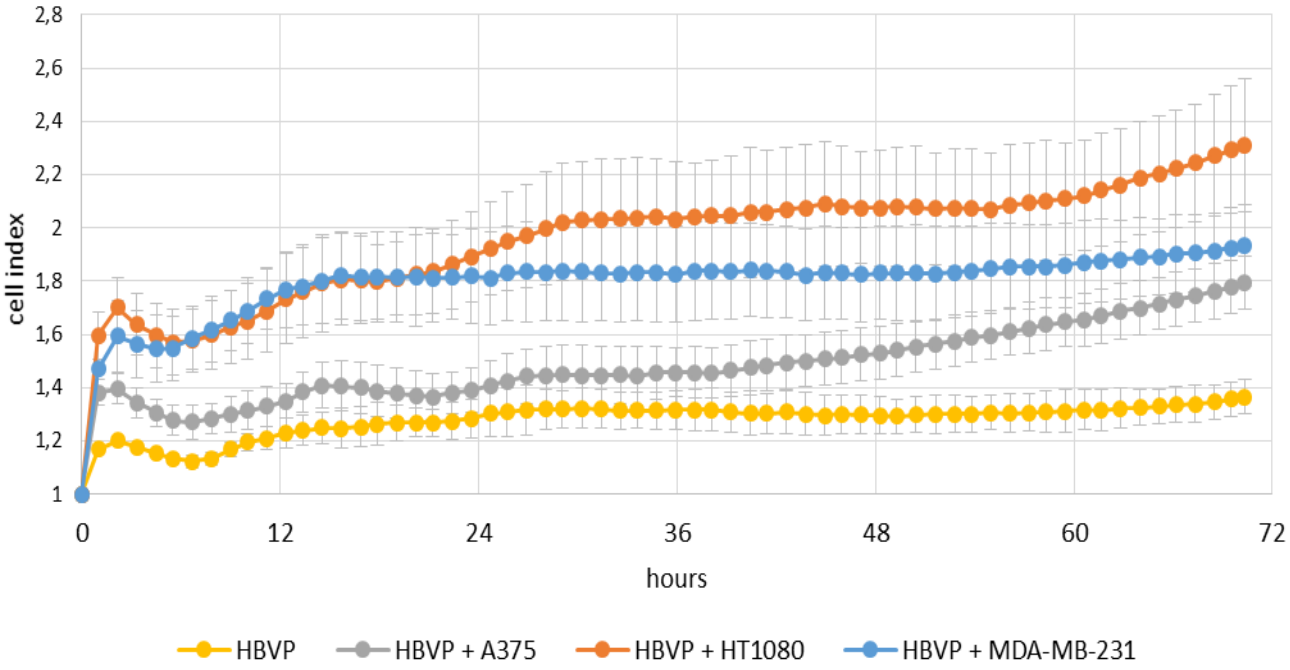

Figure 19. Direct interaction between late pericytes and tumour cell lines.

Cancer cells migration assay

To assess whether the cancer cell migratory capacity was influenced by paracrine signals, a migration assay was performed in presence of CM obtained both from pericytes cultured alone (CM HBVP) and pericytes co-cultured with tumour cells (cc-CM HBVP/A375, cc-CM HBVP/HT1080, cc-CM HBVP/MDA-MB-231) as chemoattractants. The migration of all tumour cells tested was strongly in presence of CM HBVP than in other experimental conditions. The melanoma line A375 shown the better performance (Figure 20), with a significative difference of migration in presence of CM HBVP (Figure 20, red line) respect to the positive control (DMEM with serum, figure 20, purple line) after 18 (CI 0,86 ± 0,20 vs 0,32 ± 0,09; P=0,0221) and 24 (CI 1,17 ± 0,22 vs 0,36 ± 0,10; P=0,0104) hours and high significative after 30 (CI 1,56 ± 0,24 vs 0,56 ± 0,11; P=0,0074) and 36 hours of culture (1,98 ± 0,26 vs 0,68 ± 0,14; P=0,0048). The fibrosarcoma cell line HT1080 (Figure 21) shown the same migratory trend, with a significative difference between cells in presence of CM HBVP and DMEM with serum only after 6 hours of culture (CI 1,33 ± 0,13 vs 0,50 ± 0,01; P=0,016). Also the breast carcinoma cell line MDA-MB-231 (Figure 22) followed the same migratory trend, lacking of significative differences between the CI values.

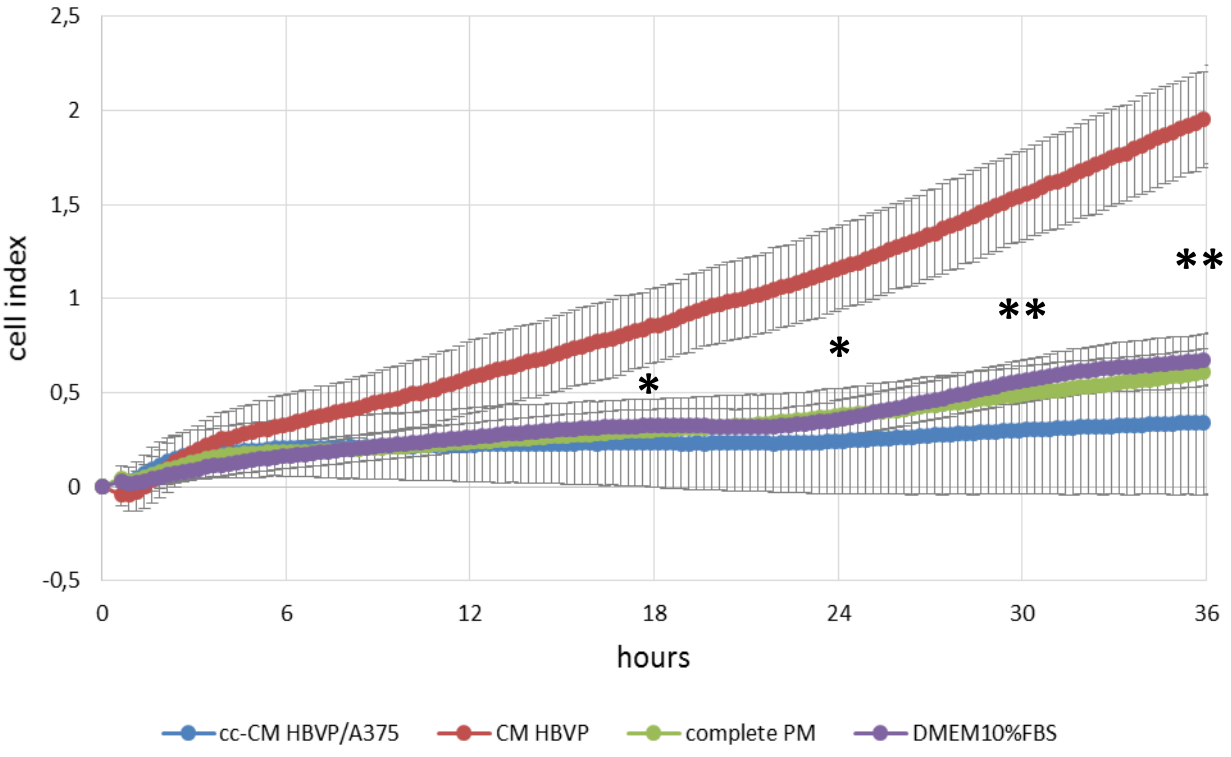

Figure 20. Migration of A375 cell line in presence of different media (* = P<0,05; ** = P<0,01).

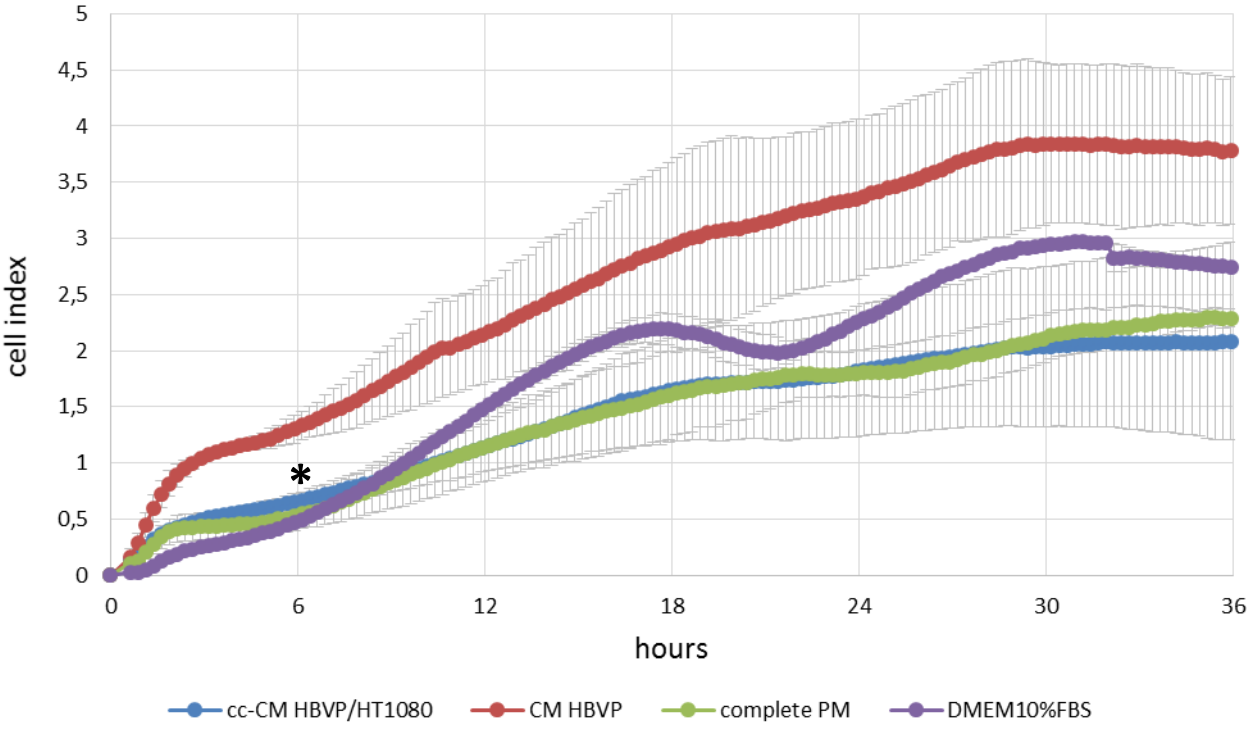

Figure 21. Migration of HT1080 cell line in presence of different media (* = P<0,05).

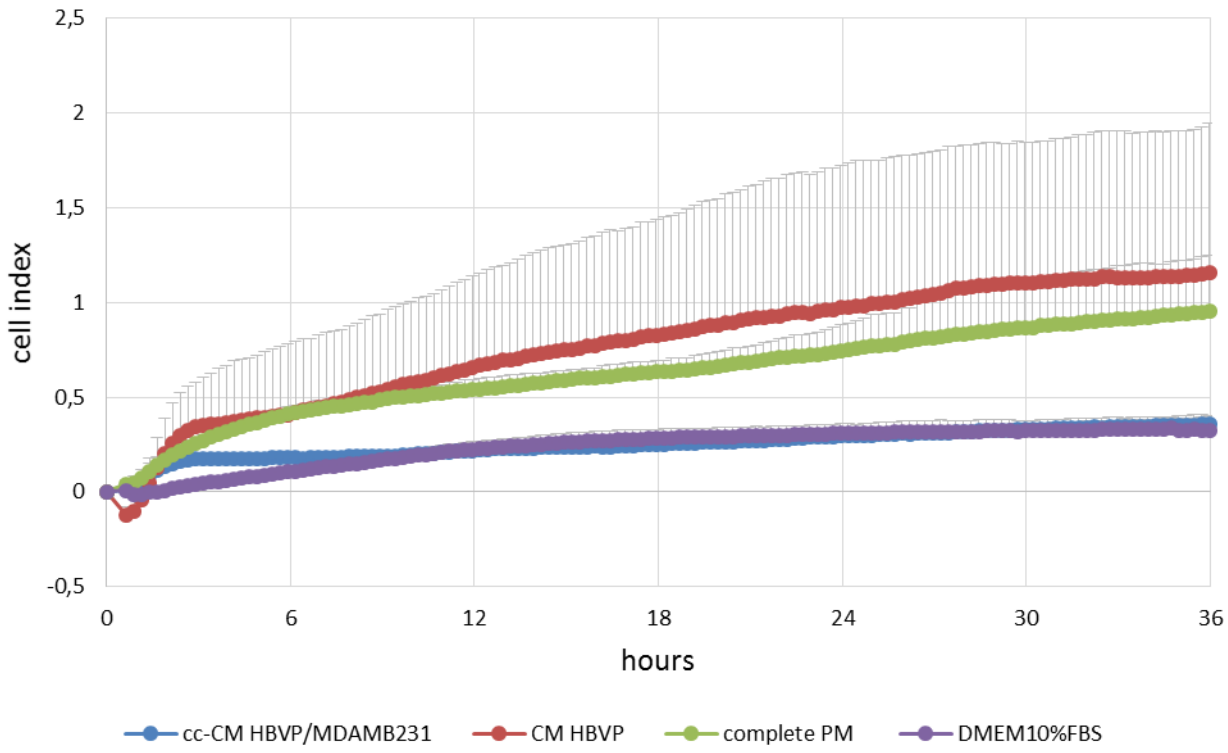

Figure 22. Migration of MDA-MB-231 cell line in presence of different media.

Co-culture conditioned media analysis

To determine the nature of the microenvironment recreated in the co-culture system, an antibody based protein array analysis was performed. The protein expression analysis was performed on CM HBVP and on cc-CM HBVP/A375, cc-CM HBVP/HT1080, cc-CM HBVP/MDA-MB-231 (Figure 23). The conditioned medium from pericytes alone composition, quantified and plotted in the reported histogram (Figure 24), was characterized by the high expression of three molecules, such as EGF (NPD 0,86 ± 0,007) , PDGF-AA (NPD 0,76 ± 0,038) and Serpin E1 (NPD 0,82 ±0,049). The protein contents of the conditioned media from the co-cultures HBVP/cancer cells (Figure 25) were enriched of factors stimulating motility and angiogenesis (such as Angiogenin, EMMPRIN, IL-8, MIF, PTX3 and VEGF) and deprived of EGF, IL-11, Il-17A and Serpin E1.

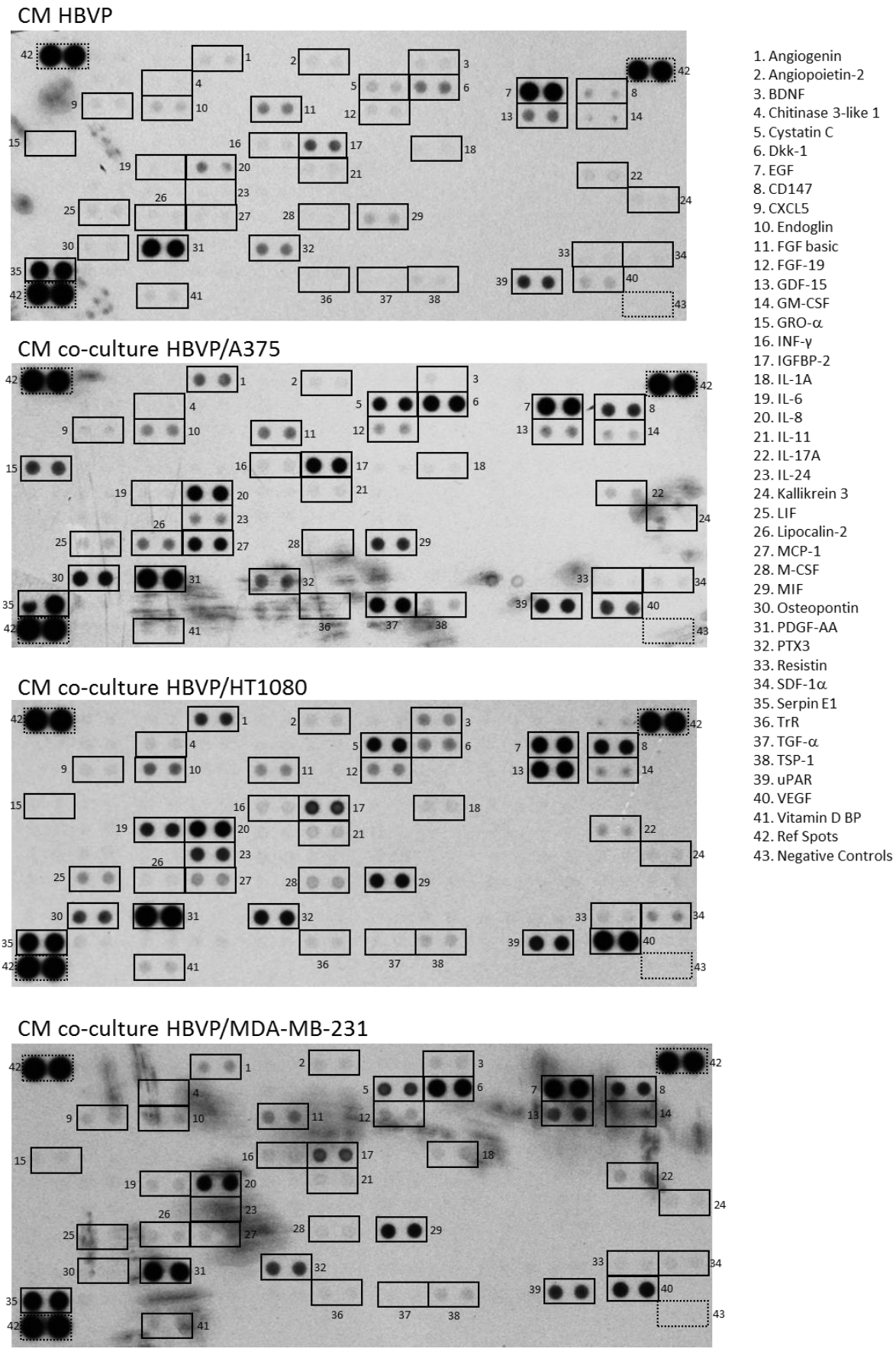

Figure 23. Protein expression in conditioned media from HBVP alone and HBVP co-cultured with melanoma (A375), fibrosarcoma (HT1080) and breast carcinoma (MDA-MB-231) cells.

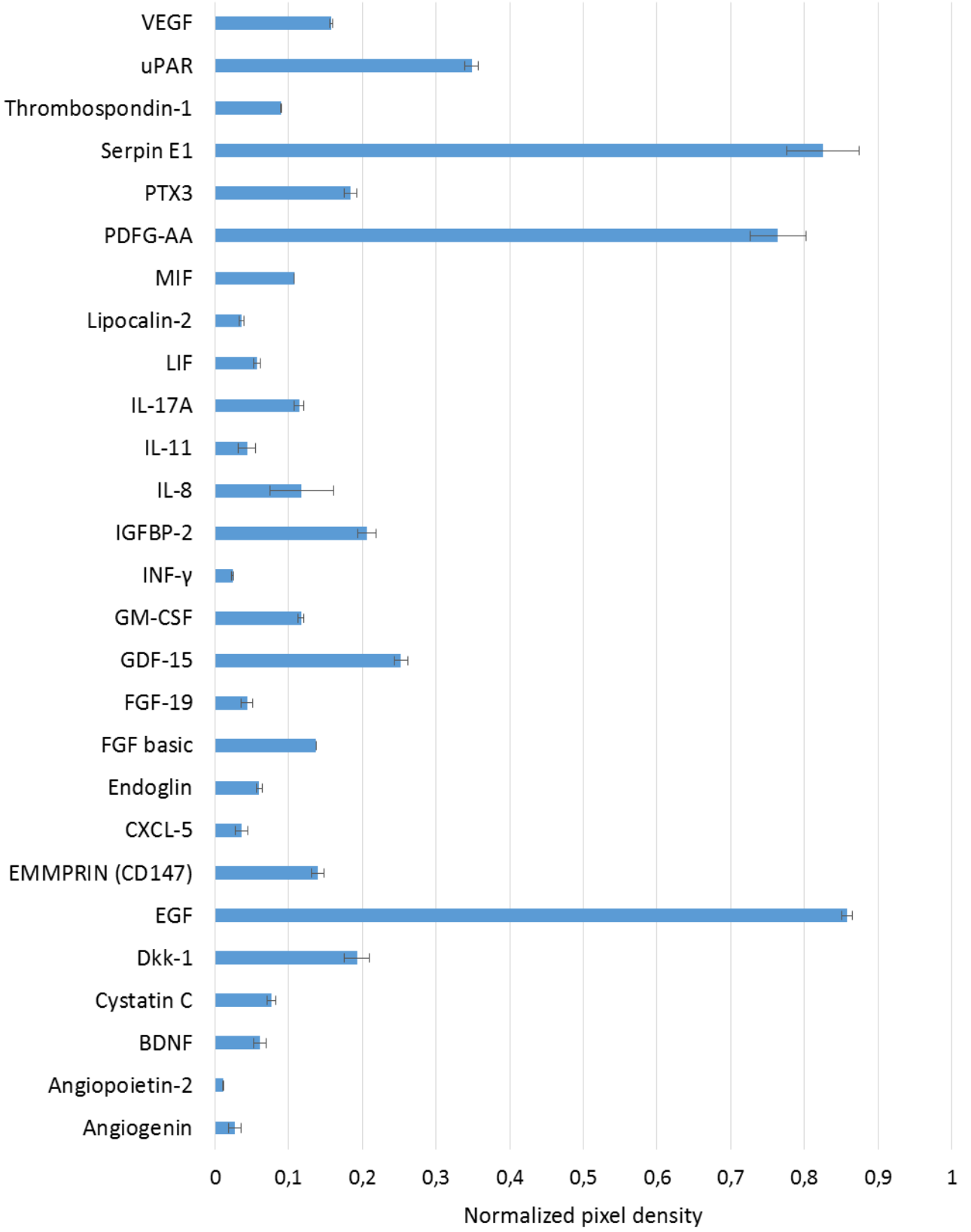

Figure 24. Protein expression of the conditioned medium from HBVP alone, quantified and plotted as normalized pixel density.

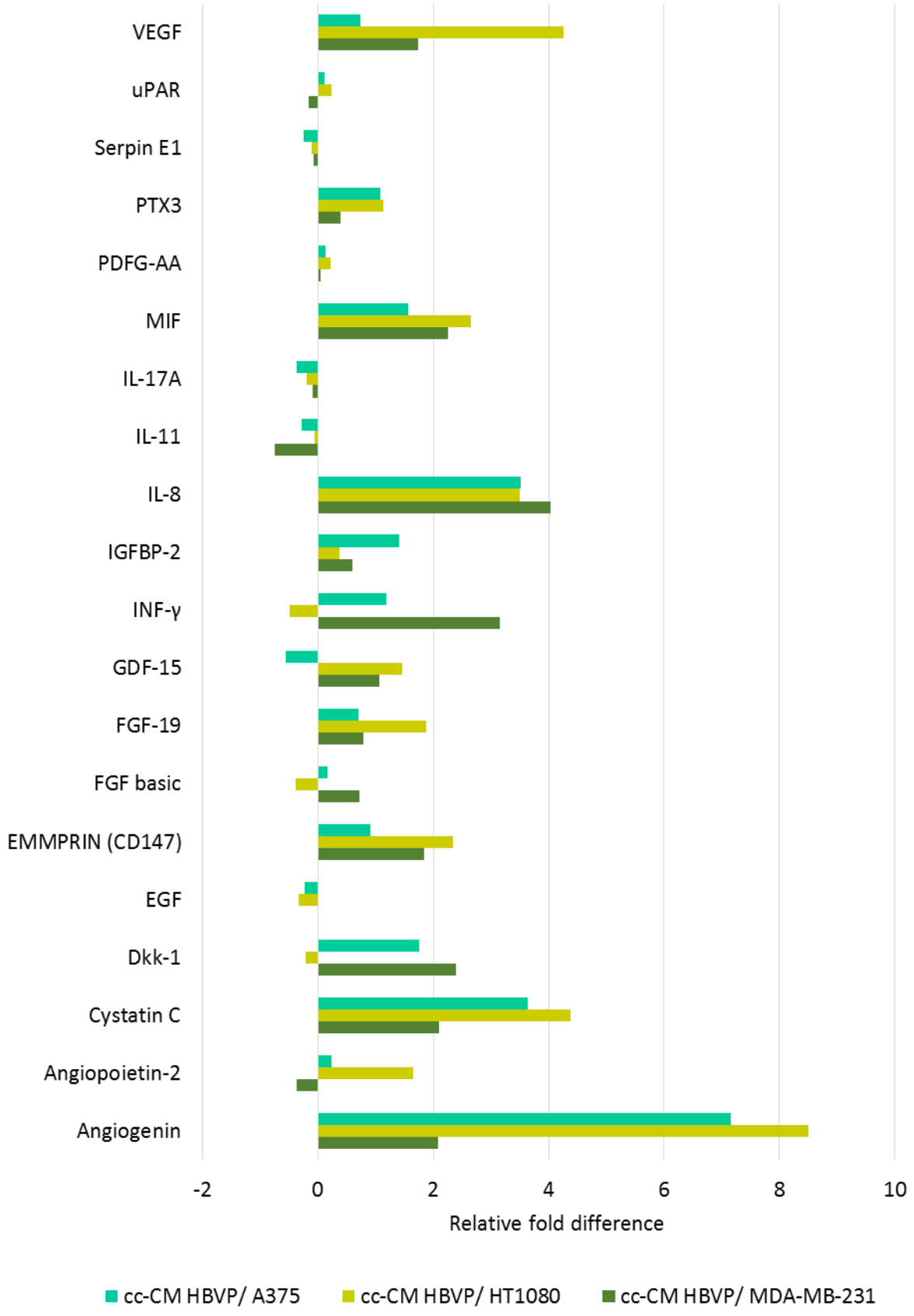

Figure 25. Protein contents of media from co-cultured HBVP/cancer cells, quantified as pixel density and expressed as relative fold differences to the conditioned medium from HBVP alone.

Discussion

Pericytes are perivascular cells whose involvement in normal and pathological angiogenesis is well known; recently, an overall analysis of the functional properties of pericytes shows that these are multifaceted cells with the ability to significantly influence tumour development and progression[46,58,59]. Pericytes, together with CAFs, immune cells and endothelial cells, are one of the main cellular components of the TME[76]. Experimental studies show that blockage of pericyte recruitment and/or their function leads to reduced tumour growth due to compromised vessel structure and blood supply[74]. On the other hand, tumour vessels with aberrations in wall coverage could facilitates tumour cell spreading and metastasis[59]. Interestingly, Morikawa and co-workers, observed several abnormalities in tumour associated pericytes including little coverage of microvessels and long cytoplasmic processes projected in tumour parenchyma[46]. This last observation reinforces the idea that pericytes not only are a microvascular component but, in malignancies, they acts as other cancer-associate stromal cells in contributing the tumorigenic characteristics. Tumour masses, in turn, are capable to transform a normal to an aberrant microenvironment modifying numerous stromal cells functions (oxidative stress, metabolism, ECM producing and stiffness)[77–79].

In this work, a phenotypic and functionally characterization of a pericytic model was performed using HBVP distinguished in "early" and "late" due to the time passed in culture. Cells were analysed evaluating the expression of a panel of markers representative of pericytes[18,57]. Changes in the expression levels of these markers were clearly present between the two cell subpopulations, above all the expression of one of the main pericytic markers NG2, that was markedly decreased from early to late pericytes. These variations were accompanied by changes in the gene expression of ECM components. In particular, early and late pericytes showed modulation of gene expression for the molecular components of the basal membrane. This modulation suggests that pericytes show a phenotypic variability depending on their maturation degree, here simulated as the time that pericytes spent in culture. In accordance with various observations published by other investigators[18,80–82], we found that the genes and markers modulation affected also their functionality, reflected into different growth rates and capacity to form tubular-like structures when deposited on a ECM layer. Our HBVP model underwent changes regarding the cell itself and its relationship with the microenvironment.

To investigate the interplay between pericytes and cancer cells, we assayed various *in vitro* conditions. The first, namely "no contact co-culture", was set up to elucidate whether the presence of cancer cells could modulate on pericytes the expression of specific markers[83], such

as CD44, CD90, NG2 and PDGFRβ. The first three markers can also be considered markers of stromal cell stemness. In our experimental condition, no significant changes were observed for CD44, CD90 and NG2/CSPG4 in term of expression. It is well known that regulation of cellular stemness is an intricate phenomenon regulate by multiple and coordinate signalling and standard co-culture conditions may not be sufficient to induce a significant switch from immature to more mature cells. These considerations may explain, almost in part, why our experimental model was not able to significantly modulate the expression of the above antigens. By contrast, we observed an enhanced expression of PDGFRβ in early pericytes co-cultured with MDA-MB-231 and with HT1080 cells. PDGFRβ is a hallmark of activate pericytes and, more in general, of stromal cells; PDGFR/PDGFRβ axis has important repercussions on pericytes, including their activation and recruitment[52,84,85]. More in general, PDGF receptors and their ligands play critical roles in several human malignancies[86–89]. In the cancer progression context, the genetic perturbation of PDGF-B expression has been used to elucidate the role of pericytes in tumour angiogenesis and growth[90]. Moreover, stromal cells, including pericytes, directly stimulate tumour cell proliferation providing various growth factors, hormones and cytokines in a context dependent manner[91,92]. On the other hand, tumour cells are capable to express PDGFs chains for proper maintenance and survive, as below discuss. Jechlinger and his group reported that metastatic potential of oncogenic mammary epithelial cells requires an PDGF/PDGFR loop and PDGF produced in carcinomas is generally thought to act on the nonepithelial tumour stroma, for instance, by promoting angiogenesis[93]. Similar observation was reported by McDermott and co-workers that found the involvement of PDGF/PDGFRs in the progression of both NSCLC and rhabdomyosarcoma[94].

In the model of direct cell-cell interaction, we found a great affinity between pericytes and the cancer cells adopted in this study. In particular, we discover that both early and mature pericytes showed a great interaction with HT1080; a discrete affinity were also observed between pericytes (early and mature) and MD-MB-231 and A375. In normal tissues, the stroma provides nutrients and regulatory signals for proper and cell survival and function. Under tumorigenic condition, the stromal compartment may provide a protective niche and stimulatory signals to cancer cells. Pericytes express several molecules of extracellular matrix which favour cell-cell and cell ECM interactions, that in turn, control multiple cellular processes, including cell polarity, proliferation, and migration. Cellular interactions with the ECM are maintained through the binding of the various ECM molecules with the cellular receptors and ligand (i.e. integrins). The surface antigen CD44 is one of the most important antigen implicated in this phenomenon through the binding

with the glycosaminoglycan namely hyaluronan[95–97]. In this study, we are seen that both early and late pericytes express highly level of CD44, and at same time, we also known that pericytes express several type of glycosaminoglycans. It is plausible that the interaction between pericytes and the cancer cells is necessary and mediated by CD44-ECM, avoiding the anchorage-dependent cell death program namely "anoikis"[98,99].

As a result of cell migration assay, we found that pericytes CM was able to induce a strong migration of the three cancer cell lines respect to the other CM; this migratory energy was especially significant for the A375 melanoma cell line. As above hypothesized, the crosstalk between pericytes and tumour may influence many aspects of cancer cells biology, including their migratory propensity. In this regard, through a protein array, we documented that the pericytes CM may be considered as a rich source of mediators and chemoattractant that, in concert, not only govern proper cell behaviour but also orchestrate cancer survival and migration. Among other factors, the most expressed factors were Serpin E1, EGF and PDGF-AA. Serpin E1 is a serine protease inhibitor known to promote tumour progression by modulating ECM degradation and for many type of cancer is considered biomarker of poor prognosis[100,101]. Recently it has also been demonstrated that in melanoma may contribute to site-specific dissemination and metastasis formation[102]. HB-EGF is well known to promote angiogenesis and pericytes coverage in tumour[103,104]. Using a differentiated pericytes-like mouse cells, C3H/10T1/2, Yu and co-workers demonstrated that addition of HB-EGF led to significant cell proliferation, even under conditions of anoxic stress. Addition of the EGF receptor inhibitor AG1478 led to complete inhibition of the proliferative effects of HB-EGF on these cells. Moreover, HB-EGF protected pericyte-like cells from anoxia-induced apoptosis and promoted cell proliferation in primary pericyte cultures. *In vivo*, administration of HB-EGF to mice subjected to intestinal I/R injury led to protection of pericytes from injury[105]. The EGF/EGFRs and PDGF-AA/PDGFRα axes engage several signalling pathways including the Ras-MAPK circuit, as well as PI3K and PLC-γ routs, which in turn, lead to stimulation of cell growth, differentiation, and migration. These have a particular impact on cancer, in fact aberrant expression of these signalling *in vivo* are often correlate with cancer cell spreading and metastasis[106–113]. As above mentioned, the HBVP/cancer cells CM influenced the migratory capacity of cancer cells in a less extend respect the HBVP CM, and when we analysed the composition of the other CM normalized to that of pericytes CM alone, we found that most factors were differentially up- or down-regulated. In general, we found that both chemoattractant

SerpinE1 and EGF were paradoxally down expressed as well as IL-11 and IL-7A. By contrast, other factors such as VEGF, IL-8, FGF-19 resulted enhanced. Concerning these apparent incongruities, we hypothesize that the reciprocal influence of the modulators may effectively govern the migratory propensity of cancer cells.

This study was developed to deeply understand the nature of pericytes, which are at the present time particularly studied due to their relationship with cancer cells as part of the TME. The obtained results sustain the thesis that pericytes and their paracrine signals are important regulators in cancer biology. The future aim will be to identify some crucial molecules, involved into the pericyte-tumour cell interaction, which could become effective targets in the anti-cancer therapy.

Acknowledgements

I would like to thank prof. Roberto Perris, who gave me the opportunity to take part of his research team for many years;

I also would like to thank prof. Enrico Maria Silini, who kindly supported me during these years;

I am grateful to dr. Domenica Mangieri, who (always?!) believed in this work and in me and strongly contributed to my professional and personal progress;

I would like to thank with all my heart my lab mates, some of them only for a short period, some other for a long time, but each of them gave me the chance to work, study, laugh, (sometime) cry, learn and grow together: dr. Alice Dallatomasina, dr. Elisa Tamburini, dr. Jade Quartararo, dr. Serena Galati, dr. Laura Rocchi, dr. Alessandra D'Angelo, dr. Elena Garusi, dr. Silvia Rossi, dr. Nicoletta Bertani, dr. Mirca Lazzaretti, dr. Chiara Foroni;

I also wish to thank all the people who work in the Department of Life Sciences that I met on my way.

Finally, special thanks go to my husband and my parents, who always encouraged and supported me with patience and love.

Appendix

Table 1. Fluorophore-conjugated primary antibodies used for cytofluorimetric analysis

Primary antibodies	Isotype	Dilution
anti-CD10-FITC	IgG2a	1:10
anti-CD34-FITC	IgG1	1:10
anti-CD44-FITC	IgG2	1:25
anti-CD45-PE-Cy5	IgG1	1:25
anti-CD73-PE	IgG1	1:25
anti-CD90-PE	IgG1	1:20
anti-CD94-PE	IgG2a	1:12
anti-CD106-FITC	IgG1	1:25
anti-CD146-PE	IgG1	1:25
anti-CD184-PE	IgG2a	1:50
anti-NG2-PE	IgG1	1:25

Table 2. Fluorophore-conjugated isotype controls antibodies used for cytofluorimetric analysis.

Isotype controls antibodies	Dilution
IgG1-FITC	1:20
IgG2a-FITC	1:20
IgG1-PE	1:20
IgG2a-PE	1:50
IgG1-PE-Cy5	1:20

Table 3. Primary antibodies used to reveal surface and cytoplasmic markers

Primary antibodies	Host	Dilution
anti-CD10	mouse	1:100
anti-CD44	rabbit	1:100
anti-CD73	mouse	1:250
anti-CD90	rabbit	1:50
anti-CD105	mouse	2 μg/ml
anti-CD147	mouse	5 μg/ml
anti-BP-1	mouse	1:100
anti-Desmin	rabbit	1:200
anti-NG2	mouse	1:5
anti-PDGFR-β	rabbit	1:200
anti-α-SMA	mouse	1:100

Table 4. Secondary antibodies used in immunocytochemistry

Secondary antibodies	Dilution
anti-mouse IgG-Alexa488	1:500
anti- rabbit IgG-Alexa488	1:500

Table 5. Genes assayed through TLDA Microfluidic card

Gene Symbol	Gene Name	Entrez Gene ID	TaqMan Assay ID
18S	Eukaryotic 18S rRNA	HSRRN18S	18S-Hs99999901_s1
ACAN	aggrecan	176	ACAN-Hs00153936_m1
ACTB	actin, beta	60	ACTB-Hs01060665_g1
AGRN	agrin	375790	AGRN-Hs00394748_m1
AMBP	alpha-1-microglobulin/bikunin precursor	259	AMBP-Hs00155697_m1
ASPN	asporin	54829	ASPN-Hs00214395_m1
B2M	beta-2-microglobulin	567	B2M-Hs00187842_m1
BCAN	brevican	63827	BCAN-Hs00222607_m1
BGN	biglycan	633	BGN-Hs00959143_m1
CD248	CD248 molecule, endosialin	57124	CD248-Hs00535574_s1
CD44	CD44 molecule (Indian blood group)	960	CD44-Hs01075861_m1
CHAD	chondroadherin	1101	CHAD-Hs00154382_m1
CILP2	cartilage intermediate layer protein 2	148113	CILP2-Hs00541922_m1
CILP2	cartilage intermediate layer protein, nucleotide pyrophosphohydrolase	8483	CILP-Hs00173647_m1
COL1A1	collagen, type I, alpha 1	1277	COL1A1-Hs00164004_m1
COL1A2	Collagen, type I, alpha 2	1278	COL1A2-Hs01028956_m1
COL2A1	collagen, type II, alpha 1	1280	COL2A1-Hs01064869_m1
COL3A1	collagen, type III, alpha 1	1281	COL3A1-Hs00943809_m1
COL4A1	collagen, type IV, alpha 1	1282	COL4A1-Hs00266237_m1
COL4A2	collagen, type IV, alpha 2	1284	COL4A2-Hs01098873_m1
COL4A3	collagen, type IV, alpha 3 (Goodpasture antigen)	1285	COL4A3-Hs01022542_m1
COL4A4	collagen, type IV, alpha 4	1286	COL4A4-Hs00164150_m1
COL4A5	collagen, type IV, alpha 5	1287	COL4A5-Hs00166712_m1
COL4A6	collagen, type IV, alpha 6	1288	COL4A6-Hs00361494_m1
COL5A1	collagen, type V, alpha 1	1289	COL5A1-Hs00609088_m1
COL5A2	collagen, type V, alpha 2	1290	COL5A2-Hs00893878_m1
COL5A3	collagen, type V, alpha 3	50509	COL5A3-Hs00210526_m1
COL6A1	collagen, type VI, alpha 1	1291	COL6A1-Hs01095585_m1
COL6A2	collagen, type VI, alpha 2	1292	COL6A2-Hs00365167_m1
COL6A3	collagen, type VI, alpha 3	1293	COL6A3-Hs00365098_m1
COL6A5	collagen, type VI, alpha 5	256076	COL6A5-Hs00542046_m1
COL6A6	collagen, type VI, alpha 6	131873	COL6A6-Hs01029204_m1
COL7A1	collagen, type VII, alpha 1	1294	COL7A1-Hs00164310_m1
COL8A1	collagen, type VIII, alpha 1	1295	COL8A1-Hs00220480_m1
COL8A2	collagen, type VIII, alpha 2	1296	COL8A2-Hs00697025_m1
COL9A1	collagen, type IX, alpha 1	1297	COL9A1-Hs00932129_m1
COL9A2	collagen, type IX, alpha 2	1298	COL9A2-Hs00156712_m1
COL9A3	collagen, type IX, alpha 3	1299	COL9A3-Hs00951243_m1
COL10A1	collagen, type X, alpha 1	1300	COL10A1-Hs00166657_m1
COL11A1	collagen, type XI, alpha 1	1301	COL11A1-Hs01097664_m1
COL11A2	collagen, type XI, alpha 2	1302	COL11A2-Hs00365416_m1
COL12A1	collagen, type XII, alpha 1	1303	COL12A1-Hs00189184_m1

COL13A1	collagen, type XIII, alpha 1	1305	COL13A1-Hs00193225_m1
COL14A1	collagen, type XIV, alpha 1	7373	COL14A1-Hs00964045_m1
COL15A1	collagen, type XV, alpha 1	1306	COL15A1-Hs00266332_m1
COL16A1	collagen, type XVI, alpha 1	1307	COL16A1-Hs00156876_m1
COL17A1	collagen, type XVII, alpha 1	1308	COL17A1-Hs00166711_m1
COL18A1	collagen, type XVIII, alpha 1	80781	COL18A1-Hs00181017_m1
COL19A1	collagen, type XIX, alpha 1	1310	COL19A1-Hs00156940_m1
COL21A1	collagen, type XXI, alpha 1	81578	COL21A1-Hs00229402_m1
COL22A1	collagen, type XXII, alpha 1	169044	COL22A1-Hs01377211_m1
COL23A1	collagen, type XXIII, alpha 1	91522	COL23A1-Hs00297526_m1
COL24A1	collagen, type XXIV, alpha 1	255631	COL24A1-Hs00537698_m1
COL25A1	collagen, type XXV, alpha 1	84570	COL25A1-Hs00261300_m1
COL27A1	collagen, type XXVII, alpha 1	85301	COL27A1-Hs00259829_m1
COL28A1	collagen, type XXVIII, alpha 1	340267	COL28A1-Hs00417144_m1
COMP	cartilage oligomeric matrix protein	1311	COMP-Hs00164359_m1
CSPG4	chondroitin sulfate proteoglycan 4	1464	CSPG4-Hs00426981_m1
CSPG5	chondroitin sulfate proteoglycan 5 (neuroglycan C)	10675	CSPG5-Hs00198108_m1
CTGF	connective tissue growth factor	1490	CTGF-Hs01026926_g1
CTHRC1	collagen triple helix repeat containing 1	115908	CTHRC1-Hs00298917_m1
CYR61	cysteine-rich, angiogenic inducer, 61	3491	CYR61-Hs00155479_m1
DCN	decorin	1634	DCN-Hs00266491_m1
DPT	dermatopontin	1805	DPT-Hs00355056_m1
ECM1	extracellular matrix protein 1	1893	ECM1-Hs00189435_m1
ECM2	extracellular matrix protein 2, female organ and adipocyte specific	1842	ECM2-Hs00154821_m1
EFEMP1	EGF containing fibulin-like extracellular matrix protein 1	2202	EFEMP1-Hs00244575_m1
EFEMP2	EGF containing fibulin-like extracellular matrix protein 2	30008	EFEMP2-Hs00973815_m1
ELN	elastin	2006	ELN-Hs00355783_m1
EMID2	collagen, type XXVI, alpha 1	136227	EMID2-Hs00294957_m1
EMILIN1	elastin microfibril interfacer 1	11117	EMILIN1-Hs00170878_m1
EMILIN2	elastin microfibril interfacer 2	84034	EMILIN2-Hs00230757_m1
EPYC	epiphycan	1833	EPYC-Hs00191912_m1
ESM1	endothelial cell-specific molecule 1	11082	ESM1-Hs00199831_m1
FBLN1	fibulin 1	2192	FBLN1-Hs00972609_m1
FBLN2	fibulin 2	2199	FBLN2-Hs00157482_m1
FBLN5	fibulin 5	10516	FBLN5-Hs00197064_m1
FBLN7	fibulin 7	129804	FBLN7-Hs00402230_m1
FBN1	fibrillin 1	2200	FBN1-Hs00171191_m1
FBN2	fibrillin 2	2201	FBN2-Hs00266592_m1
FBN3	fibrillin 3	84467	FBN3-Hs00261049_m1
FGA	fibrinogen alpha chain	2243	FGA-Hs00241027_m1
FMOD	fibromodulin	2331	FMOD-Hs00157619_m1
FN1	fibronectin 1	2335	FN1-Hs01549940_m1
FRAS1	Fraser syndrome 1	80144	FRAS1-Hs00228164_m1
FREM1	FRAS1 related extracellular matrix 1	158326	FREM1-Hs00381549_m1
FREM2	FRAS1 related extracellular matrix protein 2	341640	FREM2-Hs00872621_m1
GADPH	glyceraldehyde-3-phosphate dehydrogenase	2597	GAPDH-Hs02758991_g1

GPC1	glypican 1	2817	GPC1-Hs00892476_m1
GPC2	glypican 2	221914	GPC2-Hs00415099_m1
GPC3	glypican 3	2719	GPC3-Hs00170471_m1
GPC4	glypican 4	2239	GPC4-Hs00155059_m1
GPC5	glypican 5	2262	GPC5-Hs00270114_m1
GPC6	glypican 6	10082	GPC6-Hs00170677_m1
HAPLN1	hyaluronan and proteoglycan link protein 1	1404	HAPLN1-Hs00157103_m1
HAPLN2	hyaluronan and proteoglycan link protein 2	60484	HAPLN2-Hs00368388_m1
HAPLN3	hyaluronan and proteoglycan link protein 3	145864	HAPLN3-Hs01092469_m1
HAPLN4	hyaluronan and proteoglycan link protein 4	404037	HAPLN4-Hs00604587_m1
HAS1	hyaluronan synthase 1	3036	HAS1-Hs00987418_m1
HAS2	hyaluronan synthase 2	3037	HAS2-Hs00193435_m1
HAS3	hyaluronan synthase 3	3038	HAS3-Hs00193436_m1
HMCN1	hemicentin 1	83872	HMCN1-Hs00399043_m1
HPSE	heparanase	10855	HPSE-Hs00935036_m1
HSPG2	heparan sulfate proteoglycan 2	3339	HSPG2-Hs00194179_m1
IBSP	integrin-binding sialoprotein	3381	IBSP-Hs00173720_m1
IMPG1	interphotoreceptor matrix proteoglycan 1	3617	IMPG1-Hs00155522_m1
IMPG2	interphotoreceptor matrix proteoglycan 2	50939	IMPG2-Hs01097136_m1
KAL1	Kallmann syndrome 1 sequence	3730	KAL1-Hs01085107_m1
KERA	keratocan	11081	KERA-Hs00559942_m1
LAMA1	laminin, alpha 1	284217	LAMA1-Hs00300550_m1
LAMA2	laminin, alpha 2	3908	LAMA2-Hs00166308_m1
LAMA3	laminin, alpha 3	3909	LAMA3-Hs00165042_m1
LAMA4	laminin, alpha 4	3910	LAMA4-Hs00935293_m1
LAMA5	laminin, alpha 5	3911	LAMA5-Hs00966585_m1
LAMB1	laminin, beta 1	3912	LAMB1-Hs01055967_m1
LAMB2	laminin, beta 2 (laminin S)	3913	LAMB2-Hs00158642_m1
LAMB3	laminin, beta 3	3914	LAMB3-Hs00165078_m1
LAMB4	laminin, beta 4	22798	LAMB4-Hs00860154_m1
LAMC1	laminin, gamma 1 (formerly LAMB2)	3915	LAMC1-Hs00267056_m1
LAMC2	laminin, gamma 2	3918	LAMC2-Hs00194345_m1
LAMC3	laminin, gamma 3	10319	LAMC3-Hs00195978_m1
LEPRE1	leucine proline-enriched proteoglycan (leprecan) 1	64175	LEPRE1-Hs00964386_m1
LUM	lumican	4060	LUM-Hs00158940_m1
MATN1	matrilin 1, cartilage matrix protein	4146	MATN1-Hs00159075_m1
MATN2	matrilin 2	4147	MATN2-Hs00242753_m1
MATN3	matrilin 3	4148	MATN3-Hs00159081_m1
MATN4	matrilin 4	8785	MATN4-Hs00243631_m1
MEPE	matrix extracellular phosphoglycoprotein	56955	MEPE-Hs00220237_m1
MFAP1	microfibrillar-associated protein 1	4236	MFAP1-Hs00195537_m1
MFAP2	microfibrillar-associated protein 2	4237	MFAP2-Hs01027737_m1
MFAP3	microfibrillar-associated protein 3	4238	MFAP3-Hs00195543_m1
MFAP4	microfibrillar-associated protein 4	4239	MFAP4-Hs00412974_m1
MFAP5	microfibrillar-associated protein 5	8076	MFAP5-Hs00185803_m1
MMRN2	multimerin 2	79812	MMRN2-Hs00226971_m1

NCAN	neurocan	1463	NCAN-Hs00189270_m1
NID1	nidogen 1	4811	NID1-Hs00159600_m1
NID2	nidogen 2 (osteonidogen)	22795	NID2-Hs00201233_m1
NOV	nephroblastoma overexpressed	4856	NOV-Hs00159631_m1
NPNT	nephronectin	255743	NPNT-Hs01568128_m1
NYX	nyctalopin	60506	NYX-Hs00360869_m1
OGN	osteoglycin	4969	OGN-Hs00247901_m1
OMD	osteomodulin	4958	OMD-Hs00192325_m1
OPTC	opticin	26254	OPTC-Hs00205039_m1
PODN	podocan	127435	PODN-Hs00542259_m1
PODNL1	podocan-like 1	79883	PODNL1-Hs00227318_m1
POSTN	periostin, osteoblast specific factor	10631	POSTN-Hs01566750_m1
PRELP	proline/arginine-rich end leucine-rich repeat protein	5549	PRELP-Hs00160431_m1
PTPRZ1	protein tyrosine phosphatase, receptor-type, Z polypeptide 1	5803	PTPRZ1-Hs00960146_m1
RELN	reelin	5649	RELN-Hs01022646_m1
RPTN	repetin	126638	RPTN-Hs00403264_g1
RSPO1	R-spondin 1	284654	RSPO1-Hs00543475_m1
RSPO2	R-spondin 2	340419	RSPO2-Hs00379983_m1
RSPO3	R-spondin 3	84870	RSPO3-Hs01072567_m1
RSPO4	R-spondin 4	343637	RSPO4-Hs01382765_m1
SDC1	syndecan 1	6382	SDC1-Hs00896423_m1
SDC2	syndecan 2	6383	SDC2-Hs00299807_m1
SDC3	syndecan 3	9672	SDC3-Hs00206320_m1
SDC4	syndecan 4	6385	SDC4-Hs01120909_m1
SELPLG	selectin P ligand	6404	SELPLG-Hs00380945_m1
SMC3	structural maintenance of chromosomes 3	9126	SMC3-Hs00271322_m1
SMOC1	SPARC related modular calcium binding 1	64093	SMOC1-Hs00223283_m1
SMOC2	SPARC related modular calcium binding 2	64094	SMOC2-Hs00405777_m1
SPARC	secreted protein, acidic, cysteine-rich (osteonectin	6678	SPARC-Hs00234160_m1
SPARCL1	SPARC-like 1 (hevin)	8404	SPARCL1-Hs00949886_m1
SPOCK1	sparc/osteonectin, cwcv and kazal-like domains proteoglycan (testican) 1	6695	SPOCK1-Hs00270274_m1
SPOCK2	sparc/osteonectin, cwcv and kazal-like domains proteoglycan (testican) 2	9806	SPOCK2-Hs00360339_m1
SPOCK3	sparc/osteonectin, cwcv and kazal-like domains proteoglycan (testican) 3	50859	SPOCK3-Hs00213568_m1
SPON1	spondin 1, extracellular matrix protein	10418	SPON1-Hs01120488_m1
SPON2	spondin 2, extracellular matrix protein	10417	SPON2-Hs00202813_m1
SPP1	secreted phosphoprotein 1	6696	SPP1-Hs00960942_m1
SRGN	serglycin	5552	SRGN-Hs00160444_m1
SSPO	SCO-spondin	23145	SSPO-Hs00543603_m1
SV2A	synaptic vesicle glycoprotein 2A	9900	SV2A-Hs00372069_m1
TGFBR3	transforming growth factor, beta receptor III	7049	TGFBR3-Hs00234257_m1
THBD	thrombomodulin	7056	THBD-Hs00264920_s1
THBS1	thrombospondin 1	7057	THBS1-Hs00962908_m1
THBS2	thrombospondin 2	7058	THBS2-Hs00170248_m1
THBS3	thrombospondin 3	7059	THBS3-Hs00200157_m1
THBS4	thrombospondin 4	7060	THBS4-Hs00170261_m1

TNC	tenascin C	3371	TNC-Hs01115665_m1
TNR	tenascin R	7143	TNR-Hs00990097_m1
TNXB	tenascin XB	7148	TNXB-Hs00372889_g1
TUBA4A	tubulin, alpha 4a	7277	TUBA4A-Hs00428633_m1
UCMA	upper zone of growth plate and cartilage matrix associated	221044	UCMA-Hs00377205_m1
VCAM1	vascular cell adhesion molecule 1	7412	VCAM1-Hs01003372_m1
VCAN	versican	1462	VCAN-Hs00171642_m1
VIT	vitrin	5212	VIT-Hs00364959_m1
VTN	vitronectin	7448	VTN-Hs00169863_m1
VWF	von Willebrand factor	7450	VWF-Hs01109446_m1
WISP1	WNT1 inducible signaling pathway protein 1	8840	WISP1-Hs00365573_m1
WISP2	WNT1 inducible signaling pathway protein 2	8839	WISP2-Hs00180242_m1
WISP3	WNT1 inducible signaling pathway protein 3	8838	WISP3-Hs00180236_m1

References

1. Hanahan, D. & Weinberg, R. A. Hallmarks of cancer: the next generation. *Cell* **144,** 646–74 (2011).

2. Valastyan, S. & Weinberg, R. A. Tumor metastasis: Molecular insights and evolving paradigms. *Cell* **147,** 275–292 (2011).

3. Kumar, V., Abbas, A. K. & Aster, J. C. *Robbins and Cotran Pathologic basis of disease*. *9th edition* (2014). doi:10.1007/s13398-014-0173-7.2

4. García-Román, J. & Zentella-Dehesa, A. Vascular permeability changes involved in tumor metastasis. *Cancer Lett.* **335,** 259–269 (2013).

5. Gupta, G. P. & Massagué, J. Cancer Metastasis: Building a Framework. *Cell* **127,** 679–695 (2006).

6. Reymond, N., D'Água, B. B. & Ridley, A. J. Crossing the endothelial barrier during metastasis. *Nat. Rev. Cancer* **13,** 858–70 (2013).

7. Irmisch, A. & Huelsken, J. Metastasis: New insights into organ-specific extravasation and metastatic niches. *Exp. Cell Res.* **319,** 1604–1610 (2013).

8. Oppenheimer, S. B. Cellular basis of cancer metastasis: A review of fundamentals and new advances. *Acta Histochem.* **108,** 327–334 (2006).

9. Pantel, K. & Speicher, M. R. The biology of circulating tumor cells. *Oncogene* 1–9 (2015).

10. Joosse, S. a & Pantel, K. Biologic challenges in the detection of circulating tumor cells. *Cancer Res.* **73,** 8–11 (2013).

11. Chiang, A. C. & Massagué, J. Molecular basis of metastasis. *N. Engl. J. Med.* **359,** 2814–23 (2008).

12. Luzzi, K. J. *et al.* Multistep Nature of Metastatic Inefficiency. *Am. J. Pathol.* **153,** 865–873 (1998).

13. Seyfried, T. N. & Huysentruyt, L. C. On the Origin of Cancer Metastasis. *Crit. Rev. Oncog.* **18,** 43–73 (2013).

14. Chaffer, C. L. & Weinberg, R. a. A perspective on cancer cell metastasis. *Science* **331,** 1559–1564 (2011).

15. Giussani, M., Merlino, G., Cappelletti, V., Tagliabue, E. & Daidone, M. G. Tumor-Extracellular Matrix interactions: identification of tools associated with breast cancer progression. *Semin. Cancer Biol.* **35,** 3–10 (2015).

16. Gerhardt, H. & Semb, H. Pericytes: gatekeepers in tumour cell metastasis? *J. Mol. Med. (Berl).* **86,** 135–44 (2008).

17. Goubran, H. A., Kotb, R. R., Stakiw, J., Emara, M. E. & Burnouf, T. Regulation of tumor growth and metastasis: the role of tumor microenvironment. *Cancer Growth Metastasis* **7,** 9–18 (2014).

18. Armulik, A. *et al.* Pericytes: developmental, physiological, and pathological perspectives, problems, and promises. *Dev. Cell* **21,** 193–215 (2011).

19. Grimer, R., Judson, I., Peake, D. & Seddon, B. Guidelines for the Management of Soft Tissue Sarcomas. *Sarcoma* **2010,** 1–15 (2010).

20. Mastrangelo, G. *et al.* Incidence of soft tissue sarcoma and beyond: a population-based prospective study in 3 European regions. *Cancer* **118,** 5339–48 (2012).

21. Stiller, C. A. *et al.* Descriptive epidemiology of sarcomas in Europe: Report from the RARECARE project. *Eur. J. Cancer* **49,** 684–695 (2013).

22. Lee, C.-H. *et al.* A panel of antibodies to determine site of origin and malignancy in smooth muscle tumors. *Mod. Pathol.* **22,** 1519–1531 (2009).

23. Francis, M. *et al.* Incidence and Survival of Gynecologic Sarcomas in England. *Int. J. Gynecol. Cancer* **25,** 1–8 (2015).

24. Yamada, S. *et al.* A case of multiple brain metastases of uterine leiomyosarcoma with a literature review. *Surg. Oncol.* **20,** e127–31 (2011).

25. Gurram, M. K., Pulivarthi, S., McGary, C. T. & Defillo, A. Brain and multiorgan metastases from uterine leiomyosarcoma. *Tumori* **100,** 8e–13e (2013).

26. Tan, L. a, Kasliwal, M. K., Nag, S. & O'Toole, J. E. A rare intramedullary spinal cord metastasis from uterine leiomyosarcoma. *J. Clin. Neurosci.* **20,** 1309–12 (2013).

27. Nguyen, S. K. a & Wong, F. Right atrial metastasis of uterine leiomyosarcoma causing obstructive shock. *Curr. Oncol.* **19,** e292–4 (2012).

28. Corcoran, S. *et al.* Isolated cutaneous metastasis of uterine leiomyosarcoma: case report and review of literature. *Diagn. Pathol.* **7,** 85 (2012).

29. Tunio, M. A. *et al.* Obstructive small bowel metastasis from uterine leiomyosarcoma: a case report. *Case Rep. Obstet. Gynecol.* **2014,** 603097 (2014).

30. Alonso Gómez, J. *et al.* Uterine leiomyosarcoma metastasis to the pancreas: Report of a case and review of the literature. *J. Gastrointest. Cancer* **43,** 361–363 (2012).

31. Collins, I. M. & Thomas, D. M. Novel approaches to treatment of leiomyosarcomas. *Curr. Oncol. Rep.* **13,** 316–22 (2011).

32. Sutton, G. Uterine sarcomas 2013. *Gynecol. Oncol.* **130,** 3–5 (2013).

33. Hensley, M. L. *et al.* Adjuvant therapy for high-grade, uterus-limited leiomyosarcoma: results of a phase 2 trial (SARC 005). *Cancer* **119,** 1555–61 (2013).

34. Abdollahi, A. & Folkman, J. Evading tumor evasion: current concepts and perspectives of anti-angiogenic cancer therapy. *Drug Resist. Updat.* **13,** 16–28 (2010).

35. Folkman, J. Tumor angiogenesis: therapeutic implications. *N. Engl. J. Med.* **285,** 1182–1186 (1971).

36. Hanahan, D. & Folkman, J. Patterns and emerging mechanisms of the angiogenic switch during tumorigenesis. *Cell* **86,** 353–364 (1996).

37. Shuman Moss, L. A., Jensen-Taubman, S. & Stetler-Stevenson, W. G. Matrix metalloproteinases: changing roles in tumor progression and metastasis. *Am. J. Pathol.* **181,** 1895–9 (2012).

38. Macri, L., Silverstein, D. & Clark, R. Growth factor binding to the pericellular matrix and its importance in tissue engineering. *Adv. Drug Deliv. Rev.* **59,** 1366–1381 (2007).

39. Dvorak, H. F., Weaver, V. M., Tlsty, T. D. & Bergers, G. Tumor microenvironment and progression. *J. Surg. Oncol.* **103,** 468–474 (2011).

40. Rouget, C. Memoire sur le developpement, la structures et les proprieties des capillaires sanguins et lymphatiques. *Arch. Histol. Norm. Patol.* **5,** 603–633 (1873).

41. Zimmermann, K. W. Der feinere bau der blutcapillares. *Z. Anat. Entwicklungsgesch.* **68,** 1923 (1923).

42. Díaz-Flores, L. *et al.* Pericytes. Morphofunction, interactions and pathology in a quiescent and activated

mesenchymal cell niche. *Histol. Histopathol.* **24,** 909–69 (2009).

43. Raza, A., Franklin, M. J. & Dudek, A. Z. Pericytes and vessel maturation during tumor angiogenesis and metastasis. *Am. J. Hematol.* **85,** 593–8 (2010).

44. Ribatti, D., Nico, B. & Crivellato, E. The role of pericytes in angiogenesis. *Int. J. Dev. Biol.* **55,** 261–268 (2011).

45. Geevarghese, A. & Herman, I. M. Pericyte-endothelial crosstalk: Implications and opportunities for advanced cellular therapies. *Transl. Res.* **163,** 296–306 (2014).

46. Morikawa, S. *et al.* Abnormalities in pericytes on blood vessels and endothelial sprouts in tumors. *Am. J. Pathol.* **160,** 985–1000 (2002).

47. Virgintino, D. *et al.* An intimate interplay between precocious, migrating pericytes and endothelial cells governs human fetal brain angiogenesis. *Angiogenesis* **10,** 35–45 (2007).

48. van Dijk, C. G. M. *et al.* The complex mural cell: Pericyte function in health and disease. *Int. J. Cardiol.* **190,** 75–89 (2015).

49. Mravic, M. *et al.* From pericytes to perivascular tumours: correlation between pathology, stem cell biology, and tissue engineering. *Int. Orthop.* **38,** 1819–24 (2014).

50. Stratman, A. N., Malotte, K. M., Mahan, R. D., Davis, M. J. & Davis, G. E. Pericyte recruitment during vasculogenic tube assembly stimulates endothelial basement membrane matrix formation. *Blood* **114,** 5091–101 (2009).

51. Armulik, A. *et al.* Pericytes regulate the blood-brain barrier. *Nature* **468,** 557–61 (2010).

52. von Tell, D., Armulik, A. & Betsholtz, C. Pericytes and vascular stability. *Exp. Cell Res.* **312,** 623–9 (2006).

53. Bergers, G. & Song, S. The role of pericytes in blood-vessel formation and maintenance. *Neuro. Oncol.* **7,** 452–464 (2005).

54. Hirschi, K. K. & D'Amore, P. a. Pericytes in the microvasculature. *Cardiovasc. Res.* **32,** 687–698 (1996).

55. Rowley, J. E. & Johnson, J. R. Pericytes in chronic lung disease. *Int. Arch. Allergy Immunol.* **164,** 178–88 (2014).

56. Winkler, E. a., Sagare, A. P. & Zlokovic, B. V. The pericyte: A forgotten cell type with important implications for alzheimer's disease? *Brain Pathol.* **24,** 371–386 (2014).

57. Ribeiro, A. L. & Okamoto, O. K. Combined Effects of Pericytes in the Tumor Microenvironment. *Stem Cells Int.* **2015,** (2015).

58. Xian, X. *et al.* Pericytes limit tumor cell metastasis. *J. Clin. Invest.* **116,** 642–51 (2006).

59. Cooke, V. G. *et al.* Pericyte depletion results in hypoxia-associated epithelial-to-mesenchymal transition and metastasis mediated by met signaling pathway. *Cancer Cell* **21,** 66–81 (2012).

60. Barlow, K. D., Sanders, A. M., Soker, S., Ergun, S. & Metheny-Barlow, L. J. Pericytes on the tumor vasculature: jekyll or hyde? *Cancer Microenviron.* **6,** 1–17 (2013).

61. Welén, K., Jennbacken, K., Tesan, T. & Damber, J.-E. Pericyte coverage decreases invasion of tumour cells into blood vessels in prostate cancer xenografts. *Prostate Cancer Prostatic Dis* **12,** 41–6 (2009).

62. Correa, D., Somoza, R. A., Lin, P., Schiemann, W. P. & Caplan, A. I. Mesenchymal stem cells regulate melanoma cancer cells extravasation to bone and liver at their perivascular niche. *Int. J. Cancer* **138,** 417–

427 (2016).

63. Yonenaga, Y. *et al.* Absence of smooth muscle actin-positive pericyte coverage of tumor vessels correlates with hematogenous metastasis and prognosis of colorectal cancer patients. *Oncology* **69,** 159–66 (2005).

64. Illemann, M. *et al.* Tissue inhibitor of matrix metalloproteinase-1 expression in colorectal cancer liver metastases is associated with vascular structures. *Mol. Carcinog.* **55,** 193–208 (2015).

65. Svensson, A., Özen, I., Genové, G., Paul, G. & Bengzon, J. Endogenous brain pericytes are widely activated and contribute to mouse glioma microvasculature. *PLoS One* **10,** e0123553 (2015).

66. Vanharanta, S. & Massagué, J. Origins of Metastatic Traits. *Cancer Cell* **24,** 410–421 (2013).

67. Winkler, F. The brain metastatic niche. *J. Mol. Med.* 1213–1220 (2015). doi:10.1007/s00109-015-1357-0

68. Hamzah, J. *et al.* Vascular normalization in Rgs5-deficient tumours promotes immune destruction. *Nature* **453,** 410–414 (2008).

69. Lindblom, P. *et al.* Endothelial PDGF-B retention is required for proper investment of pericytes in the microvessel wall. *Genes Dev.* **17,** 1835–1840 (2003).

70. Lorger, M. & Felding-Habermann, B. Capturing Changes in the Brain Microenvironment during Initial Steps of Breast Cancer Brain Metastasis. *Am. J. Pathol.* **176,** 2958–2971 (2010).

71. Polyak, K. & Weinberg, R. A. Transitions between epithelial and mesenchymal states: acquisition of malignant and stem cell traits. *Nat. Rev. Cancer* **9,** 265–273 (2009).

72. Kienast, Y. & Winkler, F. Therapy and prophylaxis of brain metastases. *Expert Rev Anticancer Ther* **10,** 1763–77 (2010).

73. Bababeygy, S. R. *et al.* Hematopoietic stem cell-derived pericytic cells in brain tumor angio-architecture. *Stem Cells Dev* **17,** 11–8 (2008).

74. Keskin, D. *et al.* Targeting Vascular Pericytes in Hypoxic Tumors Increases Lung Metastasis via Angiopoietin-2. *Cell Rep.* **10,** 1066–1081 (2015).

75. Xian, X. & Hakansson, J. Pericytes limit tumor cell metastasis. *J. Clin. Invest.* **116,** 642–51 (2006).

76. Hanahan, D. & Coussens, L. M. Accessories to the crime: functions of cells recruited to the tumor microenvironment. *Cancer Cell* **21,** 309–22 (2012).

77. Kamińska, K. *et al.* The role of the cell-cell interactions in cancer progression. *J. Cell. Mol. Med.* **19,** 283–96 (2015).

78. Bhome, R. *et al.* A top-down view of the tumor microenvironment: structure, cells and signaling. *Front. Cell Dev. Biol.* **3,** 1–9 (2015).

79. Fokas, E., McKenna, W. G. & Muschel, R. J. The impact of tumor microenvironment on cancer treatment and its modulation by direct and indirect antivascular strategies. *Cancer Metastasis Rev.* **31,** 823–842 (2012).

80. Blocki, A. *et al.* Not All MSCs Can Act as Pericytes: Functional In Vitro Assays to Distinguish Pericytes from Other Mesenchymal Stem Cells in Angiogenesis. *Stem Cells Dev.* **22,** 2347–55 (2013).

81. Gerhardt, H. & Betsholtz, C. Endothelial-pericyte interactions in angiogenesis. *Cell Tissue Res.* **314,** 15–23 (2003).

82. Dar, A. *et al.* Multipotent vasculogenic pericytes from human pluripotent stem cells promote recovery of murine ischemic limb. *Circulation* **125,** 87–99 (2012).

83. Patenaude, A. *et al.* A novel population of local pericyte precursor cells in tumor stroma that require Notch signaling for differentiation. *Microvasc. Res.* **101,** 38–47 (2015).

84. Stratman, A. N., Schwindt, A. E., Malotte, K. M. & Davis, G. E. Endothelial-derived PDGF-BB and HB-EGF coordinately regulate pericyte recruitment during vasculogenic tube assembly and stabilization. *Blood* **116,** 4720–30 (2010).

85. Hellström, M., Kalén, M., Lindahl, P., Abramsson, a & Betsholtz, C. Role of PDGF-B and PDGFR-beta in recruitment of vascular smooth muscle cells and pericytes during embryonic blood vessel formation in the mouse. *Development* **126,** 3047–3055 (1999).

86. van Dijk, F., Olinga, P., Poelstra, K. & Beljaars, L. Targeted Therapies in Liver Fibrosis: Combining the Best Parts of Platelet-Derived Growth Factor BB and Interferon Gamma. *Front. Med.* **2,** (2015).

87. Zhao, Y. & Adjei, A. A. Targeting Angiogenesis in Cancer Therapy: Moving Beyond Vascular Endothelial Growth Factor. *Oncologist* **20,** 660–673 (2015).

88. Gialeli, C. *et al.* PDGF/PDGFR signaling and targeting in cancer growth and progression: Focus on tumor microenvironment and cancer-associated fibroblasts. *Curr Pharm Des* **20,** 2843–8 (2014).

89. Demoulin, J.-B. & Essaghir, A. PDGF receptor signaling networks in normal and cancer cells. *Cytokine Growth Factor Rev.* **25,** 1–11 (2014).

90. Abramsson, A., Lindblom, P. & Betsholtz, C. Endothelial and nonendothelial sources of PDGF-B regulate pericyte recruitment and influence vascular pattern formation in tumors. *J. Clin. Invest.* **112,** 1142–51 (2003).

91. Paulsson, J., Ehnman, M. & Östman, A. PDGF receptors in tumor biology: prognostic and predictive potential. *Futur. Oncol.* **10,** 1695–708 (2014).

92. Aguirre Palma, L. M., Gehrke, I. & Kreuzer, K.-A. Angiogenic factors in chronic lymphocytic leukaemia (CLL): Where do we stand? *Crit. Rev. Oncol. Hematol.* **93,** 1–12 (2014).

93. Jechlinger, M. *et al.* Autocrine PDGFR signaling promotes mammary cancer metastasis. *J. Clin. Invest.* **116,** 1–10 (2006).

94. McDermott, U. *et al.* Ligand-dependent PDGF receptor-alpha activation sensitizes rare lung cancer and sarcoma cells to PDGF receptor kinase inhibitors. *Cancer Res.* **69,** 3937–3946 (2010).

95. Klein, D. *et al.* Vascular Wall-Resident CD44+ Multipotent Stem Cells Give Rise to Pericytes and Smooth Muscle Cells and Contribute to New Vessel Maturation. *PLoS One* **6,** e20540 (2011).

96. Maria, B. L. *et al.* Targeting hyaluronan interactions in spinal cord astrocytomas and diffuse pontine gliomas. *J. Child Neurol.* **23,** 1214–1220 (2008).

97. Caspani, E. M., Crossley, P. H., Redondo-Garcia, C. & Martinez, S. Glioblastoma: A Pathogenic Crosstalk between Tumor Cells and Pericytes. *PLoS One* **9,** e101402 (2014).

98. Paoli, P., Giannoni, E. & Chiarugi, P. Anoikis molecular pathways and its role in cancer progression. *Biochim. Biophys. Acta - Mol. Cell Res.* **1833,** 3481–3498 (2013).

99. Yadav, S. S. *et al.* Anti-tumor activity of staurosporine in the tumor microenvironment of cervical cancer: An in vitro study. *Life Sci.* **133,** 21–8 (2015).

100. Placencio, V. R., Ichimura, A., Miyata, T. & DeClerck, Y. a. Small Molecule Inhibitors of Plasminogen Activator Inhibitor-1 Elicit Anti-Tumorigenic and Anti-Angiogenic Activity. *PLoS One* **10,** e0133786 (2015).

101. Harbeck, N. *et al.* Clinical relevance of the plasminogen activator inhibitor type 1--a multifaceted proteolytic

factor. *Onkologie* **24,** 238–244 (2001).

102. Klein, R. M., Bernstein, D., Higgins, S. P., Higgins, C. E. & Higgins, P. J. SERPINE1 Expression Discriminates Site-Specific Metastasis in Human Melanoma. *Exp Dermatol* **21,** 551–554 (2013).

103. Nolan-Stevaux, O. *et al.* Differential contribution to neuroendocrine tumorigenesis of parallel egfr signaling in cancer cells and pericytes. *Genes Cancer* **1,** 125–41 (2010).

104. Taylor, S. R., Markesbery, M. G. & Harding, P. a. Heparin-binding epidermal growth factor-like growth factor (HB-EGF) and proteolytic processing by a disintegrin and metalloproteinases (ADAM): A regulator of several pathways. *Semin. Cell Dev. Biol.* **28,** 22–30 (2014).

105. Yu, X., Radulescu, A., Chen, C.-L., James, I. O. & Besner, G. E. Heparin-Binding EGF-Like Growth Factor Protects Pericytes from Injury. *J. Surg. Res.* **12,** 1–12 (2012).

106. Higashiyama, S. *et al.* Membrane-anchored growth factors, the epidermal growth factor family: Beyond receptor ligands. *Cancer Sci.* **99,** 214–220 (2008).

107. Huang, P. *et al.* The role of EGF-EGFR signalling pathway in hepatocellular carcinoma inflammatory microenvironment. *J. Cell. Mol. Med.* **18,** 218–30 (2014).

108. Wei, T. *et al.* Overexpression of platelet-derived growth factor receptor alpha promotes tumor progression and indicates poor prognosis in hepatocellular carcinoma. *Oncotarget* **5,** (2014).

109. Zhang, J.-B. *et al.* Up-regulation of platelet-derived growth factor-A is responsible for the failure of re-initiated interferon alpha treatment in hepatocellular carcinoma. *BMC Cancer* **12,** 439 (2012).

110. Nabeshima, A. *et al.* Tumour-associated macrophages correlate with poor prognosis in myxoid liposarcoma and promote cell motility and invasion via the HB-EGF-EGFR-PI3K/Akt pathways. *Br. J. Cancer* **112,** 547–555 (2015).

111. Clapéron, A. *et al.* EGF/EGFR axis contributes to the progression of cholangiocarcinoma through the induction of an epithelial-mesenchymal transition. *J. Hepatol.* **61,** 325–332 (2014).

112. Chen, Y. *et al.* Glioma initiating cells contribute to malignant transformation of host glial cells during tumor tissue remodeling via PDGF signaling. *Cancer Lett.* **365,** 174–181 (2015).

113. Guardiola, S. *et al.* Peptides targeting EGF block the EGF-EGFR interaction. *ChemBioChem* (2015).